Prediction of Transporter-Based Drug Clearances and Tissue Concentrations: Relative Expression Factor Approach and Protein-Mediated Uptake Effect

Mengyue Yin

A dissertation

submitted in partial fulfillment of the

requirements for the degree of

Doctor of Philosophy

University of Washington

2023

Reading Committee:

Jashvant D. Unadkat, Chair

Nina Isoherranen

Joanne Wang

Program Authorized to Offer Degree:

Pharmaceutics

Abstract

Prediction of Transporter-Based Drug Clearances and Tissue Concentrations: Relative Expression Factor Approach and Protein-Mediated Uptake Effect

Mengyue Yin

Chair of the Supervisory Committee:
Jashvant D. Unadkat
Pharmaceutics

Clinical drug development often fails due to insufficient efficacy and safety, which can be attributed to not reaching the desired drug concentrations at their target sites (Smietana *et al.*, 2016).Therefore, for successful and cost-effective development of a new drug, it's crucial to accurately measure or predict its concentrations at the site of actions. This becomes especially critical for drugs that are active transporter substrates or undergo metabolism in the target tissue. For such drugs, *in vivo* pharmacokinetic (PK) studies cannot yield reliable predictions of tissue drug concentrations (G Patilea-Vrana and Unadkat, 2016). Moreover, direct measurement of tissue drug concentrations using imaging techniques is not always feasible (Billington *et al.*, 2019). These challenges highlight the need to accurately predict (not measure) tissue drug

concentrations. To achieve this goal, all clearances (CLs) pathways mediating drug's entry and exit from the tissue, including transporter-mediated and metabolic CLs must be accurately predicted. While metabolic drug CL predictions have been relatively successful, predicting transporter-mediated drug CL, using primary cells, remains challenging.

Given this, we have proposed the proteomics-informed relative expression factor (REF) approach to predict transporter-based drug CL. This approach utilizes the transporter-expressing cells (TECs) or vesicles (TEVs), which are more readily available. We have verified this approach by successfully predicting transporter-based CLs and tissue concentrations for several transported drugs (Storelli, Yin, *et al.*, 2022). However, the prediction fell short for the hepatic uptake CL of rosuvastatin (RSV, an organic anion-transporting polypeptide (OATP) substrate) (Kumar *et al.*, 2021). In addition, the underprediction of *in vivo* hepatic uptake CL has been widely reported for OATP-substrates (Kim *et al.*, 2019).

Numerous investigators introduced "protein-mediated uptake effect (PMUE)" and indicating that the inclusion of plasma proteins enhances the apparent intrinsic uptake CL of OATP-substrate drugs, thereby improving the prediction of hepatic CL for these drugs (Schulz *et al.*, 2023). Therefore, the primary goal of my dissertation work is to investigate if the addition of human plasma proteins can bridge the IVIVE gap of *in vivo* hepatic uptake CL of OATPs substrates, such as statins.

To do so, in **Chapter 2**, I investigated PMUE on five statins (atorvastatin (ATV), cerivastatin (CRV), fluvastatin (FLV), pitavastatin (PTV), rosuvastatin (RSV)) using OATP1B1-expressing and mock HEK293 cells with varying (0, 1%, 2%, and 5%) human serum albumin (HSA) concentrations. However, the results showed that the observed PMUE was largely an artifact of the residual statin-albumin complex remaining with the cells or labware when the uptake

experiment is terminated. The residual albumin-statin complex was estimated by quantifying the residual albumin using quantitative targeted proteomics (QTP). This residual statin-albumin complex has not been quantified by others and therefore its presence has been erroneously interpreted as actual drug uptake resulting in the false conclusion of an apparent PMUE on statin uptake.

Since human hepatocytes (plated or suspended) are widely used by researchers to measure OATP-mediated uptake of drugs, in **Aim 2** (**Chapter 3**), we investigated if the reported PMUE on statin uptake by human hepatocytes could also be explained by the residual statin-albumin complex. We hypothesized that if this apparent PMUE on human hepatocytes is also an artifact, it should be reduced when suspended hepatocytes are used. This is because when terminating uptake of drugs, the suspended hepatocytes are centrifugated through an oil layer potentially reducing the amount of residual statin-albumin complex remaining with the cells. Indeed, the results showed that the apparent PMUE on statins, when using human hepatocytes, was indeed an artifact and was much reduced when the oil-spin method was used.

With such observations in **Chapter 2 & 3**, we investigated in **Aim 3** (**Chapter 4**) if the underprediction of *in vivo* hepatic uptake CL was true for all OATP-transported drugs or specific only to RSV, using TECs/TEVs/REF approach. In **Chapter 4**, we extended the TECs/TEVs/REF approach to predict THE hepatobiliary CLs and hepatic concentrations of two additional OATP-substrates, glyburide (GLB) and pitavastatin (PTV). Then, we verified these predictions using their human PET imaging data. The hepatobiliary CLs of both GLB and PTV were well predicted (*i.e.* within two-fold of the observed values). In addition, the predicted hepatic concentration-time profiles for GLB and PTV, both fell within 2-fold range. These results, together with our previous successes, indicate that the REF approach can be used with

confidence to predict transporter-based drug CLs and tissue concentrations. Such predictions may be useful to inform dose selection in clinical trials to improve successful development of drugs.

TABLE OF CONTENTS

LIST OF FIGURES

LIST OF TABLES

ACKNOWLEDGEMENTS

Time has truly flown by, and these past five years have seen me grow immensely. There are numerous individuals who have been instrumental in this journey, and I wish to express my gratitude to each one of them.

Firstly, I extend my heartfelt thanks to my mentor, Dr. Jashvant D. Unadkat for his guidance and patience with me these past few years. He selected me to his lab during a difficult time in my life. The four-month internship in his lab was a turning point for me, reigniting my passion for science and helping me find my footing again. His approach to science and mentorship has not only boosted my confidence as a budding scientist but also deeply influenced my personal and professional growth. I am immensely grateful for the knowledge and skills he has imparted, especially in public speaking and critical thinking, which I know will serve me well throughout my career.

I am also thankful to my thesis committee – Dr. Nina Isoherranen, Dr. Ken Thummel, Dr. Joanne Wang, and Dr. Qingcheng Mao (dec.). Your insights, probing questions, and valuable suggestions have significantly shaped my dissertation research. A special thanks to Dr. Isoherranen and Dr. Wang for their meticulous reading of my dissertation and their constructive feedback. Dr. Thummel, your thought-provoking questions have always inspired deeper inquiry. Dr. Mao, your assistance has been invaluable, and you are dearly missed.

To the current and former members of the Unadkat lab, thank you for creating an environment of learning and camaraderie. Madhav, your mentorship during my internship was critical in developing my independent thinking and inspiring me to pursue the UW PCEUT program. Flavia, your readiness to help and your passion for science have been truly inspiring. Ankit, your companionship in the final year of my Ph.D. journey has been a source of strength. Together, we will “fly”.

To my fiancé Weize, your support has been my pillar through these transformative years. From teaching me PK to helping me adapt to life in the U.S., and standing by me during tough times, your presence has been a constant source of comfort and strength.

To my friends – Cindy, Winnie, Christina, Claire, Yuqian, Nan, Lili, Ziyue, Kexin – your support, understanding, and diverse perspectives have enriched my life in countless ways.

I am grateful to all the faculty and staff in the Department of Pharmaceutics for fostering a supportive and conducive learning environment.

Lastly, to my family, whose unwavering support and belief in me have been my backbone. This milestone is as much a testament to your love and faith as it is to my efforts.

DEDICATION

To my mom,

Thank you for all the sacrifices you made and your unconditional love.

Chapter 1. INTRODUCTION

1.1 SPECIFIC AIMS

Failure of drug development predominantly stems from inadequate drug efficacy and safety. One reason for lack of efficacy could be due to not achieving the desired drug concentrations at the site of action (Harrison, 2016). Hence, to reduce the failure-rate and cost when developing a new molecular entity (NME, henceforth referred to as a drug), accurate measurement or prediction of its human tissue concentrations is required. This is particularly true for a drug that is actively transported into or out of the target tissue or is significantly metabolized there. For these drugs, routine pharmacokinetic (PK) studies cannot be used to predict their tissue drug concentrations (G Patilea-Vrana and Unadkat, 2016). Although human tissue drug concentrations can be measured by imaging, routine use of these methods (such as positron emission tomography, PET) is limited by cost, low spatial resolution, and sensitivity or the use of radioactivity (Matthews *et al.*, 2012). Therefore, the only alternative is to predict, not measure, tissue drug concentrations. To make such predictions, all clearance (CL) pathways mediating the drug's entry and exit from the tissue, including transporter-mediated and metabolic CLs, must be accurately predicted.

Although prediction of metabolic drug CL is relatively successful, accurate prediction of transporter-mediated drug CL remains a challenge. One reason is that primary cells from the organs of interest are often not available (e.g. the BBB). Therefore, our laboratory has proposed the proteomics-informed relative expression factor (REF) approach to make such predictions as it does not require primary cells (Storelli, Yin, *et al.*, 2022). Instead, it uses transporter-expressing cells (TECs) or vesicles (TEVs). The REF approach is based on correcting transport CL of a drug measured in transporter-expressing cells (TECs) or vesicles (TEVs) by the ratio of the transporter abundance in the tissue of interest and the TECs/TEVs. Using this approach, we found that the *in vivo* hepatic uptake CL of rosuvastatin (RSV, an organic anion-transporting polypeptide (OATP) substrate), determined by PET imaging, was modestly underpredicted. But this underprediction was much less than when human hepatocytes were used (Kumar *et al.*, 2021). Similarly, others have reported drastic underprediction of hepatic uptake CL of OATP-substrates (Kim *et al.*, 2019; Francis *et al.*, 2021) using human

hepatocytes, though this approach has many flaws (see later for this discussion). One widely proposed reason for this underprediction is the lack of inclusion of plasma or plasma proteins in the *in vitro* uptake studies. Numerous report have shown that such inclusion increases the apparent intrinsic uptake clearance ($CL_{int,uptake}$) of OATP-substrate drugs by human hepatocytes and OATP-expressing cells (Miyauchi *et al.*, 2018; Bowman *et al.*, 2020). This phenomenon is called the protein-mediated uptake effect (PMUE) or albumin-facilitate uptake (Schulz *et al.*, 2023).

The first two aims of my dissertation investigated if the inclusion of human plasma proteins, when measuring uptake of statins by OATP1B1 cells **(Aim 1)** or human hepatocytes **(Aim 2)**, can explain the underprediction of the *in vivo* hepatic uptake CL of OATP-substrates (e.g., statins). The results of **Aim 1** (**Chapter 2**) showed that the observed PMUE on the uptake of statins by OATP1B1-expressing HEK293 cells (and mock cells) was largely an artifact of the residual statin-albumin complex remaining with the cells or labware when the uptake experiment is terminated. The residual albumin-statin complex was estimated by quantifying the residual albumin using quantitative targeted proteomics (QTP). This residual statin-albumin complex has not been quantified by others and therefore its presence has been erroneously interpreted as actual drug uptake resulting in the false conclusion of an apparent PMUE on statin uptake. Since human hepatocytes (plated or suspended) are widely used by researchers to measure OATP-mediated uptake of drugs, in **Aim 2** (**Chapter 3**), we investigated if the reported PMUE on statin uptake by human hepatocytes could also be explained by the residual statin-albumin complex. We hypothesized that if this apparent PMUE is indeed an artifact, it should be reduced when suspended hepatocytes are used. This is because when terminating uptake of drugs, the suspended hepatocytes are passaged through an oil layer potentially reducing the amount of residual statin-albumin complex remaining with the cells. Our hypothesis was found to be correct. The apparent PMUE on statins, when using human hepatocytes, was largely an artifact and was much reduced when the oil-spin method was used. Thus, mechanisms other than PMUE should be investigated for the underprediction of *in vivo* hepatic uptake CL of statins. However, before doing so, we investigated in **Aim 3** (**Chapter 4**) if such underprediction was true for all OATP-transported drugs or specific only to RSV.

The specific aims of my dissertation are:

Aim 1: To determine, using plated OATP1B1-expressing and mock HEK293 cells and QTP, if the observed PMUE on statins is largely confounded by the residual drug-protein complex.

Aim 2: To determine if the above observed PMUE is reproduced with plated human hepatocytes and if it is reduced or eliminated when using suspended (oil-spin) hepatocytes.

Aim 3: To extend the proteomics-informed REF approach to predict the human hepatobiliary CLs and hepatic concentrations of two other OATP-substrates, glyburide and pitavastatin. Then, to compare these predictions with their PET imaging data.

1.2 THE IMPORTANCE OF MEASURING OR PREDICTING TISSUE DRUG CONCENTRATIONS

Drug discovery is a lengthy, expensive process with a high attrition rate. Between the years 1996 to 2014, 90% of new molecular entities (NME) in phase 1 trials did not achieve market success (Smietana *et al.*, 2016). The primary reason for this attrition rate was lack of efficacy and safety. Among the small molecules, NMEs for the central nervous system exhibited an exceptionally high failure rate, also primarily due to insufficient efficacy (Hay *et al.*, 2014; Kesselheim *et al.*, 2015). One potential reason for this lack of efficacy is that insufficient concentrations of the drug were achieved at the site of action, along with other potential challenges of translating preclinical safety and efficacy to humans. The PD characteristics of an NME, such as efficacy or toxicity, are driven by its PK, both systemic and at the site of action, e.g., target tissue. Therefore, a clear understanding of the drug's *in vivo* disposition in both plasma and target tissues is essential.

During the drug development process, measuring or predicting the systemic PK of the drug is crucial to calculating the first in human dose and the quantitative impact of drug-drug interactions (DDIs), pharmacogenetics (PGx), disease, age, and other factors on the drug's PK. In addition, systemic PK drives the tissue PK. Thus, it is important to also predict a drug's systemic PK before its tissue PK can be successfully predicted.

However, there are circumstances where there is drug concentration disconnect between plasma and tissue. This discrepancy can arise due to involvement of active drug transporters or tissue metabolism. For many drugs, membrane transporters significantly affect not only their absorption and systemic clearance (CL), but also their distribution into tissues where their PD effects manifest (e.g., the brain and liver) (Niemi, 2010; Romaine *et al.*, 2010; Ke *et al.*, 2013; He *et al.*, 2014; Liu, 2019; Krishnan *et al.*, 2022). Take statin drugs for example, which are substrates of the hepatic uptake transporter OATPs. Statins primarily exert their lipid-lowering effects in the liver. Individuals with the SLCO1B1 c.521T>C single nucleotide polymorphism (SNP) have shown decreased OATP1B1 function. A data analysis of 16,660 patients taking 40 mg of simvastatin for 4–6 weeks revealed that the reduction in low-density lipoprotein cholesterol was 1.28% smaller per copy of the c.521C allele ($P<0.001$) (Link *et al.*, 2008). Hence, for these drugs that are active transporter substrates, besides determining the systemic PK, measuring or predicting the tissue PK of the drug is important to inform its efficacy and/or toxicity. This not only includes the drug's unbound average steady-state tissue concentrations but also its dynamic fluctuations in concentrations over a dosing interval. The methods for measuring or predicting drug tissue concentrations are discussed below.

1.3 TECHNIQUES USED FOR MEASURING TISSUE DRUG CONCENTRATIONS: EMPHASIS ON POSITRON EMISSION TOMOGRAPHY (PET)

Imaging techniques offer a noninvasive approach to measure tissue drug concentrations in humans. Several methods, including single photon emission computed tomography (SPECT), and positron emission tomography (PET), have been employed for this purpose (Mairinger *et al.*, 2022). Of these, PET stands out as a more sensitive and quantitative tool, which makes it particularly fitting for broader applications.

PET imaging requires drugs to be radiolabeled with positron-emitting radionuclides (Matthews *et al.*, 2012). The radiolabeled drugs (so-called radiotracers) are most commonly administered intravenously at a microdose and PET cameras are used to monitor the distribution of radioactivity into different tissues of the body over time with a temporal resolution in the order of minutes. Due to the possibility of correcting for tissue attenuation of the measured radioactivity, PET provides the absolute concentration of total radioactivity in tissue (*i.e.*

independent of its chemical form), typically quantified in kilobecquerels per gram tissue (kBq/g). Radioactivity concentration in tissue can be converted into mass concentration (e.g. nanogram per gram tissue) via the specific activity of the employed radiolabeled drug. Following quantification of tissue drug concentration-time profiles, these data can be further analyzed using pharmacokinetic modeling approaches to obtain distribution/elimination CL of the drug between different compartments (e.g. blood to liver, liver to bile) (Billington *et al.*, 2019).

There are several limitations of this technique: 1) This technique measures total radioactivity (drug plus any labeled metabolites) rather than that associated with only the drug in tissues. The inability to discriminate between the parent drug and its metabolite may provide misleading CL values (Langer, 2016). 2) This technique is able to measure only total drug concentration rather than unbound drug concentration. According to the free-drug hypothesis, only the unbound drug can exert pharmacological effect. Hence, the total tissue drug concentrations measured by PET imaging need to be corrected for the unbound fraction in the tissue homogenate or in the corresponding primary cell lysate, assuming these metrics reflect drug binding *in vivo*. 3) This technique cannot distinguish the amount of drug present in the blood within the tissue from that in the tissue itself (Hernández Lozano and Langer, 2020). For example, ~30% of liver volume is blood (Hwang *et al.*, 2002), which can significantly affect the estimation of actual hepatic concentrations (and for that matter, estimation of hepatobiliary CLs). In addition, PET imaging of hepatic drug concentrations cannot differentiate between drug in hepatic tissues from that in the bile ducts within the tissue (Wang *et al.*, 2021). 4) This technique presents technical and budgetary challenges which make it hard to employ routinely. Not all drugs can be radiolabeled for PET imaging. The most commonly used positron emitting radioisotopes decay with a relatively short half-life (e.g. 20 min for ^{11}C and 110 min for ^{18}F), which necessitates proximity between radiotracer production facilities and the PET scanner, ensuring injection occurs within a constrained timeframe (Langer, 2016). Due to the substantial cost, meticulous planning is crucial regarding study sample size, dose, and scan timings. In addition, due to the use of radioactivity, ethical concerns regarding the use of radiation constrains its use in vulnerable populations such as pregnant people (Matthews *et al.*, 2012).

While non-imaging techniques such as microdialysis are useful tools for tissue drug concentration measurement (Zhang *et al.*, 2019), their use is largely limited in humans to those tissues that are accessible (e.g. skin or muscle) or under special circumstances (e.g., when brain surgery is conducted) (Müller *et al.*, 1995; Stahl *et al.*, 2002).

1.4 APPROACHES USED TO PROSPECTIVELY PREDICT TISSUE DRUG CONCENTRATIONS

Given the technical and budgetary challenges associated with using imaging techniques to measure tissue drug concentrations in humans (**section 1.2**), predicting tissue drug concentrations using *preclinical* or *in silico* methods remains the only alternative. Over time, several approaches have been proposed to prospectively predict tissue drug concentrations.

1.4.1 *In vivo PK study*

For a drug that passively diffuses across the blood: tissue barrier, the unbound drug concentrations in plasma ($C_{u,p}$) have been traditionally used as a surrogate for unbound drug concentrations in tissues ($C_{u,t}$). This is generally true under two conditions: 1) the tissue has no active transport or metabolism, and 2) the sampling time of $C_{u,p}$ and $C_{u,t}$ is at true steady state after intravenous continuous infusion. However, the presence of active transporters or drug metabolism within the tissue can create asymmetry in unbound drug concentrations between tissues and plasma including at steady state . Thus, under these circumstances $C_{u,p}$ will not serve as a good predictive surrogate of $C_{u,t}$.

1.4.2 *Animal data and preclinical-to-human scaling*

Tissue drug concentrations can be readily measured in animals, enabling preclinical-to-human scaling to predict drug distribution in humans. This approach obviously requires sacrificing the animals, so time-course data are often limited to predict tissue -to-plasma drug concentration ratios (Kp). Moreover, this approach of predicting

tissue Kp is fraught with interspecies differences in protein abundance, catalytic activity and substrate selectivity of the transporters and metabolic enzymes that determine the PK of a drug (Walker *et al.*, 2017).

1.4.3 *In vitro to in vivo extrapolation (IVIVE) of drug CLs and tissue drug concentrations*

The tissue drug concentrations are determined by the clearance (CL) pathways that mediate drug's entry into and exit (including metabolism) from the tissue. Here, we are relying on the well-stirred hepatic model for the liver tissue drug concentration discussion, while other hepatic models such as series compartment model may have different considerations (Li and Jusko, 2022, 2023). Taking liver as an example, the hepatic concentrations of any drug that distributes into and then is eliminated by the liver are determined by all hepatobiliary CLs, namely sinusoidal influx ($CL_{s,uptake}$), sinusoidal efflux ($CL_{s,efflux}$), biliary (CL_{bile}), and metabolic CL (CL_{met}). Therefore, one can first predict these *in vivo* CLs through *in vitro* systems and scaling factors (more details in **section 1.5**) and then incorporate the predicted *in vivo* CLs into the compartmental or PBPK model to predict tissue drug concentrations (**Fig 1.1**). While IVIVE of metabolic CL has been successful, such success remains a challenge for a drug that is transported. Given this, the discussion below is focused on how to accurately predict transporter-based CLs and drug concentrations in the tissue of interest (e.g. liver). To do so, transport-mediated CLs of a drug are measured *in vitro* (e.g. primary cells, TECs or TEVs), and activity/abundance/physiological scaling factors are employed to extrapolate these *in vitro* CLs to *in vivo* (IVIVE). Then these *in vivo* CLs are incorporated into a compartmental or PBPK model to predict tissue drug concentrations.

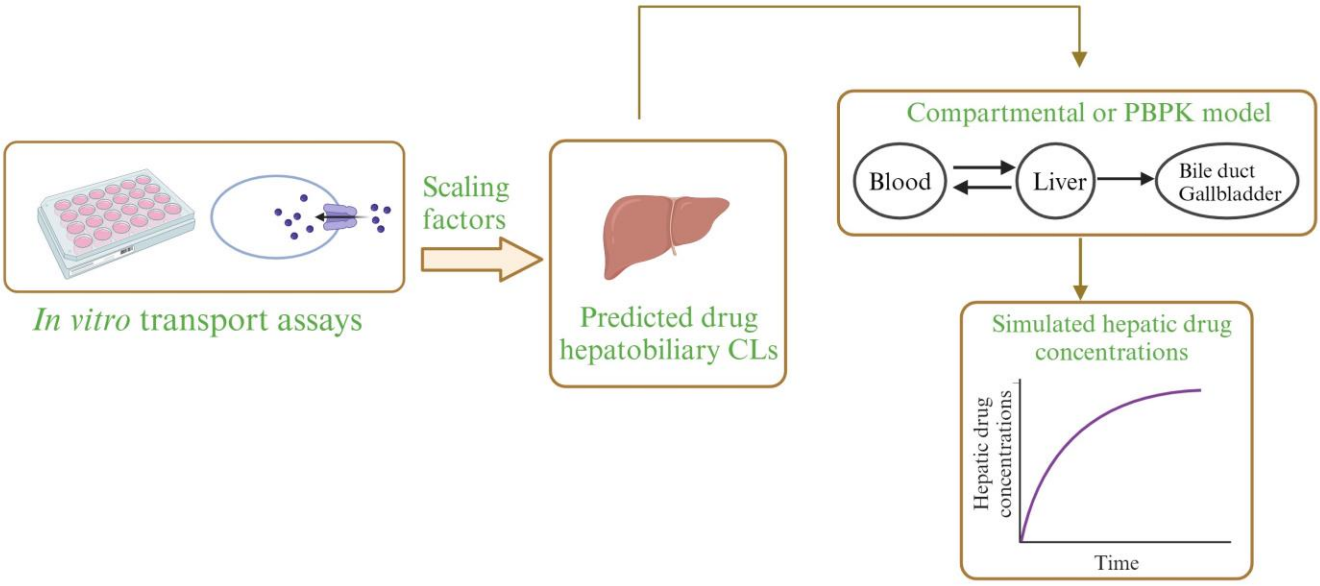

Figure 1.1. Schematic of the IVIVE approaches to predict drug CL and tissue drug concentrations.

Taking liver as an example, the *in vivo* hepatobiliary CLs are predicted through *in vitro* models (e.g. hepatocytes or TECs/TEVs) and scaling factors (see details in **section 1.5** below) and the *in vivo* hepatobiliary CLs are incorporated into a compartmental or PBPK model to predict hepatic drug concentrations.

1.4.4 *Approaches to retrospectively verify the predicted tissue drug concentrations*

To evaluate the performance of the aforementioned approaches, they must be verified using either PET imaging data (Billington *et al.*, 2019) or PD outcomes (*i.e.*, efficacy and toxicity observations or PD biomarkers). For example, rosuvastatin (RSV), a 3-hydroxy-3-methylglutaryl-CoA reductase inhibitor, inhibits the conversion of acetyl-CoA to mevalonic acid (MVA) – a pivotal step in hepatic cholesterol synthesis. Thus, the unbound hepatic RSV concentrations are crucial in determining its efficacy in reducing cholesterol concentrations. A PBPK/PD model for RSV developed by Rose *et al.*, established a correlation between predicted hepatic RSV concentrations and its PD response (based on plasma MVA concentrations). Simulations revealed that the impact of OATP1B1 genotypes on RSV's PD was consistent with hepatic RSV concentrations rather than plasma RSV concentrations (Rose *et al.*, 2014). This highlights the potential of using PD biomarkers to verify the prediction of tissue drug concentration, especially when there is a significant disconnect between plasma and tissue drug concentrations.

1.5 IN VITRO MODELS AND SCALING FACTORS FOR IVIVE OF TRANSPORTER-MEDIATED CLS

1.5.1 *Primary cells and physiological scaling factors (PSF)*

The *in vivo* intrinsic uptake or efflux CL ($CL_{int,in\ vivo}$) of a drug can be predicted by scaling its *in vitro* intrinsic uptake or efflux CL ($CL_{int,in\ vitro}$), quantified using primary cells, by a physiological scaling factor (PSF). The PSF includes the number of cells in the tissue of interest or the membrane/total protein content (*i.e.* mg membrane/total protein or number of cells per gram of tissue) (**Fig 1.2**).

$$CL_{int,in\ vivo} = CL_{int,in\ vitro} \times PSF \qquad Eq.\ 1.1$$

Due to its straightforward implementation and ready availability of human hepatocytes, PSF is the preferred method for IVIVE of hepatic uptake/efflux CL during drug development. However, primary human cells from other organs important in drug distribution (e.g. BBB), elimination (e.g. kidneys) or absorption (e.g. intestines) are not readily available or verified. Also, the primary cells and PSF approach assumes that the transporter activity/abundance *in vitro* (in the primary cells) is the same as that *in vivo*, which may not be the case (Kumar *et al.*, 2019). Transporter activity/abundance can differ between primary cells and organ of origin (due to the isolation process, cryopreservation and culture time/conditions). For example, total and plasma membrane abundance of biliary efflux transporters is dramatically increased in sandwich-cultured human hepatocytes (SCHH) compared to the liver tissue from which the hepatocytes are isolated (Kumar *et al.*, 2019). Moreover, human hepatocyte and PSF approach underpredicts transporter-based hepatic *in vivo* uptake CL of OATP-substrates (Jones *et al.*, 2012; Kumar *et al.*, 2021). Therefore, alternative approaches, such as relative activity factor (RAF) or relative expression factor (REF) need to be explored.

1.5.2 *Relative activity factor (RAF)*

There are two relative activity factor (RAF) approaches: $RAF_{in\ vivo}$ and $RAF_{in\ vitro}$, which are discussed in detail in our recent review (Storelli, Yin, *et al.*, 2022). Briefly, the $RAF_{in\ vivo}$ relies on the availability of data on CL of

a probe drug, that is mediated by a single transporter, both *in vitro* (in primary cells or in transporter-transfected cells) and *in vivo* (Mathialagan *et al.*, 2017). If such a probe drug is available, the ratio of its intrinsic uptake or efflux CL *in vitro vs. in vivo*, yields the $RAF_{in\ vivo}$ value (**Fig 1.2**):

$$RAF_{in\ vivo} = \frac{CL_{int,in\ vivo,probe}}{CL_{int,in\ vitro,probe}} \qquad Eq.\ 1.2$$

Then, the *in vitro* CL_{int} of drug X transported by the same transporter as the probe drug, can be scaled to *in vivo* as follows:

$$CL_{int,in\ vivo} = CL_{int,in\ vitro} \times RAF_{in\ vivo} \qquad Eq.\ 1.3$$

One advantage of $RAF_{in\ vivo}$ approach is that it does not require the use of PSF (**Fig 1.2**). However, such selective transporter probes are rarely available. In that event, an alternative scalar, $RAF_{in\ vitro}$, can be used (Mitra *et al.*, 2018):

$$RAF_{in\ vitro,i} = \frac{CL_{int,in\ vitro,probe,primary\ cells,i}}{CL_{int,in\ vitro,probe,transfected\ cells,i}} \qquad Eq.\ 1.4$$

Briefly, the active $CL_{int,in\ vitro}$ of the probe drug through the ith transporter is calculated using both transporter-transfected cells and hepatocytes, resulting in the $RAF_{in\ vitro}$ for each transporter. Then, for drug X, its active $CL_{int,in\ vitro}$ for each transporter is scaled with the corresponding $RAF_{in\ vitro}$ value and summed. This summed value, plus the *in vitro* passive diffusion ($CL_{int,pd,in\ vitro}$) of drug X, can then be scaled to obtain $CL_{int,in\ vivo}$ using a PSF (Eq. 1.5)

$$CL_{int,in\ vivo} = (\left[\sum_{i=1}^{n} CL_{int,in\ vitro,i} \times RAF_{in\ vitro,i}\right] + CL_{int,pd,in\ vitro}) \times PSF \qquad Eq.\ 1.5$$

Similar to the PSF approach, the use of $RAF_{in\ vitro}$ requires the availability of primary cells and assumes that the transport activity *in vitro* in the hepatocytes is identical to that *in vivo*.

For both RAF approaches, either the passive CL_{int} of the probe substrate is assumed to be negligible or the ratio of the *in vitro* passive and active CL_{int} of drug X and the probe drug is assumed to be identical.

1.5.3 *Proteomics-informed relative expression factor (REF)*

With the emergence of quantitative targeted proteomics (QTP) and availability of transporter abundance data *in vivo*, the REF approach has recently gained a lot of attention (Storelli, Yin, *et al.*, 2022). The CL_{int} via a transporter is defined as the ratio of J_{max} over K_m (when the drug concentration is < K_m). J_{max} represents the product of transporter turnover rate (k_{cat}; rate at which substrates are actively translocated across the cell membrane) and transporter abundance. The REF approach assumes that the difference in transporter activity *in vitro vs. in vivo* is predominantly attributed to the difference in transporter abundance, and that K_m and k_{cat} are identical *in vitro* and *in vivo*. Therefore, transporter-based CL_{int} can be scaled from *in vitro* to *in vivo* using the REF:

$$CL_{int,in\ vivo,active} = \sum_{i=1}^{n} CL_{int,in\ vitro,active,i} \times REF_i \qquad Eq.\ 1.6$$

$$REF_i = \frac{[Transporter]_{tissue,i}}{[Transporter]_{in\ vitro,i}} \qquad Eq.\ 1.7$$

where $[Transporter]_{tissue,i}$ and $[Transporter]_{in\ vitro,i}$ are the abundance of the i^{th} transporter in human tissue and the *in vitro* model, respectively. Therefore, REF requires measurement of transporter abundance for each transporter of interest, in both the *in vitro* system and in the tissue of interest.

In contrast to the RAF approach, the REF approach is capable of handling multiple drug transporters because transporter-expressing cells or vesicles (TECs/TEVs) can be used (**Fig 1.2**). This is particularly advantageous for tissues where primary cells are unavailable (e.g. BBB, kidney, intestinal enterocytes). In addition, TECs/TEVs are more accessible, reproducible, higher throughput and cost-effective.

In comparison to the RAF method, the REF approach offers more flexibility. It is not limited by the need for selective probe substrates. The REF method can also be applied to multiple organs provided transporter abundances are available. But, the REF approach can be applied only if the transporters of interest can be quantified in the human tissue of interest.

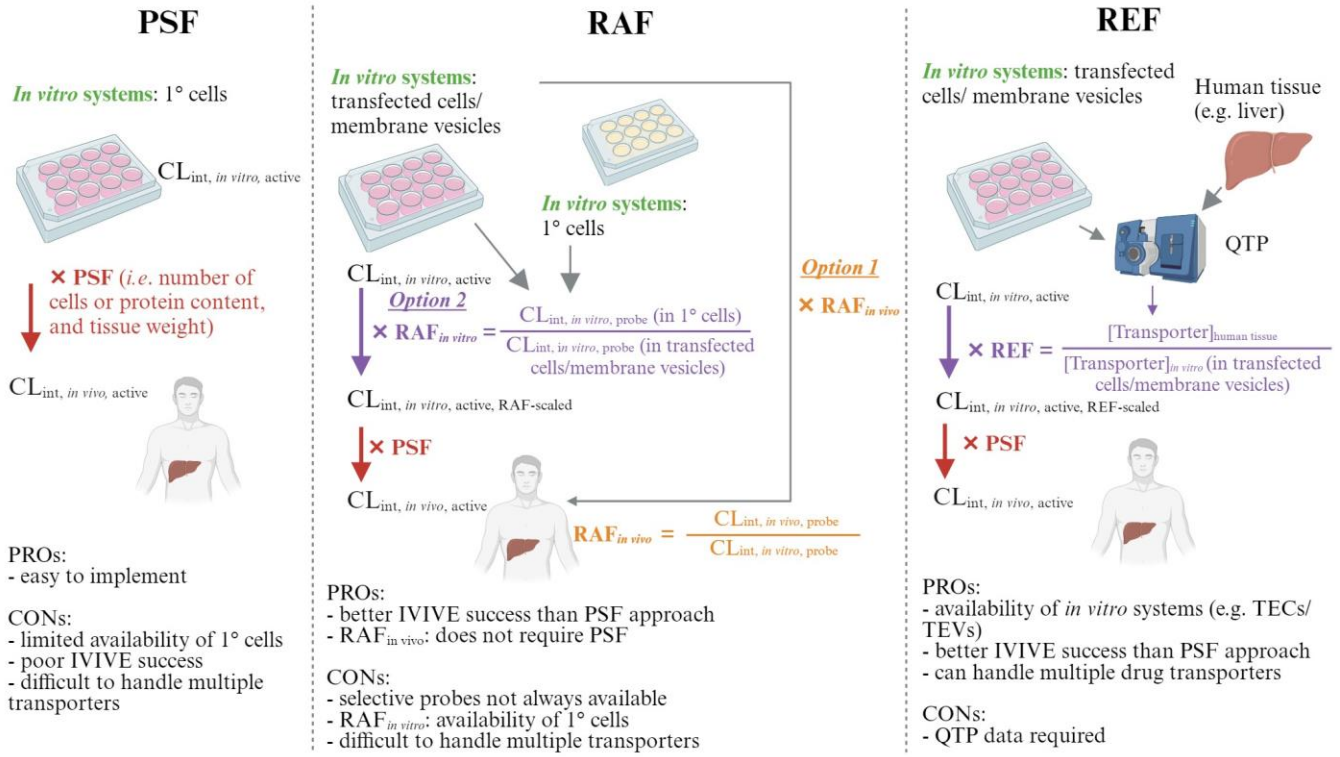

Figure 1.2. Schematic framework and pros and cons of different scaling approaches for IVIVE of transporter-mediated CL.

1°, primary; $CL_{int,in\ vitro,active}$, *in vitro* active intrinsic CL; $CL_{int,in\ vitro,active,RAF\text{-}scaled}$ or $CL_{int,in\ vitro,active,REF\text{-}scaled}$ *in vitro* active intrinsic CL scaled by RAF or REF; $CL_{int,in\ vitro\ probe}$, *in vitro* intrinsic CL of the probe substrate; $CL_{int,in\ vivo\ probe}$, *in vivo* intrinsic CL of the probe substrate used for the RAF approach; PSF, physiological scaling factor; QTP, quantitative targeted proteomics; RAF, relative activity factor; REF, relative expression factor. Figure was adapted from (Storelli, Yin, *et al.*, 2022).

Using this promising approach, we have successfully predicted *in vivo* metformin hepatic uptake CL, RSV biliary efflux CL and the brain and fetal exposure of several transported substrates (Sachar *et al.*, 2020; Anoshchenko *et al.*, 2021; Storelli *et al.*, 2021; Storelli, Li, *et al.*, 2022). However, we found that the TECs/TEVs/REF approach marginally underpredicted RSV hepatic uptake CL and hepatic concentrations (fell at the bottom of our acceptance criterion *i.e.* 2-fold range). In contrast, the SCHH (using the PSF) underpredicted these values to a much greater extent because SCHH underestimated the RSV sinusoidal uptake CLs and overestimated the biliary efflux CLs (Storelli, Li, *et al.*, 2022).

Underprediction of the OATPs-mediated hepatic uptake CL, using PSF, is common and often drastic (Jones *et al.*, 2012; Wood *et al.*, 2017; Kim *et al.*, 2019). One reason for such underprediction could be that the *in vitro*

hepatocyte uptake studies do not include blood constituents (e.g. plasma proteins) that may modulate OATP-mediated uptake of drugs. Indeed, when plasma or plasma proteins (e.g. human serum albumin, HSA) are included in the *in vitro* uptake assays, the *in vitro* intrinsic uptake CL ($CL_{int,uptake)}$ of highly protein-bound OATP substrates (e.g. statins), by human hepatocytes or OATP-expressing cells, is enhanced (Bowman *et al.*, 2019, 2020). This phenomenon called the "protein-mediated uptake effect (PMUE)" is widely believed to be responsible for the underprediction of OATP-mediated hepatic uptake CL using human hepatocytes and PSF (Francis *et al.*, 2021). Therefore, two of the three specific aims of this dissertation are focused on determining if this PMUE is a real phenomenon and whether it can improve the performance of IVIVE of hepatic uptake CL of OATP substrates (e.g., RSV). For these reasons, this phenomenon and its potential mechanisms are described in detail below.

1.6 PROTEIN-MEDIATED UPTAKE EFFECT (PMUE)

The concept of protein-mediated hepatic uptake (PMUE, also called "albumin-facilitated uptake") describes the phenomenon that highly protein-bound compounds have more efficient hepatic uptake than that accounted for by their unbound concentrations determined *in vitro*. During 1980s, several single-pass isolated perfused rat liver (IPRL) studies conducted with diverse compounds, such as taurocholate (Forker and Luxon, 1981), oleate (Weisiger and Ma, 1987), and warfarin (Tsao *et al.*, 1988), demonstrated the aforementioned albumin-facilitated uptake process. Taking the taurocholate study as an example, when the perfusate bovine serum albumin (BSA) concentration was 0.5 g/dL, the perfused rat liver removed 97% of the taurocholate from the afferent circulation. However, a 10-fold increase in BSA concentration (5 g/dL) decreased the unbound taurocholate concentration by 81% but produced only a 50% reduction in the apparent taurocholate uptake rate (Fig.1.3, adapted from (Forker and Luxon, 1981)). This suggests that uptake was not solely determined by unbound taurocholate concentration; bound taurocholate seemed to also play a significant role.

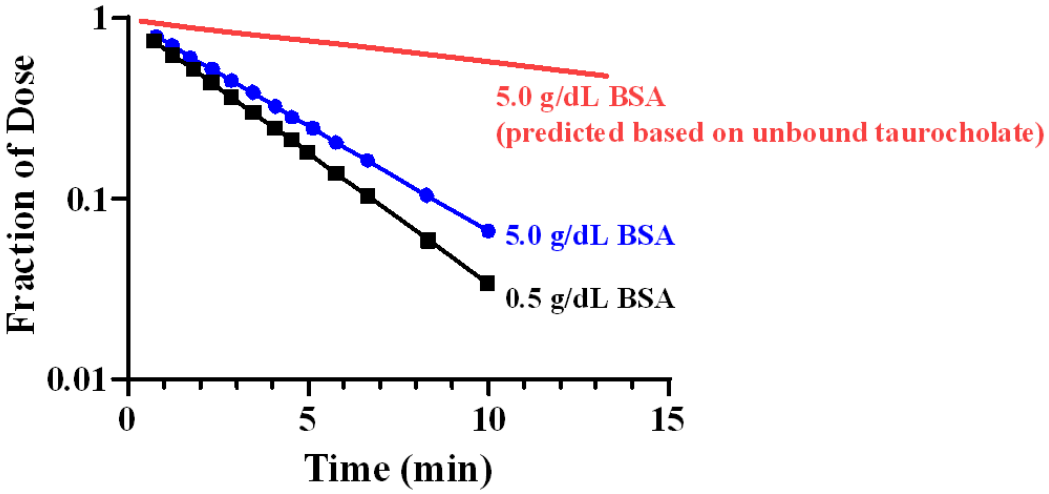

Figure 1.3. Representative taurocholate disappearance from the afferent circulation when the perfusate BSA concentration was 0.5 g/dl and 5.0 g/dl (Adapted from (Forker and Luxon, 1981)).

The solid red line represents the predicted result for 5.0 g/dl BSA based on the assumption that uptake is determined by only the unbound taurocholate perfusate concentration.

More recently it has been noted that as fraction unbound in plasma ($f_{u,p}$) decreases, underprediction of hepatic CL with primary cells and PSF increases (Baker and Parton, 2007). Furthermore, recent studies from both us and others have shown that, when conducting *in vitro* uptake studies, adding plasma or albumin to hepatocytes or transporter-expressing cells can result in an increased observed $CL_{int,uptake}$, thereby improving the IVIVE performance of hepatic CL (Liang *et al.*, 2020; Bi *et al.*, 2021; Kumar *et al.*, 2021). Based on the *ex vivo* and *in vitro* observations, multiple mechanisms to explain the PMUE, primarily for hepatic uptake of drugs, have been postulated. These potential mechanisms are summarized below.

1.6.1 *Potential PMUE mechanisms*

In general, the proposed mechanisms for PMUE can be broadly classified into three categories. That is the presence of plasma or plasma proteins results in:

1) **Increased local unbound drug concentration ($C_{u,local}$)**, which results from specific or non-specific interactions between plasma proteins and receptors or cell membranes. If this mechanism holds true, one should observe an equal increase in both active and passive uptake of drugs in *in vitro* uptake assays in

the presence of plasma protein. In addition, the PMUE should be greater for compounds with greater degree of protein-binding.

2) **Increased transporter-mediated intrinsic uptake CL ($CL_{int,uptake}$) of the drug**, which is due to the interplay (e.g. allosterisim) between plasma proteins (or soluble endogenous factors in plasma) and transporters. If this mechanism holds true, one should observe an increase in transporter-mediated (not passive) $CL_{int,uptake}$ in *in vitro* uptake assays. In addition, the PMUE should be greater for compounds with larger fraction transported (ft) relative to the total uptake.
3) **Endocytosis of the drug-protein complex**. If this mechanism holds true, the increased drug uptake should be comparable to endocytosis kinetics. In addition, the PMUE should be greater for compounds with greater protein-binding.

1.6.1.1 Increased local unbound drug concentration ($C_{u,local}$)

1.6.1.1.1 Hepatocyte surface albumin receptor hypothesis

One of the earliest hypotheses to explain PMUE proposed the presence of a specific albumin-receptor on the hepatocyte cell surface (Weisiger *et al.*, 1981). When the drug-albumin complex binds to the albumin receptor, it will trigger drug dissociation. Thus, the $C_{u,local}$ of drug increases resulting in greater amount of drug being taken up into the hepatocytes.

Oleate was one of the first ligands used to suggest this mechanism (Weisiger *et al.*, 1981). Using single pass isolated perfused rat liver (IPRL), when increasing ^{14}C-oleate concentration but keeping bovine serum albumin (BSA) concentration constant in the perfusate, hepatic oleate uptake increased linearly relative to total oleate concentration but nonlinearly relative to the unbound oleate concentration. This suggests that both unbound oleate and bound oleate can be taken up by the liver. Then, ^{125}I-albumin was used to evaluate the possibility of albumin binding to hepatocytes and there appeared to be a single high-affinity binding site specific for albumin. This binding was hypothesized to trigger the release of the drug from the drug-albumin complex and increase the $C_{u,local}$ of the drug (Weisiger *et al.*, 1981).

While the albumin receptor hypothesis provides a compelling narrative, subsequent research has cast doubt over its applicability to other drugs. First, the specific albumin receptor theory would not be able to account for the enhanced CL seen for compounds in the presence of β-lactoglobulin to which they bind (Nunes *et al.*, 1988; Burczynski *et al.*, 2001). Second, Weisiger *et al.* demonstrated that exogenously administered albumin facilitated the uptake of (bromosulphophthalein) BSP in perfused skate livers even though skates lack albumin (Weisiger *et al.*, 1984). Third, using affinity chromatography, researchers failed to identify any solubilized membrane proteins on albumin-agarose gels (Stremmel *et al.*, 1983). Collectively, these findings challenge the validity of the albumin receptor hypothesis to explain the PMUE.

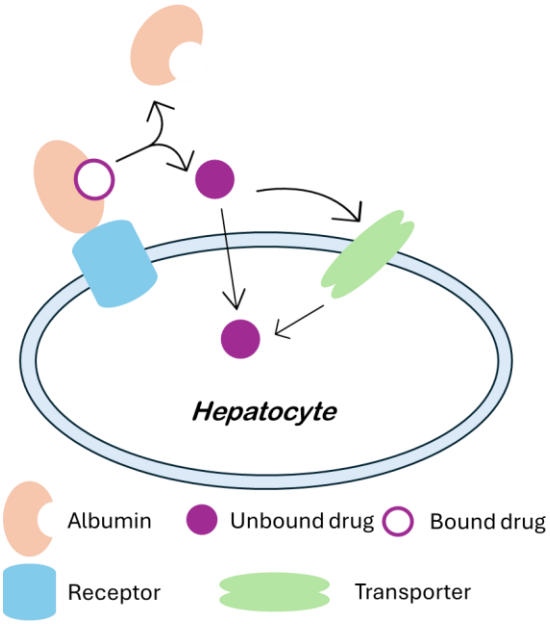

Figure 1.4. Albumin receptor hypothesis.

Drug-albumin complex binds to a specific albumin receptor on the hepatocyte surface, triggering drug dissociation and uptake into hepatocytes.

1.6.1.1.2 Facilitated dissociation mechanism

Recently, attention has been redirected to more general interactions between hepatocyte cell surface and the drug-protein complex. The plasma membrane of polarized hepatocytes is rich in negatively charged acidic and zwitterionic phospholipids (Burczynski *et al.*, 2001). Therefore, in the space of Disse, the charged residues on the surface of albumin should favor strong ionic forces binding the plasma protein to these phospholipids (**Fig 1.5**). According to the facilitated dissociation mechanism, these electrostatic attractions will reduce the

diffusional distance for the drug-protein complex and cause conformational changes of both protein and phospholipid headgroups. Therefore, the dissociation of the drug from albumin and the $C_{u,local}$ of drug will increase.

Horie *et al.* utilized absorption and electron spin resonance spectroscopy to show that albumin undergoes conformational change when interacting with hepatocyte membranes, potentially impacting protein binding (Horie *et al.*, 1988). Further evidence supporting the facilitated dissociation mechanism emerged from experiments involving modified albumin. Van der Sluijs *et al.* examined the hepatic uptake of BSP using lactosylated albumin. Compared to albumin, this protein modification decreased the hepatic uptake of BSP, despite the unbound fraction (f_u) remaining largely unchanged. This effect was attributed to a significant reduction in the BSP dissociation rate constant (k_{off}) when bound to lactosylated albumin (Sluijs *et al.*, 1987).

Recently, Miyauchi *et al.* revisited a previously developed Facilitated Dissociation Model (FDM) by Tsao *et al.* (Tsao *et al.*, 1988) to predict the *in vivo* $CL_{int,uptake}$ from *in vitro* data (Miyauchi *et al.*, 2018, 2021). According to FDM, the uptake of highly albumin-bound drugs can occur not only from the unbound drug in the space of Disse (where the equilibrium with the drug-protein complex is governed by the dissociation equilibrium constant K_D), but also from the additional amount of the drug dissociated from the drug-protein complex at the hepatocyte surface. The intrinsic (unbound) uptake CL in the presence of protein ($CL_{int,uptake}(+)$) and the apparent (total) uptake CL ($CL_{app,uptake}$) in the presence of protein is described below (Miyauchi *et al.*, 2018, 2022):

$$CL_{app,uptake} = fu \times CL_{int,uptake}(+) = \frac{K_D}{K_D+[Alb]} \times (CL_{int,uptake}(-) + \frac{CL_{bound,uptake} \times B_{max} \times \frac{[Alb]}{K_D}}{K_{D,m}+[Alb]}) =$$

$$\frac{K_D}{K_D+[Alb]} \times CL_{int,uptake}(-) \times (1 + \frac{\frac{CL_{bound,uptake} \times B_{max} \times [Alb]}{CL_{int,uptake}(-)}}{K_D \times (K_{D,m}+[Alb])}) \qquad \textit{Eq. 1.8}$$

$CL_{int,uptake}(+)$ and $CL_{int,uptake}(-)$ represent the intrinsic (unbound) uptake CL in the presence/absence of plasma protein, respectively; $CL_{bound,uptake}$ represents the uptake CL of the additional amount of the unbound drug dissociated from the drug-albumin complex due to the conformational change at the hepatocyte cells surface;

K_D represents drug dissociation constant; B_{max} is the hepatocyte surface binding capacity; $K_{D,m}$ is the dissociation constant of the protein (unbound protein or drug-bound protein) from the hepatocyte surface.

Miyauchi *et al.* later determined that the value of $\frac{CL_{bound,uptake} \times B_{max}}{CL_{int,uptake}(-)}$ (defined as Extent of Facilitated Dissociation, EFD) was 11 μM by fitting **Eq. 1.8** to the previously obtained hepatocyte uptake data for 10 OATP1B substrates at different HSA concentrations (Kim *et al.*, 2019; Miyauchi *et al.*, 2022). They concluded that this EFD is a drug-independent parameter and can be applied in the future to estimate the $CL_{app,uptake}$ of drugs in the presence of HSA. In addition, Miyauchi *et al.* fixed $K_{D,m}$ as 46 μM, assuming the dissociation constant of protein from the hepatocyte surface is drug-independent. As a result, to estimate $CL_{app,uptake}$ and employ it to predict *in vivo* hepatic uptake CL, one only needs to obtain $CL_{int,uptake}$ (-) and K_D, which can be determined experimentally (Miyauchi *et al.*, 2022).

Although this approach is considered to be plausible and simple, there are concerns about the assumptions, particularly whether EFD and $K_{D,m}$ are truly compound-independent: 1) the EFD determined by other investigators for 19 OATP-substrates was ~5.2 μM (Bi *et al.*, 2021), only half of the EFD proposed by Miyauchi *et al.* (Miyauchi *et al.*, 2022); 2). In Miyauchi's earlier study, $K_{D,m}$ values were found to be 24.4 μM for 1-anilino-8-naphthalene sulfonate (ANS) and 199 μM for pitavastatin, both differ considerably from the proposed 46 μM (Miyauchi *et al.*, 2018; Kim *et al.*, 2019). Also, when incorporating the $CL_{app,int}$ in the presence of 5% HSA into the IVIVE of 10 OATP substrates, their hepatic uptake CL was underestimated, and a scaling factor of 2.44 was required to ensure predictions for all 10 OATP substrates fell within 5-fold of their *in vivo* values (Kim *et al.*, 2019). This suggests that the PMUE is not able to entirely bridge the IVIVE discrepancy.

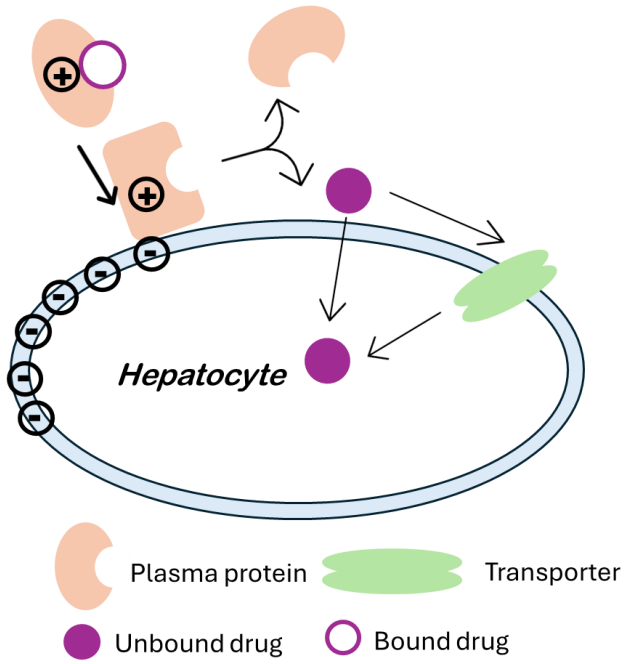

Figure 1.5. The facilitated-dissociation mechanism hypothesis.

Interaction of the drug-protein complex with the plasma membrane induces a conformational change in the protein. The conformational change affects the structure of the binding pocket and decreases the affinity of the drug to the protein. As a result, the drug is released directly at the hepatocyte surface, where hepatic uptake can occur.

1.6.1.2 Increased transporter-mediated $CL_{int,uptake}$

1.6.1.2 Transporter induced protein binding shift (TIPBS)

Most recently, Bowman *et al.* proposed a transporter-induced protein-binding shift (TIPBS) as a mechanism of PMUE (Bowman *et al.*, 2019, 2020). Many of the earlier hypotheses were developed before the transporter field emerged. The consistently poor IVIVE predictions were observed for compounds that are substrates of transporters and exhibit high protein binding (Soars, Grime, *et al.*, 2007; Kumar *et al.*, 2021). The TIPBS hypothesis posits that, the high affinity binding of the drug to membrane transporters such as OATPs, may be able to change the equilibrium of the binding between the drug and plasma protein. If a highly protein-bound drug has a greater affinity for a transporter compared to the protein, the transporter will "pull" the drug from the protein before the drug can naturally dissociate from the protein and reach a binding equilibrium (**Fig 1.6**). Under this circumstance, in the presence of proteins, the measured unbound K_m for the transporter will decrease, and thus the apparent transporter-mediated $CL_{int,uptake}$ will increase. Supporting this hypothesis, using statins (known as OATPs substrates) and plasma, Bowman *et al.* demonstrated an increase in drug affinity (decrease in measured unbound K_m) and therefore an increase in $CL_{int,uptake}$ in both suspended human hepatocytes and plated OATP1B1- and OATP1B3-expressing HEK293 cells (Bowman *et al.*, 2019, 2020).

TIPBS is plausible since most transporter substrates have higher affinity for the transporter (K_m) than plasma proteins (K_D). Additionally, the observed PMUE is less prominent for compounds like repaglinide, which have a smaller active uptake component (Bowman *et al.*, 2019). Of note, the fundamental basis of TIPBS is the interaction between the protein, drug, and the transporter, implying that only transporter-mediated uptake (and not passive diffusion) should be influenced. Additionally, the TIPBS-based PMUE should be only observed on drugs with high hepatic extraction. However, several observations are inconsistent with TIPBS. Bowman *et al.* noted an increase in passive diffusion of drugs, into both hepatocytes and cells expressing OATPs-, in the presence of plasma proteins (Bowman *et al.*, 2019, 2021). Also, in their studies, they noticed a decrease in J_{max} which could not be explained by TIPBS. Others have identified hepatic PMUE on compounds that are not transporter-substrates, like tolbutamide and midazolam (Bi *et al.*, 2021). Furthermore, drugs like PTV, which demonstrate PMUE, do not fall in the high extraction ratio category (Bowman *et al.*, 2019, 2020). Collectively, TIPBS alone cannot fully explain the PMUE phenomenon.

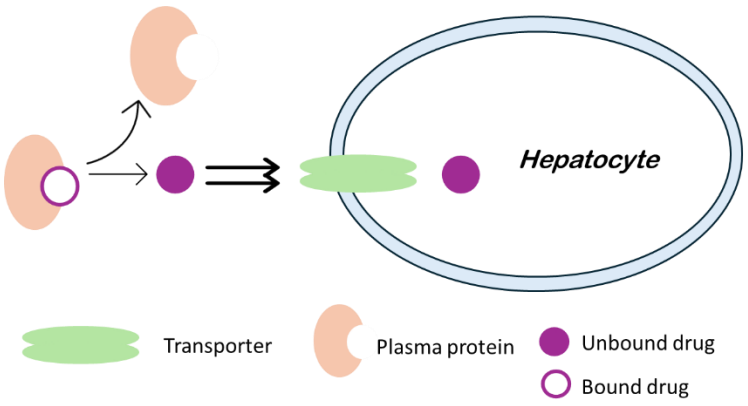

Figure 1.6. Transporter induced protein binding shift (TIPBS).

Due to the high affinity of the substrate for the uptake transporter, transporters can directly strip drugs from plasma protein.

1.6.1.3 Allosteric effect and substrate channeling

Several other hypotheses have been proposed to explain the PMUE, including allosteric effect, and substrate channeling. For example, OATPs are known to be allosteric (Kindla *et al.*, 2011). It is possible that proteins or endogenous factors in the plasma that bind to the OATP transporters, could cause a conformational change of OATPs and increase their transport efficiency. Parenthetically we note here that in preliminary experiments, plasma water did not affect the uptake of RSV by OATP1B1-expressing cells. Another possible mechanism is

substrate channeling. In this scenario, the plasma protein could directly channel the drug to membrane transporters. Such protein-protein interactions may potentially influence the observed kinetic parameters of the transporter, such as K_m and V_{max}. These measured parameters would represent a combination of both the free drug's interaction with the transporter and the bound drugs' interaction with the transporter. However, while substrate channeling has been observed between intracellular proteins, such as cellular retinoic acid-binding protein (Nelson *et al.*, 2016; Yabut and Isoherranen, 2022), it remains unclear whether similar interactions would occur between plasma drug binding proteins (e.g., albumin) and membrane drug transporters (e.g., OATPs). Given the lack of in-depth experimental investigations to support these mechanisms in the context of PMUE, they are not further discussed here. Nonetheless, they should be re-examined if experimental evidence emerges to support or refute these hypotheses.

1.6.1.4 Endocytosis

Epithelial cells such as kidney or intestine epithelial cells can internalize, by endocytosis, large molecules like inulin or dextran (Doherty and McMahon, 2009). Therefore, the PMUE could be due to endocytosis, *i.e.*, the drug-albumin complex could enter the hepatocytes via receptor-mediated endocytosis or non-specific pinocytosis (**Fig 1.7**). For hepatocytes, a plausible participant in such a receptor-driven process is the neonatal Fc receptor (FcRn) (Baker and Bradley, 1966; Sand *et al.*, 2015). Evidence supporting this hypothesis is lacking. It is also worth noting that while albumin binds to FcRn under acidic pH conditions within early endosomes, the complex subsequent recycles to the cell surface, where its binding affinity to albumin diminishes because of the rise in pH. These data suggests that the FcRn's role is in recycling albumin rather than facilitating its uptake (Sand *et al.*, 2015). Also, the uptake rates of large solutes through endocytosis are typically much slower than the uptake clearance rates by transporters. The reported hepatic endocytosis rate is limited to 0.008 ml/min/mg protein (approximately 0.007 ml/min/10^6 cells; (Scharschmidt *et al.*, 1986)). However, the reported rate of the increase in hepatic uptake in the presence of plasma proteins (> 6 ml/min/10^6 cells) is more than 800-fold of the albumin endocytosis rate (Scharschmidt *et al.*, 1986; Francis *et al.*, 2021). Consequently, endocytosis as a primary mechanism of the PMUE appears to be kinetically inconsistent with the observed PMUE.

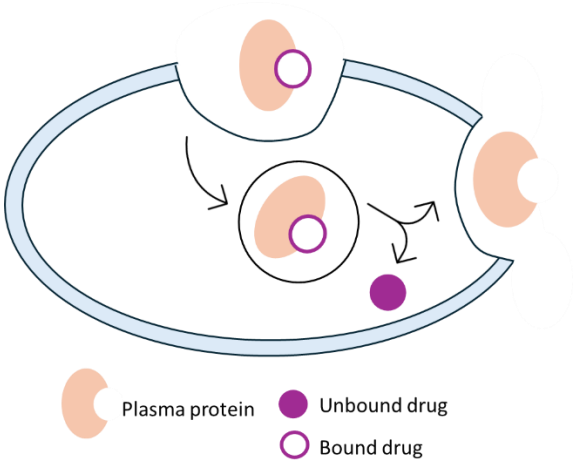

Figure 1.7. Endocytosis.

The drug-protein complex enters hepatocytes via endocytosis. In the cytosol, the drug is released, while the plasma protein is recycled to the extracellular space.

Table 1.1. Overview of hypotheses to explain the observed PMUE on drug uptake by hepatocytes

Hypothesis	**Expected observations**	**Experimental approach to test the hypothesis**	**Caveats**
Albumin-receptor hypothesis	The PMUE should be observed only with albumin; both active and passive uptake should increase to the same extent in the presence of albumin	Evaluate the PMUE on both passive and active uptake of drugs; Investigate the PMUE using other plasma proteins such as α-1-acid-glycoprotein 1 (AAG); Conduct parallel artificial membrane permeability assay (PAMPA) with/without plasma proteins	Presence of albumin receptor on hepatocytes cell surface has not been confirmed; PMUE is observed with proteins other than albumin; The observed PMUE on drug passive uptake ≠ active uptake
Facilitated Dissociation Mechanism	Both active and passive uptake should increase to the same extent in the presence of plasma proteins	Evaluate PMUE on both passive and active uptake of drugs Experiments comparing mobile and immobilized plasma proteins to determine whether PMUE requires direct contact between plasma proteins and the hepatocyte surface	The observed PMUE on drug passive uptake ≠ active uptake
TIPBS	PMUE should be observed only on active uptake of high extraction ratio drugs; binding affinity for the transporter should be higher than for plasma proteins	Evaluate PMUE on both low and high extraction ratio drugs as well those not transported	The PMUE has been observed on passive uptake and low extraction ratio drugs; PMUE has been observed for non-transported drugs such as midazolam
Endocytosis	The increase in rate of drug uptake in the presence of plasma proteins should be similar to the rate of endocytosis of the drug-protein complex	Imaging methods to quantify the movement of drug-albumin complex across the hepatocyte membrane	Kinetically implausible – hepatocyte albumin endocytic clearance is much smaller than the observed PMUE on hepatic drug uptake clearance

1.6.2 *Experimental conditions employed in the PMUE investigations*

Diverse experimental conditions are used to investigate the PMUE. To understand the influence of these conditions on the PMUE interpretation, catalogued below are the experimental models and tools featured in these investigations. First, the range of the systems includes (human or rat) hepatocytes, human proximal tubule endothelial cells, transporter-expressing cells (e.g. OATPs, OATs), liver slices to the isolated perfused rat liver (Francis *et al.*, 2021). For human hepatocyte studies, most researchers use suspended (oil-spin) hepatocytes, while a minority use plated hepatocytes. Second, the source of plasma proteins used in the studies includes plasma, serum, albumin from humans, bovine, rat, monkey, or pigs. Several studies also included α-1-acid-glycoprotein 1 (AAG) and β-lactoglobulin. Albumin concentrations in these investigations typically range from 0.1% to 5% (Francis *et al.*, 2021). In some studies, the human *in vitro* models (e.g. hepatocytes) were not paired with human plasma proteins, instead BSA or rat plasma was used. Third, most compounds analyzed in these studies are substrates for uptake transporters with a few exceptions, such as midazolam which is not transported and passively diffuses across the cell membrane (Bi *et al.*, 2021).

Collecting this information aids in the re-evaluation of potential PMUE mechanisms. For example, the albumin receptor hypothesis would suggest PMUE is exclusive to albumin. If the endocytosis theory holds, PMUE should be evident in HEK293 cells and not hepatocytes since the former express receptors like megalin which can mediate endocytosis. Furthermore, the TIPBS hypothesis should restrict PMUE to transporter substrates that exhibit high extraction ratio. At present, there is no consensus on which methodology should be applied in future investigations.

1.6.3 *Can PMUE bridge the IVIVE gap in predicting hepatic uptake CL?*

We and others have observed underprediction of OATP-mediated hepatic CL_{uptake} of drugs using the TECs/REF approach and/or hepatocytes using PSF (see **section 1.5.3**). To determine if PMUE can bridge the REF-based underprediction of the *in vivo* RSV hepatic CL_{uptake} measured by PET imaging (Billington *et al.*, 2019), we included 100% human plasma or 5% HSA (*i.e.* physiological concentration) in the uptake experiments (Kumar *et al.*, 2021). As expected, the transporter-mediated RSV $CL_{int,uptake}$ in the presence of plasma or HSA was

increased, but the increase was modest, only about 2-fold. Although, the predicted *in vivo* RSV hepatic CL_{uptake} increased, it barely fell within the lower limit of the predefined two-fold success criterion. Therefore, while PMUE can improve the IVIVE performance, it doesn't entirely bridge the IVIVE gap. This conclusion aligns with findings from another study where a comprehensive analysis showed that after inclusion of the PMUE, the predicted hepatic CL of only 51% of the OATP-transported drugs fell within 2-fold of their observed *in vivo* values (Francis *et al.*, 2021).

Interestingly, during our preliminary investigations of the PMUE, we made two observations from our and published data that were inconsistent with the potential mechanisms outlined in **section 1.6.1**: 1) both the slope and the intercept of the statin uptake curve (using OATP1B1 expressing cells) increased in the presence of plasma (Bi *et al.*, 2021) and 2) the magnitude of increase in transporter-mediated and passive $CL_{int,uptake}$ were different with latter being greater than the former (Bowman *et al.*, 2020). The intercept of an uptake curve is usually interpreted as non-specific binding of the drug (and the drug-protein complex if protein is included) to the cells/labware. Therefore, we hypothesized that the observed PMUE on OATP-mediated drug uptake, is largely confounded by the residual drug-protein complex. The answer to this question is crucial in understanding the role of the PMUE and its implication in improving current IVIVE methodologies.

Specific Aim 1 of this dissertation tested the residual drug-protein complex hypothesis by quantifying the uptake of a cocktail of statins by OATP1B1 with varying concentrations of HSA (0, 1%, 2%, and 5%). The residual statin-albumin complex was quantified using quantitative target proteomics. The statin cocktail consisted of five statins (atorvastatin (ATV), cerivastatin (CRV), fluvastatin (FLV), pitavastatin (PTV), rosuvastatin (RSV), **Fig. 1.8**, **Table 1.2**). They are OATPs substrates with varying degrees of protein-binding. They were chosen based on reported underpredictions of their hepatic CLs (Varma *et al.*, 2014; Kim *et al.*, 2019; Li *et al.*, 2020, 2021; Bi *et al.*, 2021). Plated OATP1B1-expressing and mock HEK293 cells were used as *in vitro* models to distinguish the active from passive uptake of the statins. The results from Aim 1 showed that the observed PMUE on ATV, FLV and RSV in the presence of HSA was mostly an artifact caused by the residual statin-HSA complex that is not washed away completely when the uptake is terminated. In contrast, this was not the case for OATP1B1-mediated uptake of PTV and passive uptake of CRV (**Chapter 2**).

While the above results were obtained with plated OATP1B1 HEK293 cells, can they also apply to uptake determined using suspended (oil-spin) hepatocytes where the PMUE has also been observed (Kim *et al.*, 2019; Liang *et al.*, 2020; Li *et al.*, 2021)? Suspended (oil-spin) hepatocytes utilize rapid centrifugation through oil as the uptake termination strategy. Theoretically, this model does not have a washing step and therefore the residual drug-protein complex should be reduced or eliminated when uptake studies are conducted with the suspended (oil-spin) *vs.* plated hepatocytes. It's worth noting that most researchers use suspended (oil-spin) hepatocytes when investigating the PMUE. In addition, suspended human hepatocytes are widely used in the pharmaceutical industry to evaluate hepatic uptake of drug candidates. Therefore, in **Specific Aim 2**, we determined if the apparent PMUE observed with plated or suspended (oil-spin) human hepatocytes, was also largely confounded by the residual drug-protein complex. And, if it was, we hypothesized that it would be reduced when suspended hepatocytes are spun through an oil layer. Using the same experimental design as that used for OATP1B1 cells, the uptake of a cocktail of five statins by plated and suspended (oil-spin) human hepatocytes was quantified in the presence and absence of 5% HSA, both at 37˚C (active + passive uptake) and at 4˚C (passive uptake). The amount of residual statin-albumin was quantified by quantitative targeted proteomics. The results (**Chapter 3)** from both plated and suspended hepatocytes suggest that the increase in passive uptake of all five statins, in the presence of 5% HSA, was completely explained by the residual stain-HSA complex. Except for ATV and CRV, this was also the case for the total uptake (at 37˚C) of the statins. In conclusion, the PMUE on the uptake of ATV or CRV by plated and suspended hepatocytes appears to be a real phenomenon. Nevertheless, the increase in transporter-mediated uptake clearance of ATV and CRV (into suspended hepatocytes) by 5% HSA was modest (1.2 to 1.5-fold *vs.* buffer) and much lower than that observed with plated hepatocytes (1.9 to 7.1-fold vs. buffer). These data suggest that the observed PMUE on the uptake of ATV and CRV is also likely an artifact not captured by quantitative targeted proteomics. Therefore, including this PMUE in IVIVE of hepatic CL is unlikely to bridge the underprediction of the *in vivo* hepatic CL of statins.

Table 1.2. Overview of the physicochemical properties and IVIVE discrepancy of the five statins

	MW	LogD7.4	PKa	$f_{u,p}$[1]	Hepatic uptake transporter(s)[2]	Observed $CL_{h,p}$[3] (mL/min/kg)	Observed IVIVE discrepancy of hepatic CL[4]	Reported PMUE (SHH+5% HSA)[4]
Atorvastatin	558.6	1.3	4.4	0.02~0.0478	OATP1B1/1B3/2B1; NTCP	8.93	11	3.18
Cerivastatin	459.6	1.9	4.5	0.0073~0.0176	OATP1B1/1B3/2B1	2.70	2.2	3.10
Fluvastatin	411.5	1.12	4.4	0.004~0.009	OATP1B1/1B3/2B1; NTCP	7.25	33	6.83
Pitavastatin	421.5	1.2	4.1	0.005~0.008	OATP1B1/1B3/2B1; NTCP	5.56	17	2.44
Rosuvastatin	481.5	-0.33	4.3	0.134~0.158	OATP1B1/1B3/2B1; NTCP	6.83	12	2.48

MW: molecular weight; $f_{u,p}$: unbound fraction in plasma; $CL_{h,p}$: hepatic plasma CL; SHH: suspended human hepatocytes; HSA: human serum albumin; PMUE: protein-mediated uptake effect

[1] Data obtained from (Keith A. Riccardi *et al.*, 2019) and (Kim *et al.*, 2019)

[2] Data obtained from Certara DIDB

[3] Data collected from (Bi *et al.*, 2021)

[4] Data obtained from (Kim *et al.*, 2019)

Atorvastatin **Cerivastatin** **Fluvastatin** **Pitavastatin** **Rosuvastatin**

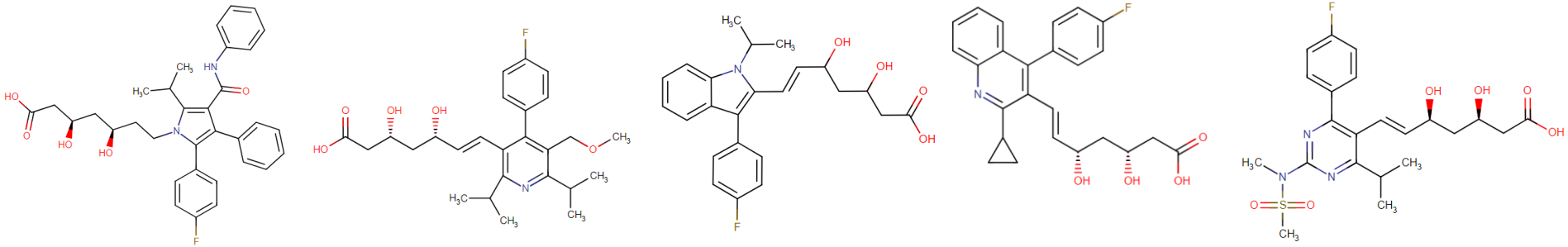

Figure 1.8. Chemical structures of atorvastatin, cerivastatin, fluvastatin, pitavastatin and rosuvastatin.

Having discounted the observed PMUE as largely an artifact, we wanted to determine if the underprediction of the *in vivo* hepatic CL_{uptake} of RSV using TECs/REF approach was unique to RSV or was also the case for other OATPs substrates. Parenthetically, we have found that the TECs/TEVs/REF approach yields excellent predictions of hepatic uptake of non-OATP substrates (e.g. metformin) and BBB or placental efflux of P-gp substrates (e.g. betamethasone) (Sachar *et al.*, 2020; Anoshchenko *et al.*, 2021; Storelli *et al.*, 2021). While others have shown such underprediction of hepatic uptake CL for a wide range of OATP substrates, the IVIVE approach taken by these investigators is flawed. That is, they assume that the sinusoidal uptake is the rate-determining step (RDS) in the hepatic CL of these drugs (Kim *et al.*, 2019). Without quantifying all hepatobiliary CLs of drugs, such an assumption cannot be made. It is likely that for most of these drugs, all hepatobiliary CLs (*i.e.*, uptake, efflux and metabolic) are the RDS. In that event, equating the *in vivo* hepatic CL of the drug with the uptake CL quantified *in vitro* could result in the *in vivo* hepatic CL to be well-predicted when in fact the discrepancy is large. The only solution to this problem is to estimate all the hepatobiliary CLs, including the uptake CL, by PET imaging (Billington *et al.*, 2019). When such data are available, they should be used (not the total hepatic CL) to verify the prediction of transporter-based hepatobiliary CL of drugs.

Based on the above information, we sought to extend the TECs/TEVs/REF approach to other OATPs substrates, to predict their hepatobiliary CLs and hepatic drug concentrations. Then, these predictions were to be verified using the PET imaging data and the correct *in vivo* CLs estimated by PET imaging data. Therefore, **specific Aim 3 of this dissertation** extends the TECs/TEVs/REF approach to predict the hepatobiliary CLs and hepatic concentrations to two additional OATP substrates, glyburide and pitavastatin, for which PET imaging data are available either from our collaborators or in the literature.

1.7 EXTENDING THE PROTEOMICS-INFORMED TECS/TEVS/REF APPROACH TO PREDICT HEPATOBILIARY CLS AND HEPATIC CONCENTRATIONS OF OATP-TRANSPORTED DRUGS, GLYBURIDE AND PITAVASTATIN

Glyburide and pitavastatin were selected because: 1) they are excellent OATPs-substrate as evidenced by both *in vitro* studies and clinical DDI studies. (Fujino *et al.*, 2005; Zheng *et al.*, 2009; Bi *et al.*, 2013; Li *et al.*, 2017;

Bouchghoul *et al.*, 2021)2) their human PET-imaged hepatic concentrations are available (Marie *et al.*, 2022; Nakaoka *et al.*, 2022). 3) underprediction of their *in vivo* hepatobiliary CLs (albeit estimated incorrectly) using human hepatocytes and PSF has been reported (Li *et al.*, 2017; Kim *et al.*, 2019).

Glyburide (GLB), also known as glibenclamide, is a second-generation sulfonylurea widely prescribed to treat type 2 diabetes. It potently stimulates pancreatic insulin secretion and may also reduce muscle and liver resistance to insulin action. The CL pathway of GLB involves initial hepatic uptake through the OATPs followed by hepatic metabolism via CYP2C9 (major route) and CYP3A4/5 (minor route) enzymes (Naritomi *et al.*, 2004; Zhou *et al.*, 2010). GLB is metabolized to the hydroxy metabolites with roughly 50% of the metabolites excreted in urine and 50% of the metabolites excreted in bile (Feldman, 1985). The physicochemical properties of GLB are summarized in **Table 1.3**. In a recent PET study, using the integration plot approach (see below), our collaborators estimated the hepatic uptake rate constant (k_{uptake}) to be 0.066 ± 0.025 min^{-1} (Marie *et al.*, 2022).

Pitavastatin (PTV) is an inhibitor of the enzyme 3-hydroxy-3-methylglutaryl-CoA reductase and is effective for the treatment of hyperlipidemia. The oral bioavailability of PTV is 80% due to its metabolic stability (Hoy, 2017). Its primary elimination pathway is through hepatic uptake by OATPs and NTCP transporters and biliary excretion of the unchanged drug (95% of the dose) by P-gp and BCRP (Hirano *et al.*, 2004; Duan *et al.*, 2017). Due to the cyclopropyl group in its molecular structure, only a small fraction of PTV undergoes hepatic metabolism by CYP2C9 (Fujino *et al.*, 2003). PTV undergoes reversible metabolism to its lactone (Fujino *et al.*, 2003). Only 2–4% of the dose is excreted unchanged in the urine. The physicochemical properties of PTV are summarized in **Table 1.3**. Using the integration plot approach, a recent PET study in seven Japanese males estimated the hepatic uptake CL and canalicular efflux CL for PTV to be 7.68 mL/min/kg (uptake) and 0.111 mL/min/kg (biliary), respectively (Nakaoka *et al.*, 2022).

The integration plot approach assumes negligible sinusoidal efflux or biliary CL of the drug during the initial uptake phase. Ignoring this CL will result in underestimation of CL_{uptake}. Therefore**, in specific Aim 3**, I will fit a compartmental model to the blood, hepatic and gall bladder (PTV only) concentrations to generate the *in vivo*

hepatobiliary CLs of GLB and PTV. Then, the REF-predicted CLs as well as hepatic concentrations of these drugs will be compared with the corresponding values estimated from PET imaging.

Table 1.3. Physicochemical properties and PK data of glyburide and pitavastatin.

Parameter	Glyburide	Pitavastatin
	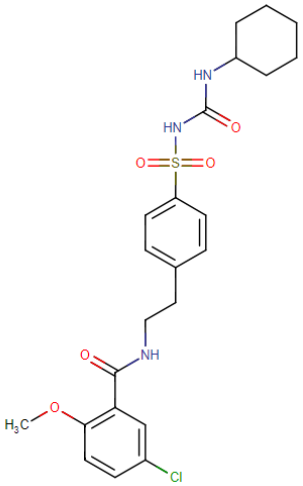	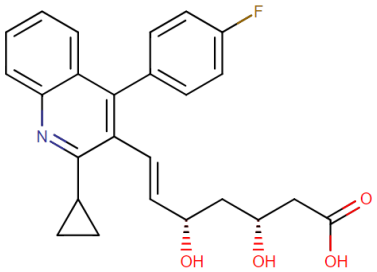
MW	494.0	421.46
pKa	5.38	5.31
$logD_{7.4}$	2.23	1.2
$f_{u,p}$[1]	0.013	0.008
$R_{B/P}$[1]	0.55	0.58
Metabolizing enzyme[2]	CYP2C9, CYP3A4/5	CYP2C8, CYP2C9, UGT1A3/2B7
Transporters[2]	OATP1B1, OATP1B3?, OATP2B1?, MRP3?, MRP4?, BRCP, P-gp	OATP1B1, OATP1B3, OATP2B1, NTCP, BCRP, P-gp, MRP3, MRP4
$CL_{total,blood}$[3]	2.30 mL/min/kg	9.81 mL/min/kg
$CL_{h,blood}$[3]	2.30 mL/min/kg	9.78 mL/min/kg
$CL_{r,blood}$[4]	negligible	0.030 mL/min/kg
Bioavailability[5]	80%	80%
Volume of distribution[5]	0.077 L/kg	2.0 L/kg
Terminal $t_{1/2}$[5]	Ranging from 1.5-1.75 hrs	~12 hrs

MW, molecular weight; $f_{u,p}$, unbound fraction in plasma; $R_{B/P}$, blood-to-plasma ratio; $CL_{total,blood}$, total blood clearance; $CL_{h,blood}$, hepatic blood clearance; $CL_{r,blood}$, renal blood clearance

[1] Data obtained from (Keith A. Riccardi *et al.*, 2019)

[2] Data obtained from Certara DIDB; "?": data from different studies are controversial

[3] Data obtained from (Otoom *et al.*, 2001; Catapano, 2010; Saito, 2011)

[4] Data obtained from (Morgan *et al.*, 2012)

[5] Data obtained from (Neugebauer *et al.*, 1985; Pearson, 1985; Rydberg *et al.*, 1995), DrugBank and U.S. Food and Drug Administration approval package

1.8 SPECIFIC AIMS

To reiterate, the specific aims of my dissertation are:

Aim 1 (Chapter 2): To determine, using plated OATP1B1-expressing and mock HEK293 cells and QTP, if the observed PMUE on statins is largely confounded by the residual drug-protein complex.

Aim 2 (Chapter 3): To determine if the above observed PMUE is reproduced with plated human hepatocytes and if it is reduced or eliminated when using suspended (oil-spin) hepatocytes.

Aim 3 (Chapter 4): To extend the proteomics-informed REF approach to predict the human hepatobiliary CLs and hepatic concentrations of two other OATP-substrates, glyburide and pitavastatin. Then, to compare these predictions with their PET imaging data.

Chapter 2. IS THE PROTEIN-MEDIATED UPTAKE OF DRUGS BY OATPS A REAL PHENOMENON OR AN ARTIFACT?

The work presented in this chapter was previously published in *Drug Metabolism and Disposition* 2022 Sep;50(9):1132-1141. Mengyue Yin is the first author responsible for research design, conducting experiments, data analysis, and manuscript writing. Both Flavia Storelli and Jashvant D. Unadkat were co-authors involved in the research design, data analysis, and contributed to manuscript writing.

2.1 ABSTRACT

Plasma proteins or human serum albumin (HSA) have been reported to increase the in vitro intrinsic uptake clearance ($CL_{int,uptake}$) of drugs by hepatocytes or organic anion transporting polypeptide (OATP)-transfected cell lines. This, so called protein-mediated uptake effect (PMUE), is thought to be due to an interaction between the drug-protein complex and the cell membrane causing an increase in the unbound drug concentration at the cell surface resulting in an increase in the apparent $CL_{int,uptake}$ of the drug. To determine if the PMUE on OATP-mediated drug uptake is an artifact or a real phenomenon, we determined the effect of 1%, 2%, and 5% (w/v g/dL) HSA on OATP1B1-mediated (HEK293 transfected cells) and passive $CL_{int,uptake}$ (Mock HEK293 cells) of a cocktail of five statins. In addition, we determined the non-specific binding (NSB) of the statin-HSA complex to the cells/labware. The increase in uptake of atorvastatin, fluvastatin and rosuvastatin in the presence of HSA was completely explained by the extent of NSB of the statin-HSA complex, indicating that the PMUE for these statins is an artifact. In contrast, this was not the case for OATP1B1-mediated uptake of pitavastatin and passive uptake of cerivastatin suggesting that the PMUE is a real phenomenon for these drugs. Additionally, the PMUE on OATP1B1-mediated uptake of pitavastatin was confirmed by a decrease in its unbound IC_{50} in the presence of 5% HSA *vs.* HBSS buffer. These data question the utility of routinely including plasma proteins or HSA in uptake experiments and the previous findings on PMUE on OATP-mediated drug uptake.

2.2 INTRODUCTION

Successful *in vitro* to *in vivo* extrapolation (IVIVE) of transporter-mediated hepatic drug clearance (CL_h) is important in drug development. Underprediction of *in vivo* CL_h of highly protein-bound organic anion transporting polypeptide (OATP)-substrate drugs, is widely reported when using IVIVE approaches (Soars, McGinnity, *et al.*, 2007; Jones *et al.*, 2012; Wood *et al.*, 2017; Bowman and Benet, 2018; Miyauchi *et al.*, 2018). The mechanistic basis of this discrepancy is not clear. Numerous investigators, including us, have suggested that the absence of plasma proteins in the *in vitro* uptake studies is a contributor to this *in vitro* to *in vivo* discrepancy in CL_h (Miyauchi *et al.*, 2018, 2021; Bowman *et al.*, 2019, 2020, 2021; Kim *et al.*, 2019; Liang *et al.*, 2020; Bi *et al.*, 2021; Francis *et al.*, 2021; Kumar *et al.*, 2021). These investigations have demonstrated that inclusion of plasma or plasma proteins in the *in vitro* uptake studies increases the apparent $CL_{int,uptake}$ of OATP substrate drugs by hepatocytes and OATP-expressing cells. This phenomenon is called the protein-mediated uptake effect (PMUE). That is, plasma proteins present *in vivo* increase the CL_h of OATP substrate drugs beyond that quantified by *in vitro* uptake studies conducted in protein-free buffer. Indeed, IVIVE of CL_h of OATP substrate drugs is improved when plasma/plasma proteins are included in the *in vitro* uptake studies (Mao *et al.*, 2018; Miyauchi *et al.*, 2018; Poulin and Haddad, 2018; Kim *et al.*, 2019; Liang *et al.*, 2020; Kumar *et al.*, 2021).

Several potential mechanisms for the PMUE have been proposed (Bowman and Benet, 2018; Bteich *et al.*, 2019). Of these, the most accepted is the protein-lipid interaction (PLI) mechanism. This mechanism hypothesizes that an *in vivo* interaction between the drug-protein complex and the lipid membrane of the cell results in enhanced dissociation of the drug-protein complex and, therefore, increased local unbound drug concentration at the cell surface. Consequently, in the presence of plasma proteins, the *in vivo* apparent $CL_{int,uptake}$ of the drug is greater than that estimated from *in vitro* uptake studies conducted in the absence of proteins.

If the PLI hypothesis is correct, the following should be observed in the *in vitro* OATP uptake studies in the presence *vs.* absence of plasma proteins: 1) the OATP-mediated and passive $CL_{int,uptake}$ of the drug should

increase to the same extent (if unbound substrate concentration << K_m); 2) the slope (*i.e.* the $CL_{int,uptake}$), but not the intercept, of the unbound concentration-normalized uptake *vs.* time curve should increase. However, all publications supporting the PLI mechanism report an increase in both slope and intercept of the uptake curve in the presence of plasma or plasma proteins (e.g. human serum albumin, HSA) (Nunes *et al.*, 1988; Miyauchi *et al.*, 2018; Li *et al.*, 2020; Liang *et al.*, 2020; Bi *et al.*, 2021). An increase in the intercept is usually interpreted as non-specific binding (NSB) of the drug to the cells/labware. Therefore, we hypothesized that the PLI mechanism, and therefore the PMUE on OATP-mediated drug uptake, is an artifact caused by NSB, and not a real phenomenon.

The PMUE may be an artifact because of the way in which *in vitro* uptake CL of a drug is routinely determined. Ideally, drug uptake should measure the intracellular concentration of the drug when the uptake experiment is terminated by washing the cells with cold drug-free buffer. However, in practice, it is analytically impossible to distinguish between intracellular drug and that bound to the cell surface/labware. If the drug uptake study is conducted in the presence of plasma proteins, the amount of drug bound to the proteins in the media will be large relative to the unbound drug concentration in the media and that taken up by the cells. Consequently, any remaining drug-protein complex bound to the cells/labware (*i.e.* residual drug-protein complex), will be erroneously interpreted as drug taken into the cells. Such erroneous interpretation will result in an increase in intercept and, if the NSB is time-dependent, an apparent increase in slope (*i.e.* $CL_{int,uptake}$) of drug uptake profile.

To test our hypothesis that the PMUE is due to NSB, we determined the total, active (OATP1B1-mediated) and passive $CL_{int.uptake}$ of a cocktail of five OATP1B1-transported statins, namely atorvastatin (ATV), cerivastatin (CRV), fluvastatin (FLV), pitavastatin (PTV), and rosuvastatin (RSV) in the absence (protein-free buffer) and presence of 1%, 2%, or 5% (w/v g/dL) HSA. These statins were chosen as they have varying degrees of binding to albumin and their uptake by OATP1B1 has been shown to demonstrate PMUE (Bowman *et al.*, 2019, 2020; Kim *et al.*, 2019; Liang *et al.*, 2020; Bi *et al.*, 2021). Albumin, and not plasma, was chosen to simplify the number of plasma proteins included in the incubations. Total $CL_{int.uptake}$ of the statins was determined by using OATP1B1-transfected HEK293 cells while passive $CL_{int.uptake}$ was determined using Mock or OATP1B1-

transfected HEK293 cells incubated with high unbound concentration of rifampicin (500 μM) (henceforth called OATP1B1_RIF cells). The NSB of HSA was determined by quantifying the residual albumin by quantitative targeted proteomics. Finally, to confirm or refute that the PMUE is an artifact, we determined a parameter that should be independent of NSB of the statin-HSA complex, namely the unbound inhibitory capacity of a statin ($IC_{50,u,}$ unbound inhibitor concentration that results in 50% inhibition) towards OATP1B1-mediated transport of another statin.

2.3 MATERIALS AND METHODS

2.3.1 *Chemicals and Reagents*

The dithiothreitol (DTT), iodoacetamide (IAA), mass spectrometry grade trypsin, total protein quantification bicinchoninic acid assay (BCA) kit, Hank's balanced salt solution with calcium and magnesium (HBSS) were obtained from Thermo Scientific (Rockford, IL). Dulbecco's modified Eagle's medium (DMEM), fetal bovine serum (FBS), nonessential amino acids, geneticin, blasticidin S HCl, penicillin, and streptomycin solution were obtained from Thermo Fisher Scientific (Waltham, MA). Atorvastatin (ATV), cerivastatin (CRV), fluvastatin (FLV), pitavastatin (PTV), rosuvastatin (RSV), diclofenac sodium salt (DCL), rifampicin (RIF), human serum albumin (HSA, fatty acid free, Purity $\geqslant$ 96%) and formic acid was purchased from Sigma-Aldrich (St. Louis, MO). Bovine serum albumin (BSA) and HEPES buffer were purchased from MP Biomedicals (Solon, OH). Synthetic signature peptides for HSA were obtained from New England Peptides (Boston, MA). High-performance liquid chromatography (HPLC)-grade acetonitrile and sodium dodecyl sulfate (SDS) were purchased from Fischer Scientific (Fair Lawn, NJ). Formic acid was purchased from Sigma-Aldrich (St. Louis, MO). All reagents were analytical grade. The Calbiochem ProteoExtract Native Membrane Extraction kit and the Centrifree® Ultrafiltration Device was purchased from EMD Millipore Corporation (Billerica, MA). Poly-D-lysine-coated 24-well plates were purchased from Corning (Kennebunk, ME). OATP1B1-expressing and Mock human embryonic kidney (HEK) 293 cells were generously provided by Dr. Yurong Lai of Gilead Sciences Inc. (Foster City, CA).

2.3.2 *Uptake of Statins by OATP1B1-Expressing or Mock HEK293 cells in the Absence or Presence of 1%, 2% and 5% HSA*

OATP1B1-expressing or Mock HEK293 cells were seeded in 24-well poly-D-lysine-coated plates at a density of 3×10^5 cells per well with 1 ml of high glucose DMEM medium (containing 10% FBS, 100 U/mL penicillin and streptomycin. 25 mM HEPES and 0.1 mM MEM non-essential amino acid solution) for 48 hours at 37°C, 90% relative humidity, and 5% CO_2. OATP1B1-expressing HEK293 cells were supplemented with 600 µg/mL geneticin and 10 µg/mL blasticidin.

For the uptake assays, OATP1B1-expressing or Mock HEK293 cells were rinsed twice with 1 mL of warm HBSS buffer (37℃, pH 7.4). Then, the cells were pre-incubated with HBSS buffer or HSA solution (1%, 2%, or 5% HSA w/v in HBSS buffer) for 10 minutes. After aspiration of these solutions from the wells, statin uptake was initiated by adding 0.5 mL of a cocktail containing approximately unbound 0.2 µM ATV, 0.1 µM CRV, 0.2 µM FLV, 0.2 µM PTV and 1 µM RSV. The above uptake studies with OATP1B1-expressing cells were repeated in the presence of RIF (unbound concentration 500 µM). Statin uptake was terminated at designed time points (5s, 30s, 60s and 120s, all within the linear range) by aspirating the drug solution and washing the cells three times with ice-cold HBSS buffer. Then, the cells were lysed using the quench solution (80% acetonitrile containing 1 nM diclofenac sodium salt as an internal standard). After centrifuging the lysate at 18,000 g for 20 minutes, 10 µL of the supernatant was injected onto the liquid chromatography-tandem mass spectrometer (LC-MS/MS) to quantify the cell-lysate statin concentration. For every experiment, extra wells were included for total protein quantification by the BCA assay following cell lyses by 1 ml 2% SDS. Three to five independent experiments were conducted, each in triplicate. Of note, the final dimethyl sulfoxide (DMSO) concentration (used to make the statin stock solution) was maintained at 1% (v/v) in each uptake experiment. After the uptake study, the total, unbound (and bound) statin concentration in the uptake media (HBSS or HSA) in every uptake study was estimated using ultrafiltration as described below. The unbound RIF concentration was estimated based on its published binding to albumin (Boman and Ringberger, 1974).

2.3.3 *Inhibitory Effect of Atorvastatin (ATV), Pitavastatin (PTV) or Fluvastatin (FLV) on OATP1B1-Mediated Uptake of RSV in the Absence or Presence of HSA*

The uptake of rosuvastatin (nominal unbound concentration 1 µM) by the OATP1B1-expressing cells was determined (over 1 min) in the presence of the inhibitors ATV, PTV or FLV. The range of nominal unbound concentrations of ATV was 0-200 µM (in HBSS or 2% HSA solution), for PTV was 0-100 µM in HBSS and 0-25 µ M in 5% HSA solution, and for FLV was 0-100 µM in HBSS buffer, 0-2 µM in 2% HSA solution and 0-1 µM in 5% HSA solution (different nominal unbound concentrations and the percent of HSA used was dictated

by the solubility of the statins). The total, unbound (and bound) substrate and inhibitor concentrations were estimated using ultrafiltration as described below.

2.3.4 *Quantification of the Statin Unbound Fraction in 1%, 2% and 5% HSA Solution*

The unbound fraction of the statins in the uptake solution was determined using the Centrifree® Ultrafiltration Device as per the manufacturer's specifications. The fraction unbound of the statins was corrected for NSB of the statins to the ultrafiltration device determined by filtering 500 µL of the statin HBSS solution used in the above uptake experiments. Briefly, the samples were centrifuged at 37℃ for 2 minutes at 1,200 g to keep the filtrate volume <15% of the initial volume. After centrifugation, 10 µL of the statin solution/filtrate was diluted up to 1 mL or 10 mL by the quench solution described above. Then, after centrifuge at 18,000 g for 20 minutes, 10 µL of the supernatant was injected onto the LC-MS/MS systems.

2.3.5 *Quantification of Statins by Liquid Chromatography–Tandem Mass Spectroscopy (LC-MS/MS)*

All the above samples were analyzed on AB Sciex Triple Quad 6500 (SCIEX, Farmingham, MA) coupled with Waters Acquity UPLC system (Waters, Hertfordshire, UK). Ten microliters of the sample were injected onto a UPLC column (ACQUITY UPLC® BEH C18 column, 1.7 µm, 2.1 mm x 50 mm, Waters). The LC-MS/MS conditions are summarized in Suppl. Table. 1 of (Yin *et al.*, 2022).

2.3.6 *Quantification of Residual Albumin in Cell Lysates Using Quantitative Target Proteomics*

The residual albumin in the cell lysates (*i.e.* the NSB of albumin-drug complex) was measured in the absence and presence of HSA (1%, 2% and 5%) using either the relative quantification approach (when the unlabeled HSA surrogate peptide was not immediately available) or the absolute quantification approach (when the unlabeled HSA surrogate peptide was available).

2.3.7 *Relative Quantification of Residual Albumin in the Cell Lysates in the Absence or Presence of 1%, 2% and 5% HSA*

After termination of uptake in the above uptake studies (excluding the $IC_{50,u}$ studies), the cells were lysed for 1 hour at 4°C with (200µL/well) equal mixture of 2% SDS and EBII buffer from the Calbiochem ProteoExtract Native Membrane Extraction kit. Following reduction, alkylation and digestion by trypsin as previously described (Storelli *et al.*, 2021), 10 µL of a mixture of the stable-labeled surrogate peptides (details described in Suppl. Table 1 of (Yin *et al.*, 2022)), prepared in 80% acetonitrile plus 0.2% formic acid and 5 µL of 80% acetonitrile plus 0.2% formic acid was added to 40 µL of trypsin digest (in 50 mM ammonium bicarbonate buffer). After centrifugation (5000g, 4°C, 5min), 5 µL of supernatant was injected onto the LC-MS/MS system (described above) and analyzed using the settings and procedure described in Suppl. Table 1 of (Yin *et al.*, 2022). Any measured HSA under the HBSS condition (in OATP1B1-expressing HEK293 cells) was assumed to be endogenous and identical to that in Mock HEK293 cells and unaffected by the addition of the statins.

2.3.8 *Absolute Quantification of Residual Albumin in the Cell Lysates in the Presence of 5% HSA*

To estimate the amount of statin-HSA complex non-specifically bound to the cells, absolute quantification of HSA in the cell lysates is required at all time points of the uptake studies. For these experiments, the pre-incubation step was eliminated from the uptake studies primarily to replicate the NSB of the statin-HSA complex during the uptake phase of the experiments. In addition, the pre-incubated albumin will not carry any drug into the cells and any remaining albumin from the pre-incubation mixture (after aspiration) will be negligible relative to that added when the uptake study is conducted in the presence of HSA. The absolute amount of albumin in the cell lysates was quantified as described above except that the calibrators (14.2 – 455 nM of the unlabeled albumin surrogate peptide) and quality control samples (28.7, 56.8, 114 nM of the unlabeled albumin surrogate peptide) were included in the LC-MS/MS analyses. These were prepared by spiking 5 µl of the unlabeled peptide standard and 10 µL of the labeled peptide (both in 80% acetonitrile and 0.2% formic acid solution) to 40 µL of 50 mM ammonium bicarbonate buffer.

2.3.9 *Data and Statistical Analyses*

2.3.9.1 Determination of OATP1B1-Mediated and Passive Apparent Intrinsic Uptake Clearance ($CL_{int,uptake}$) of statins

The initial uptake rate was estimated from the slope of the drug uptake *vs.* time profile (passive: in Mock cells or OATP1B1_RIF cells; total: in OATP1B1-expressing cells) using simple linear regression in GraphPad Prism version 9 (GraphPad Software, San Diego, CA). The apparent $CL_{int,uptake}$ was calculated as the ratio of the initial uptake rate and the measured unbound concentration of the drug in HBSS or HSA-containing buffer. To allow comparison across the statins, the uptake data presented in the figures were normalized to a nominal 1 µM unbound concentration of each statin. The OATP1B1-mediated apparent $CL_{int,uptake}$ was calculated by subtracting the apparent passive $CL_{int,uptake}$ (in Mock or OATP1B1_RIF cells) from the apparent total $CL_{int,uptake}$ (in OATP1B1-expressing cells).

2.3.9.2 Estimation of the $IC_{50,u}$ or the Degree of Inhibition of OATP1B1-Mediated RSV Uptake by ATV, FLV or PTV

First, the total % RSV uptake in the presence of the inhibitor (expressed relative to the uptake in the absence of the inhibitor) was corrected for the % passive uptake of RSV to derive the % OATP1B1-mediated RSV uptake. The % passive uptake of RSV was assumed to equal % RSV uptake at maximum inhibitor concentration and was comparable to the passive uptake obtained in Mock or OATP1B1_RIF cells. Then, the $IC_{50,u}$ value of ATV or PTV was estimated by fitting an inhibition model to the % OATP1B1-mediated RSV uptake as a function of the unbound inhibitor concentrations using GraphPad Prism version 9 (GraphPad Software, San Diego, CA):

$$\%\ OATP1B1\text{-}mediated\ RSV\ uptake = 100\% / [1+(IC_{50}/unbound\ inhibitor\ concentration)^{HillSlope}] \quad \textbf{Eq. 2.1}$$

2.3.9.3 Estimation of the Residual Statin-HSA Complex Amount in the Cell Lysates in the Presence of 5% HSA

The bound statin (*i.e.* statin-HSA complex) amount per well was the difference between the total statin amount and the unbound statin amount per well calculated as the total or unbound statin concentration per well times 500 µL uptake media per well.

Assuming the ratio of the residual HSA and the total HSA (in 500 µL) equals the ratio of the residual bound statin and the total bound statin (in 500 µL), the amount of residual statin-HSA complex at different uptake times was estimated as follow:

$$Residual\ bound\ statin\ (pmol/well) = Total\ bound\ statin\ \ (pmol/well) \times \frac{Residual\ HSA\ \ (pmol/well)}{Total\ HSA\ (pmol/well)} \quad \textbf{Eq. 2.2}$$

Where the total HSA per well [5% (w/v) HSA in 500 µL] was 0.36 µmol, based on HSA molecular weight of 69367 g/mol (https://www.uniprot.org/uniprot/P02768), and the residual HSA was quantified by proteomics as described above.

2.3.9.4 Calculation of Increased Apparent Uptake in the Presence of 5% HSA vs. HBSS

To take into consideration small variation in the measured unbound statin concentration and the total protein content in HSA *vs.* HBSS uptake studies, statin uptake at each time point in these studies was corrected (Eq. 3) for these variables before estimating the increased apparent uptake in the presence of 5% HSA *vs.* HBSS.

$$Normalized\ statin\ uptake\ in\ HBSS = Apparent\ statin\ uptake\ in\ HBSS\ (pmol/well) \times \frac{Unbound\ statin\ concentration\ in\ 5\%HSA\ (\mu M)}{Unbound\ statin\ concentration\ in\ HBSS\ (\mu M)} \times \frac{Total\ protein\ amount\ in\ 5\%\ HSA\ (mg/well)}{Total\ protein\ amount\ in\ HBSS\ (mg/well)} \quad \textbf{Eq. 2.3}$$

Where the unbound statin concentration was measured using ultrafiltration and the total protein amount was determined by the BCA assay. Then, the increase in statin uptake in the presence of HSA *vs.* HBSS at each time point was estimated as follows:

$$Increased\ apparent\ uptake\ in\ the\ presence\ of\ 5\%\ HSA\ vs. HBSS\ = Apparent\ statin\ uptake\ in\ 5\%\ HSA - \ normalized\ statin\ uptake\ in\ HBSS \quad \textbf{Eq. 2.4}$$

2.3.9.5 Statistical analysis

Estimates of the NSB of statin-HSA complex to the cells and the measured increase in statin uptake in the presence of 5% HSA (**Fig. 2.4**) as well as the $IC_{50,u}$ of the statins in absence and presence of HSA (**Fig. 2.5**), were statistically compared by the unpaired (**Fig. 2.4**) or the paired (**Fig. 2.5**) Student's t-test using GraphPad Prism version 9 (GraphPad Software, San Diego, CA).

2.4 RESULTS

2.4.1 *Unbound Fraction in 1%, 2% and 5% HSA*

The extent of protein binding of the five statins followed the order FLV > PTV > CRV > ATV > RSV (**Table 2.1**; corrected for the NSB of statins to the ultrafiltration device 0.03 to 0.44). Three statins (CRV, FLV and PTV) were highly protein bound drugs (> 0.97), with fraction unbound in 5% HSA ($fu_{5\%HSA}$) ranging between 0.003 to 0.023. No difference in $fu_{5\%HSA}$ values was noted for each drug when determined singly (data not shown) *vs.* as a cocktail. The $fu_{5\%HSA}$ values (physiologically relevant, **Table 2.1**) of the statins were in agreement with their reported fraction unbound values in plasma (fu_p) except for the highly protein-bound statin FLV ($f_{u.5\%HSA}$ 0.003 *vs.* $f_{u,p}$ 0.009).

Table 2.4. Fraction unbound (f_u) of the statins in buffer containing 1%-5% human serum albumin (HSA) compared with that reported in human plasma

Compound	**$f_{u,\ 1\%\ HSA}$**	**$f_{u,2\%\ HSA}$**	**$f_{u,5\%\ HSA}$**	**Reported $f_{u,p}$[#]**
Atorvastatin	0.202 ± 0.041	0.102 ± 0.038	0.056 ± 0.014	0.048
Cerivastatin	0.058 ± 0.008	0.035 ± 0.007	0.023 ± 0.004	0.018
Fluvastatin	0.012 ± 0.002	0.006 ± 0.001	0.003 ± 0.0007	0.00922
Pitavastatin	0.032 ± 0.006	0.018 ± 0.002	0.008 ± 0.001	0.0080
Rosuvastatin	0.41 ± 0.04	0.27 ± 0.03	0.13 ± 0.01	0.16

Data are mean ± SD of 10~12 uptake experiments and were corrected for NSB of the statin to the ultrafiltration device.

[#] Fraction unbound in human plasma ($f_{u,p}$), determined using equilibrium dialysis, was obtained from (K. A. Riccardi et al., 2019).

2.4.2 *The Presence of HSA Increased the Apparent In Vitro Uptake of Statins into Both OATP1B1-Expressing and Mock HEK293 Cells.*

In the presence of HSA (with the unbound statin concentration kept approximately the same), slope of the uptake curves (**Fig. 2.1**) increased with the increase in HSA concentration, suggesting a PMUE on the statins. However, the ratio (HSA/HBSS) of the $CL_{int,uptake}$ (a reflection of the slope), also interpreted as the PMUE, was much smaller for OATP1B1-expressing cells (1.0 to 4.4 for 5%HSA) *vs.* Mock or OATP1B1_RIF cells, especially for ATV and RSV (< 2) (**Fig. 2.1 & 2.2**; Suppl. Fig. 1 of (Yin et al., 2022)). In contrast, the ratio of the slope (HSA/HBSS) of the uptake curve for the Mock cells (passive uptake) was 3 to 16, with the largest ratios following the order FLV **(Fig. 2.1Ci**) > PTV (**Fig. 2.1Di**) > RSV (**Fig. 2.1Ei**). The same trend was observed for OATP1B1_RIF cells (Suppl. Fig. 1 of (Yin et al., 2022)). Indeed, this apparent PMUE on statin uptake was confirmed when the apparent total, OATP1B1-mediated and passive *in vitro* $CL_{int,uptake}$ of the statins was estimated (Suppl. Table 2 of (Yin et al., 2022)). The ratio (HSA/HBSS) of the apparent passive $CL_{int,uptake}$ (*i.e.* in Mock cells) was greater than that of the apparent OATP1B1-mediated $CL_{int,uptake}$ (**Fig. 2.2**).

Interestingly, for OATP1B1-expressing cells, Mock and OATP1B1_RIF cells, not only the slopes, but also the y-intercepts of uptake curves were considerably increased in the presence of HSA (**Fig. 2.1**; Suppl. Fig. 1 of (Yin et al., 2022)). The y-intercept under the 2% and 5% HSA conditions was approximately 2- and 5-fold of that in 1% HSA condition, respectively (**Fig. 2.3A-2.3E**).

2.4.3 *The Amount of HSA Non-Specifically Bound to the Cells/Labware Increased in the Presence of Increasing HSA Concentration*

Using quantitative targeted proteomics, we confirmed the presence of residual HSA in the cell lysate after the cells had been washed thrice with the ice-cold wash buffer (**Fig. 2.3F**). As was the case for the y-intercept (**Fig. 2.3A-2.3E**), the amount of HSA non-specifically bound to the cells/labware at 1 minute was directly proportional (1:1) to the HSA concentration used to conduct the uptake experiment (**Fig. 2.3F**).

2.4.4 *The Amount of Statin-HSA Complex Non-Specifically Bound to the Cells (except for Pitavastatin/OATP1B1 Cells or Cerivastatin/Mock Cells) Completely Explained the Increase in the Apparent Uptake in the Presence of 5% HSA*

The NSB of statin-HSA complex completely explained the increase in apparent uptake of ATV, FLV and RSV by OATP1B1-expressing, Mock and OATP1B1_RIF HEK293 cells in the presence of HSA (**Fig. 2.4A**, **2.4C**, **2.4E**; Suppl. Fig. 2A, 2C, 2E of (Yin *et al.*, 2022)). Surprisingly, the amount of PTV-HSA and CRV-HSA complex non-specifically bound to the OATP1B1-expressing cells/labware explained only 35% and 27% of the increase in total uptake in the presence of 5% HSA (*vs.* HBSS buffer) (**Fig. 2.4Di**, **2.4Bi**, **2.4Bii**), implying that the PMUE on total (passive + active) uptake of PTV and CRV is a real phenomenon. Moreover, in the presence of 5% HSA, the increase in passive uptake of PTV, but not that of CRV, was completely explained by NSB (**Fig. 2.4Dii**, **2.4Bii**; Suppl. Fig. 2D, 2B of (Yin et al., 2022)), implying the PMUE on only the OATP1B1-mediated PTV uptake and on passive uptake of CRV.

2.4.5 *PMUE on OATP1B1-Mediated Pitavastatin Uptake was Confirmed by its Lower Unbound OATP1B1 IC_{50} in the Presence vs. Absence of 5% HSA*

The unbound IC_{50} ($IC_{50,u}$) of PTV was decreased by more than 80% in the presence (p=0.03) of 5% HSA *vs.* HBSS buffer (**Fig. 2.5A**). Conversely, no difference in the $IC_{50,u}$ of ATV (negative control) was observed between HBSS and 2% HSA conditions (p=0.3) (**Fig. 2.5B**; due to solubility issues, these studies could not be conducted with 5% HSA). While the $IC_{50,u}$ of FLV could not be determined in the presence of HSA due to the same solubility issue, we did not observe greater inhibitory effect of FLV on RSV uptake in the presence *vs.* absence of HSA (**Fig. 2.5C**).

2.5 DISCUSSION

To our knowledge, this is the first study to show that, except for PTV, the previously reported *in vitro* PMUE on OATP1B1-mediated uptake of statins is likely an artifact caused by NSB of the statin-HSA complex to cells/labware. Such an artifact is not surprising. We were able to detect this artifact because we used a rigorous experimental strategy that included appropriate controls and measures not employed by others on the same subject. First, we estimated the PMUE on not only the total uptake of the statins, but also on OATP1B1-mediated and passive uptake of the statins. Second, we expressed ALL our data with respect to the media unbound statin concentration. Except for the $IC_{50,u}$ studies, these concentrations were maintained below the reported K_m for their OATP1B1-mediated transport (Lau *et al.*, 2006; Van De Steeg *et al.*, 2013; Izumi *et al.*, 2015; Mitra *et al.*, 2018). Third, we quantified by targeted quantitative proteomics, the NSB of HSA (after the cells were washed thrice) at each uptake time point for each HSA concentration used. This allowed us to estimate the confounding contribution of NSB of the statin-HSA complex (at 5% HSA) to the "apparent" PMUE on the OATP1B1-mediated and passive uptake of statins. Finally, to confirm or refute that the PMUE observed for the statins was an artifact, we determined the inhibitory capacity ($IC_{50,u}$) of selective statins (ATV, FLV and PTV) on OATP1B1-mediated RSV uptake in the absence and presence of HSA. If the PMUE is an artifact caused by NSB, the $IC_{50,u}$ of these statins should be invariant in the absence or presence of HSA. This is because the $IC_{50,u}$ of a drug (if the substrate concentration is $<K_m$) is determined ONLY by the local unbound drug concentration or the interaction of the drug and the protein (in this case OATP1B1) and not dependent on passive diffusion or NSB of the drug. If the PMUE is a real phenomenon, the $IC_{50,u}$ of the drug in the presence of plasma proteins should be significantly lower than that determined in the absence of plasma proteins.

Our finding of an increase in the slope (apparent $CL_{int,uptake}$) of the time course of statin uptake by the OATP1B1-expressing cells in the presence of HSA *vs.* HBSS (**Fig. 2.1**) is consistent with PMUE on OATP1B1-mediated apparent uptake of the statins reported by others (Kim *et al.*, 2019; Liang *et al.*, 2020; Bi *et al.*, 2021). To gain insight into the above observations, we deconvoluted the apparent PMUE on the OATP1B1-mediated uptake *vs.* that on passive uptake observed in the Mock and OATP1B1_RIF cells (**Fig. 2.2**).

Surprisingly, we found that the PMUE was much greater on passive uptake (in Mock or OATP1B1_RIF cells) compared with OATP1B1-mediated uptake of the statins (**Fig. 2.2**). In addition, the PMUE on passive uptake increased as the HSA concentration increased while this change was much more modest (as expected) for the active uptake of the statin (**Fig. 2.2**). These data are NOT consistent with the PMUE caused by the PLI mechanism since this mechanism would result in the magnitude of the PMUE that would be identical for both the apparent OATP1B1-mediated and passive uptake of the statins. In contrast, our observations are consistent with the NSB hypothesis provided the NSB is time-dependent (*i.e.* increases during the duration of the uptake experiments).

To confirm the NSB hypothesis, we quantified the amount of HSA remaining in the uptake experiments (*i.e.* NSB of HSA) at 1min. Not surprisingly, the amount of HSA remining in the cell lysate was proportional to the HSA concentration used in the incubation media (**Fig. 2.3F**). Moreover, over the duration of the uptake experiments, the amount of residual HSA increased with time (**Fig. 2.4**). Collectively, both these observations indicate that the so-called PMUE is likely an artifact of how uptake experiments are conducted. Indeed, as expected, NSB of the statin-HSA complex (5% HSA) to the cells/labware explained all the increase in ATV, FLV, and RSV uptake by OATP1B1-expressing cells at each time point of the uptake study (**Fig. 2.4**). Surprisingly, this was not the case for PTV or CRV (**Fig. 2.4Bi** and **2.4Di**). Since the uptake by the OATP1B1-expressing cells is a combination of active and passive uptake, we asked whether these observations were caused by a PMUE (or lack thereof) on the passive or active uptake of the statins or both. We found that the apparent PMUE on the uptake (both passive and active) of ATV, FLV, and RSV by OATP1B1-expressing cells was an artifact caused by NSB of the statin-HSA complex to the cells/labware (**Fig. 2.4A**, **2.4C** and **2.4E**). However, this was not the case for OATP1B1-mediated uptake of PTV (Fig. 4Di) or the total uptake of CRV (**Fig. 2.4Bi**, **2.4Bii**). Interestingly, the ratio of CRV-HSA NSB to CRV uptake increase was almost identical in OATP1B1-expressing cells (27%, **Fig. 2.4Bi**) *vs.* Mock cells (28%, **Fig. 2.4Bii**), suggesting the total CRV uptake increase in the presence of 5% HSA is predominantly due to an increase in passive uptake of CRV.

To confirm that the PMUE on OATP1B1-mediated PTV uptake is a real phenomenon, we determined the unbound inhibitory capacity ($IC_{50,u}$) of PTV towards OATP1B1 transport of RSV (**Fig. 2.5A**). As a negative control, we also determined the $IC_{50,u}$ of ATV and FLV because their apparent PMUE could be completely explained by NSB (**Fig. 2.5B-C**). The $IC_{50,u}$ of PTV decreased in the presence of HSA *vs.* HBSS but not for ATV (**Fig. 2.5A-B**). Due to the higher fraction of ATV bound to HSA and limitations caused by poor solubility of ATV, the $IC_{50,u}$ for ATV could be determined only at 2% HSA. For the same reasons, FLV $IC_{50,u}$ could not be determined in either 2% HSA or 5% HSA. Nevertheless, there was no clear difference between the ability of FLV to inhibit RSV uptake by OATP1B1-expressing cells in the absence or presence of HSA (**Fig. 2.5C**). Collectively, these results show that the presence of HSA results in a real PMUE on PTV, but not on ATV or FLV, uptake by OATP1B1. These results align well with the conclusions drawn from our proteomics data.

The above observations raise some intriguing questions. Why is the NSB of the statin-HSA complex time-dependent and not instantaneous? Is this because there is time-dependent endocytosis of the statin-HSA complex by the HEK293 cells? HEK293 cells do express the albumin receptor for endocytosis (Choi *et al.*, 1999; Urae *et al.*, 2020). Therefore, it is possible that the change in slope of the uptake curve of ATV, FLV and RSV, in the presence of HSA was due, at least in part, to endocytosis of statin-HSA complex. However, this mechanism should explain the PMUE for ALL the statins. It does not. Also, it cannot account for the decrease in OATP1B1 $IC_{50,u}$ of PTV in the presence of HSA and it is unable to explain why the proteomics data do not completely explain the apparent PMUE on passive uptake of CRV. Thus, other mechanisms must be invoked to explain our intriguing observations.

"Transporter-induced protein-binding shift (TIPBS)" has been proposed as another possible mechanism for the PMUE on OATP1B1/OATP1B3-mediated uptake of drugs (Baik and Huang, 2015; Bowman *et al.*, 2019). According to this mechanism, the PMUE should be observed for only high extraction drugs. However, this mechanism cannot explain the PMUE on passive uptake of CRV and the minimal PMUE on active uptake of RSV, a high extraction ratio drug (**Fig. 2.4**)(Billington *et al.*, 2019). In addition, PTV, for which PMUE is

observed, is a low extraction drug (NDA-022363, 2009). Finally, given that OATPs are known to be allosteric (Kindla *et al.*, 2011), does HSA, PTV-HSA complex or another constituent of HSA/plasma bind to the OATP1B1 transporter causing a conformational change of OATP1B1 resulting in a reduction in the $IC_{50,u}$ of PTV? Preliminary studies in our laboratory, using human plasma filtrate, did not produce any PMUE on OATP1B1-mediated uptake of statins including PTV or CRV (data not shown) suggesting that this is not a viable hypothesis.

A key question is whether our findings apply to other statins (e.g. pravastatin) or other OATP1B1 substrate drugs, when OATP1B1 cells or human hepatocytes are used to determine drug uptake. Published data using hepatocytes show an increase in the intercept of uptake curves, a PMUE on both active and passive uptake of drugs with the effect on passive uptake being greater than the active uptake of the drugs (Miyauchi *et al.*, 2018; Bowman *et al.*, 2020; Liang *et al.*, 2020; Bi *et al.*, 2021; Li *et al.*, 2021). Overall, these observations imply the NSB of drug-protein complex may occur when using hepatocytes. There is no clear evidence that hepatocytes demonstrate endocytosis of albumin. Thus, whether the PMUE in hepatocytes is affected by endocytosis or NSB needs further investigation (in **CHAPTER 3**).

Our studies do have some limitations. First, to quantify the amount of statin-HSA complex to the cells/labware, we assumed that the binding of the statin to albumin at the cell surface was the same as that measured *in vitro* using ultrafiltration. If the latter underestimated unbound drug concentration at the cell surface, it may explain the PMUE observed on CRV (**Fig. 2.4B**; Suppl. Fig. 2B of (Yin *et al.*, 2022)). If this explanation is correct, it is puzzling that this PMUE was not of equal magnitude on the active *vs.* passive uptake of CRV (Suppl. Table 2 of (Yin *et al.*, 2022)). Moreover, this explanation cannot explain our PTV data as the passive uptake of PTV was completely explained by NSB. Second, whether our observations will translate to plasma or other transporters is unknown. There could be protein constituents in plasma other than albumin that may result in a true PMUE on OATP1B1 drug uptake (but see above for our preliminary data).

While many questions remain, here we aim to raise concerns about interpretation of the so called PMUE on OATP1B1 drug uptake reported by others. Notably, in the last four years, more than 20 reports (too numerous to cite) have been published that the PMUE on OATP1B1 drug uptake is a real phenomenon. But, none of them have considered the possibility that this could be an artifact of NSB of the drug-protein complex to the cells/labware. If the PMUE for OATP1B1 drug substrates is an artifact, it is not necessary to include albumin or plasma in OATP1B1-mediated uptake experiments because such inclusion unnecessarily complicates uptake studies and considerably raises their cost. In addition, including the PMUE in IVIVE does not appear to result in successful predictions of transporter-based CL_h (Kim *et al.*, 2019; Li *et al.*, 2020, 2021; Bi *et al.*, 2021). Therefore, future focus should be delineating the underlying mechanisms causing the underprediction of OATP-mediated CL_h.

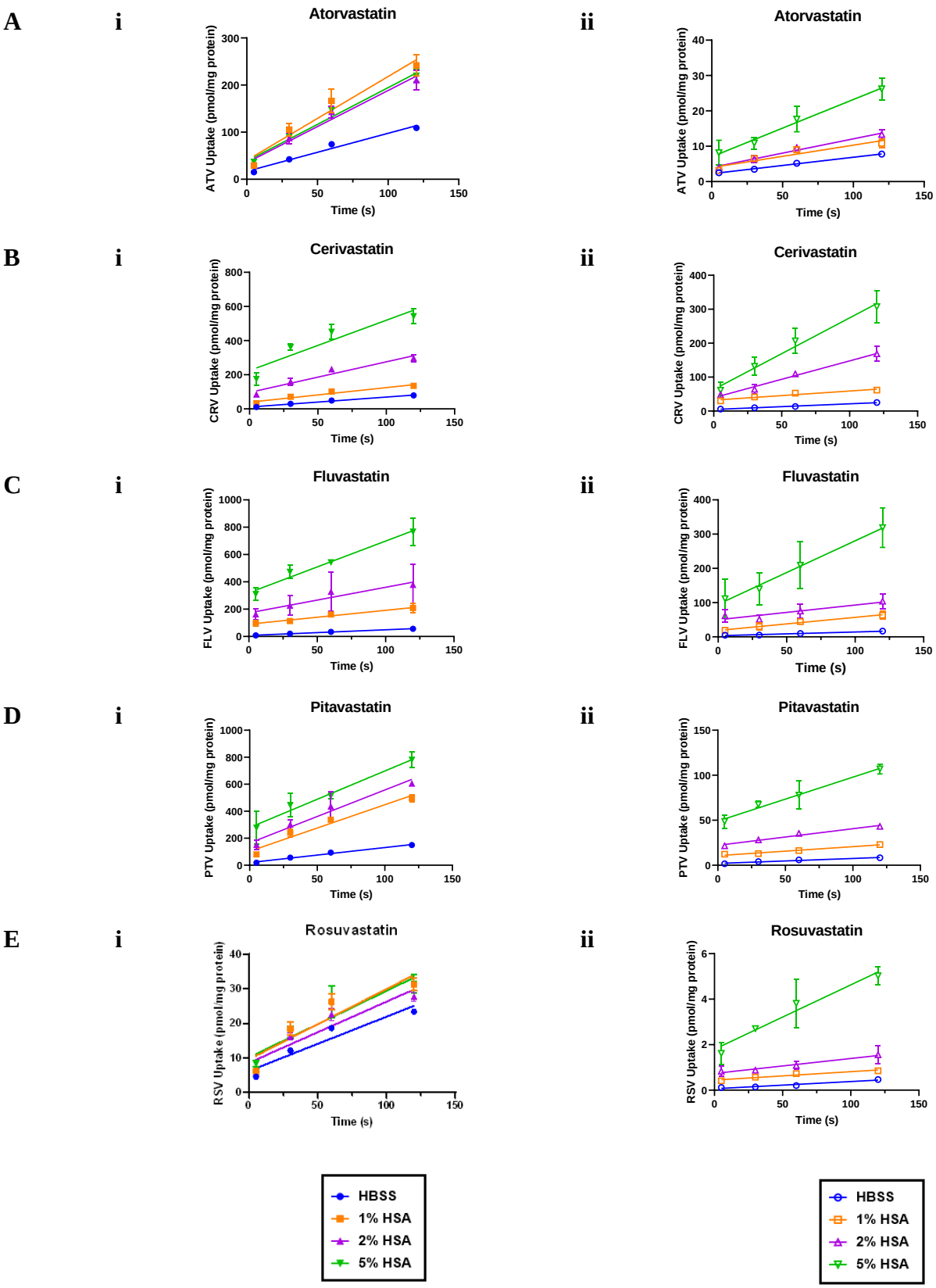

Figure 2.1. The statin uptake-time profiles for OATP1B1-expressing (left panel) and Mock HEK293 cells (right panel).

The increase in the slope of the uptake curves in the presence of HSA vs. HBSS suggests a PMUE on the $CL_{int,uptake}$ of the statins. The increased intercept in the presence of HSA indicates NSB of statin-HSA complex to the cells/labware. Data shown are mean ± standard deviation (SD) of statin uptake (normalized to 1 μM unbound concentration) and are representative of three to five independent experiments, each conducted in triplicate at each time point.

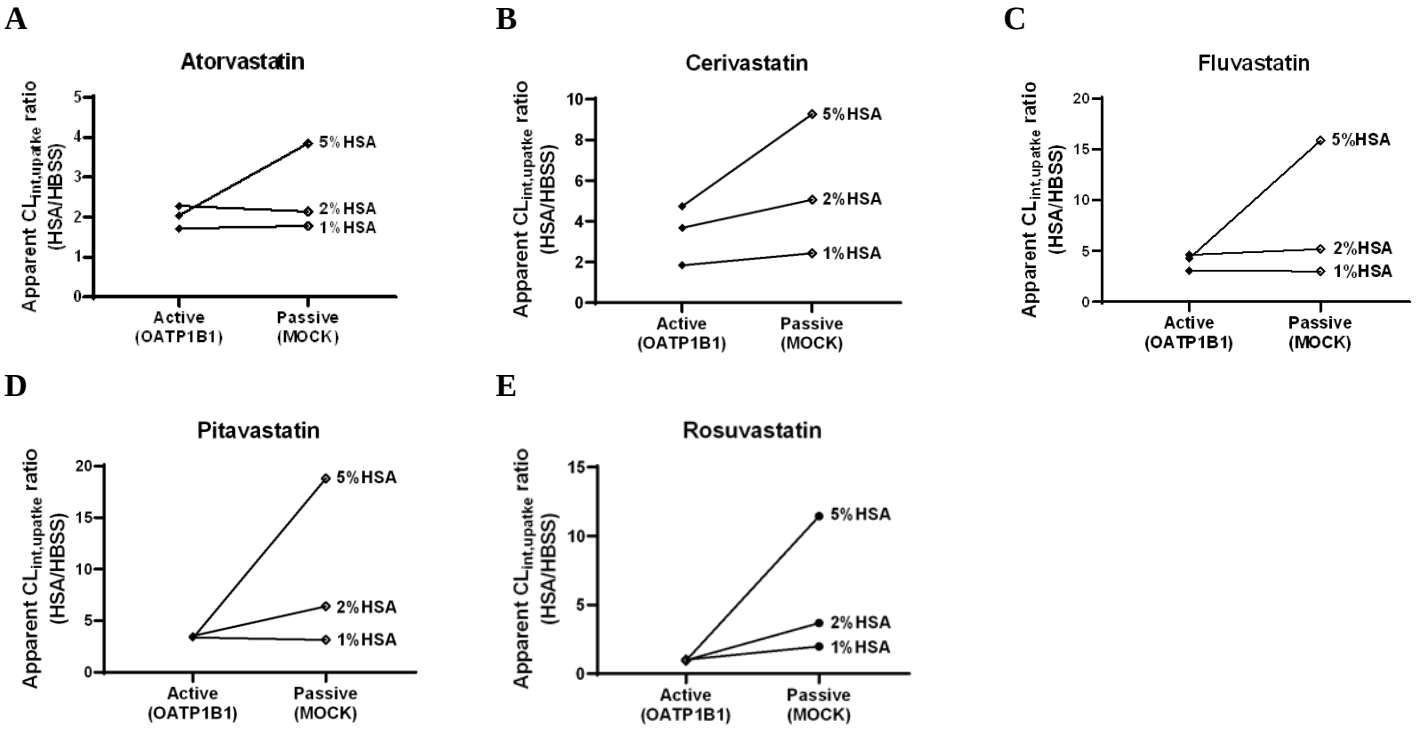

Figure 2.2. The ratio of the apparent active and passive $CL_{int,uptake}$ of the statins in the presence of HSA *vs.* HBSS.

These data indicate that the PMUE on $CL_{int,uptake}$ of the statins was greater on passive *vs.* OATP1B1-mediated uptake. Data shown are mean of 3-5 independent experiments.

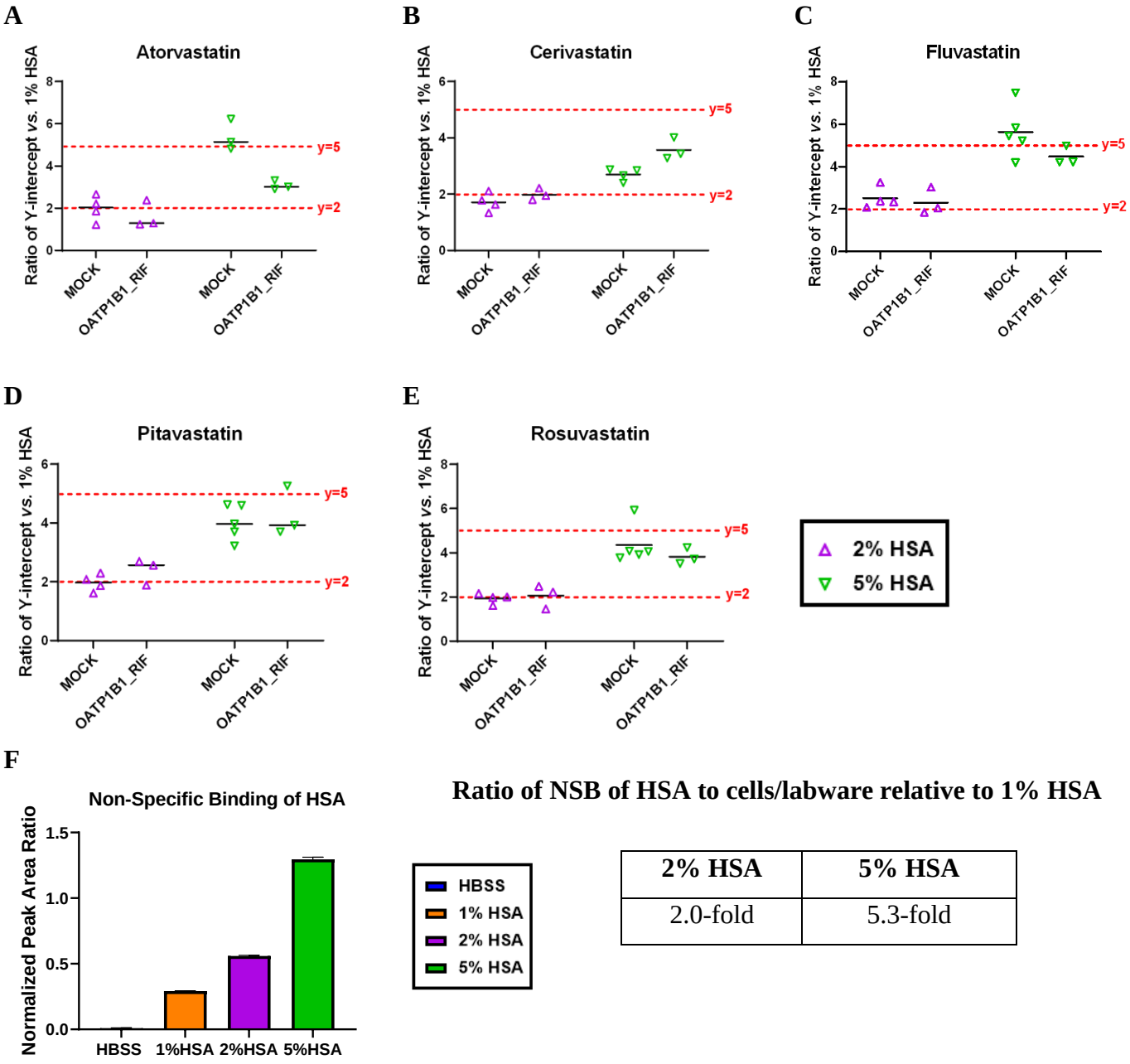

2% HSA	5% HSA
2.0-fold	5.3-fold

Figure 2.3. The ratio of Y-intercept of the uptake curve for the 2% or 5% HSA conditions (*vs.* 1% HSA), for ATV (A), CRV (B), FLV (C), PTV (D), and RSV (E) uptake by the Mock or OATP1B1_RIF HEK293 cells.

In general, the intercept increased in proportion to the % of HSA used (A-E) indicating NSB of the statin-HSA complex to the cells/labware. This was subsequently confirmed by quantifying the relative amount of HSA remaining in the cell lysate (2% HSA or 5% HSA *vs.* 1% HSA) as quantified at 1 minute by the peak area ratio (PAR) of the HSA and Na^+K^+-ATPase peptide (membrane marker) using targeted proteomics (F). Data shown in F are mean ± SD and are representative of three independent experiments, each conducted in triplicate.

OATP1B1-expressing HEK293 cells | **Mock HEK293 cells**

A **i**

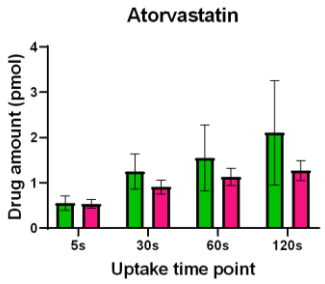

ii

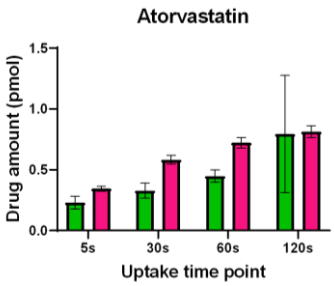

B **i**

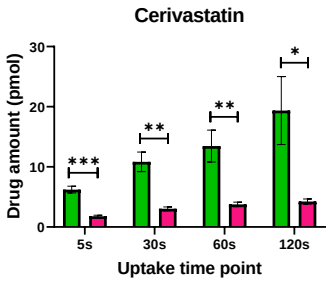

ii

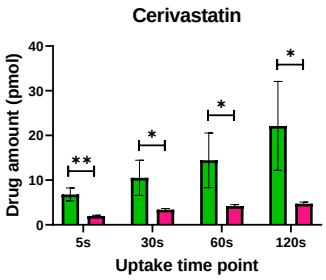

C **i**

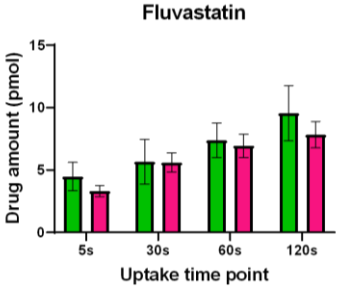

ii

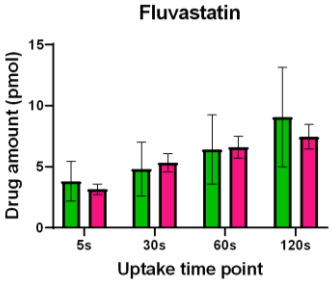

D **i**

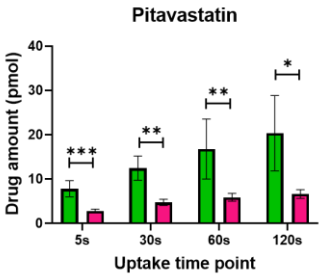

ii

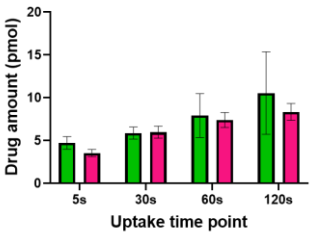

E **i**

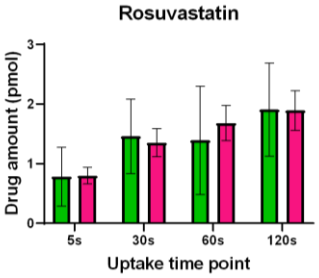

ii

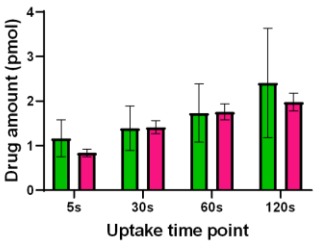

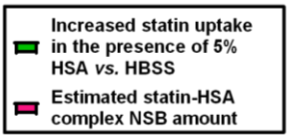

Figure 2.4. Comparison of the amount of statin non-specifically bound to the cells (as statin-HSA complex; pink bars) and the increase in statin taken up by OATP1B1-overexpressing (Ai-Ei) or Mock (Aii-Eii) HEK293 cells in the presence of 5% HSA *vs.* HBSS (green bars).

The increase in the uptake of ATV, FLV and RSV in the presence of 5% HSA (vs. HBSS) can be completely explained by the NSB of the stain-HSA complex to the OATP1B1-expressing or Mock HEK293 cells. However, this was not the case for PTV (OATP1B1-expressing cells) or CRV (both cells). The uptake data shown have been corrected for small differences in unbound concentration and total protein content between each experiment. Data shown are mean ± SD of three independent experiments, each conducted in triplicate. Statistical comparison between the increase in statin uptake in the presence of 5% HSA and NSB was performed using the Student's t test (* p <0.05; ** p<0.01; *** p<0.001).

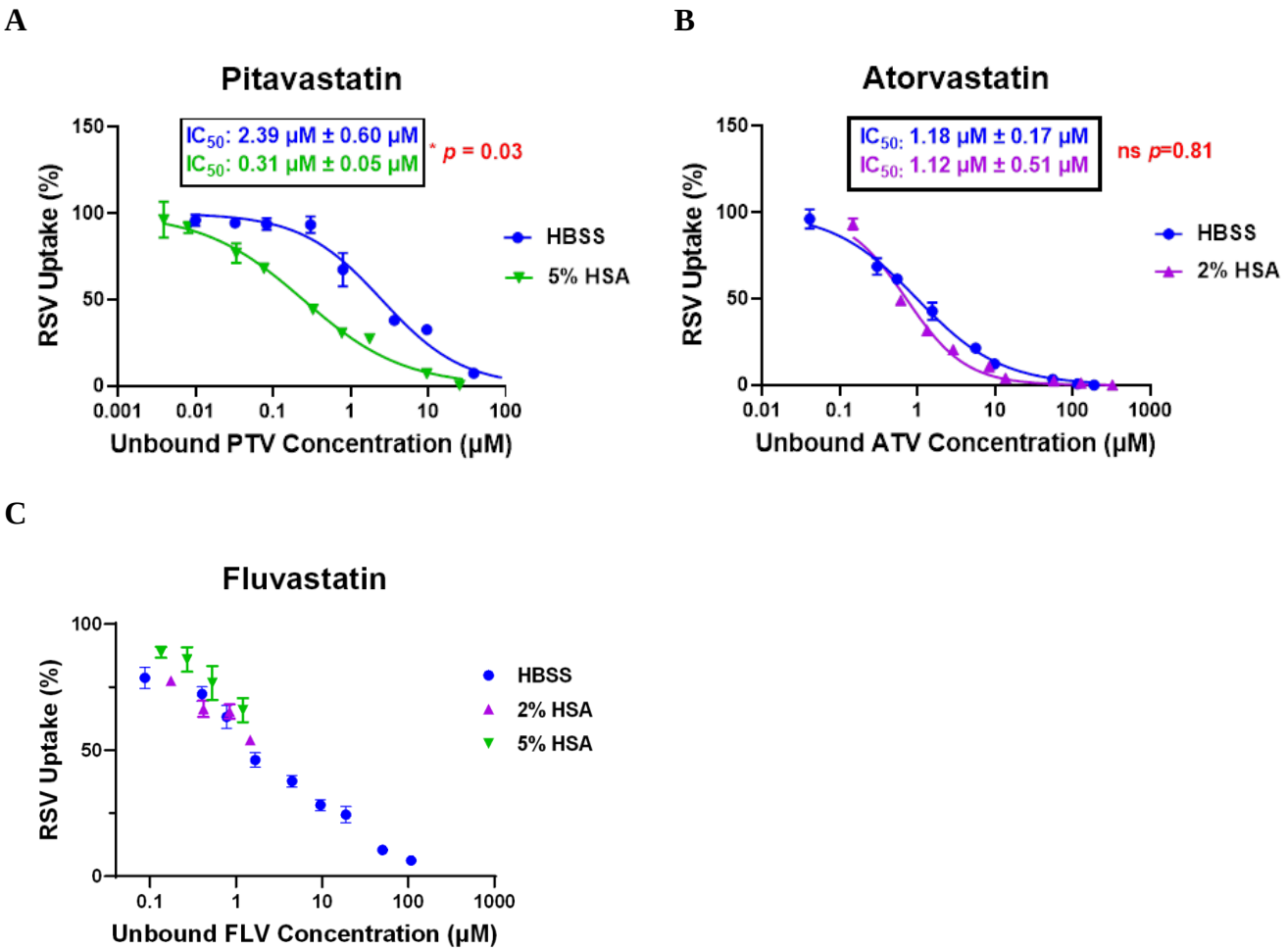

Figure 2.5. Unbound OATP1B1 IC_{50} ($IC_{50,u}$) of PTV (A) or ATV (B) and inhibition of OATP1B1 by various concentrations of FLV (C), using RSV as a substrate.

The $IC_{50,u}$ of PTV decreased in the presence of HSA while that of ATV did not. In addition, OATP1B1 inhibition by FLV in the presence of HSA was not different from that in HBSS. These data suggest that the PMUE on OATP1B1-mediated PTV uptake appears to be a real phenomenon. % RSV uptake was the OAPT1B1-mediated uptake, i.e. the total % RSV uptake corrected for the % passive uptake of RSV (see methods). The data shown are mean ±SD and representative of three independent experiments, each conducted in triplicate. Solid line is the model fit to the data. $IC_{50,u}$ data shown are mean ±SD of three independent experiments, each conducted in triplicate. *$IC_{50,u}$ in the presence of HSA *vs.* HBSS (A, B) was statistically compared using the paired Student's t test.

2.6 ABBREVIATIONS USED

ATV, atorvastatin; BCA, bicinchoninic acid assay; CL, clearance; CL_h, hepatic clearance; $CL_{int,uptake}$, intrinsic uptake clearance; CRV: cerivastatin; DCL, diclofenac sodium salt; DMEM, Dulbecco's modified Eagle's medium; DMSO, dimethyl sulfoxide; DTT, dithiothreitol; FBS, fetal bovine serum; FLV, fluvastatin; HBSS, Hank's balanced salt solution; HEK, human embryonic kidney; HPLC, high-performance liquid chromatography; HSA, human serum albumin; IAA, iodoacetamide; IC_{50}, inhibitor concentration that produces 50% inhibition of uptake; IVIVE, *in vitro* to *in vivo* extrapolation; LC-MS/MS, liquid chromatography tandem mass spectrometry; NSB, non-specific binding; OATP, organic anion transporting polypeptide; PLI, protein-lipid interaction; PMUE, protein-mediated uptake effect; PTV, pitavastatin; RIF, rifampicin; RSV, rosuvastatin; SDS, sodium dodecyl sulfate.

Chapter 3. INTERPRETATION OF PROTEIN-MEDIATED UPTAKE OF STATINS BY HEPATOCYTES IS CONFOUNDED BY THE RESIDUAL STATIN-PROTEIN COMPLEX

The work presented in this chapter was previously published in *Drug Metabolism and Disposition 2023 Oct;51(10):1381-1390.* Mengyue Yin is the first author, participating in the research design, conducting experiments, performing data analysis, and writing the manuscript. Kazuya Ishida, Xiaomin Liang, Yurong Lai, and Jashvant D. Unadkat contributed to the research design and the writing of the manuscript.

3.1 ABSTRACT

Inclusion of plasma (or plasma proteins) in human hepatocyte uptake studies narrows, but does not close, the gap in *in vitro* to *in vivo* extrapolation (IVIVE) of organic anion transporting polypeptide (OATP)-mediated hepatic clearance (CL_h) of statins. We have previously shown that this "apparent" protein-mediated uptake effect (PMUE) of statins by OATP1B1-expressing cells, in the presence of 5% human serum albumin (HSA), is mostly an artifact caused by residual statin-HSA complex remaining in the uptake assay (**CHAPTER 2**). We determined if the same was true with plated human hepatocytes (PHH), and if this artifact can be reduced using suspended human hepatocytes (SHH) and the oil-spin method. We quantified the uptake of a cocktail of five statins by PHH and SHH in the absence and presence of 5% HSA. After terminating the uptake assay, the amount of residual HSA was quantified by quantitative targeted proteomics. For both PHH and SHH, except for atorvastatin and cerivastatin, the increase in total, active and passive uptake of the statins, in the presence of 5% HSA, was explained by the estimated residual stain-HSA complex. In addition, the increase in active statin uptake by SHH, where present, was marginal (<50%); much smaller than that observed with PHH. Such a marginal increase cannot bridge the gap in IVIVE of CL_h of statins. These data disprove the prevailing hypotheses for the *in vitro* PMUE. A true PMUE should be evaluated using the uptake data corrected for the residual drug-HSA complex.

3.2 INTRODUCTION

Accurate *in vitro* to *in vivo* extrapolation (IVIVE) of transporter-mediated hepatic clearance (CL_h) is important in drug development. Human hepatocytes, incubated with protein-free drug buffer, are routinely employed to estimate *in vitro* hepatic intrinsic uptake drug clearance ($CL_{int,uptake}$). Then, physiological scaling factors and hepatic CL models (e.g. the well-stirred model), are used to extrapolate the $CL_{int,uptake}$ to *in vivo* CL_h. A key assumption made in this IVIVE is that uptake of the drug is the rate-determining step in CL_h. Irrespective of whether this assumption is made, such IVIVE of transporter-mediated CL_h of organic anion transporting polypeptide (OATP) substrates (e.g. statins) has been significantly underpredicted (Soars *et al.*, 2007; Jones *et al.*, 2012; Kim *et al.*, 2019; Kumar *et al.*, 2021; Storelli *et al.*, 2022). One reason for such under-prediction could be that the *in vitro* hepatocyte uptake studies do not include blood constituents (e.g. plasma proteins) that may modulate OATP-mediated uptake of drugs. Indeed, when plasma or plasma proteins (e.g. human serum albumin, HSA) are included in the *in vitro* uptake assays, the $CL_{int,uptake}$ of highly protein-bound OATP drug substrates (e.g. statins), by human hepatocytes or OATP-expressing cells, is enhanced. This phenomenon is called the "protein-mediated uptake effect (PMUE)" (Kim *et al.*, 2019; Liang *et al.*, 2020; Bi *et al.*, 2021; Li *et al.*, 2021; Miyauchi *et al.*, 2021; Schulz *et al.*, 2023).

Several potential mechanisms for the PMUE have been proposed. In general, they can be categorized as: 1) protein-lipid interaction (PLI) (or facilitated dissociation model (FDM)) where the drug-protein complex interacts with the cell membrane and causes a conformational change in the protein, leading to the release of the bound drug. As a result, under the free-drug hypothesis, both the local unbound drug concentration, as well as passive and active uptake of the drug should be equally increased (Kim et al., 2019; Miyauchi et al., 2018). 2) Transporter-induced protein binding shift (TIPBS) occurs where the highly efficient transporter strips the bound drug from the protein (Bowman *et al.*, 2019). In this case, only the transporter-mediated uptake of the drug will increase but the passive uptake of the drug will not. However, none of these hypotheses are compatible with our observations or those of others in OATP-expressing cells and hepatocytes, respectively (Bowman *et al.*, 2020; Liang *et al.*, 2020; Yin *et al.* 2022). We (Yin *et al.*, 2022) (in **CHAPTER 2**) and others (Bowman *et al.*, 2020) have found that the PMUE on transporter-mediated (active) and passive uptake of drugs is not equal; the

latter is much greater than the former. In addition, in the presence of plasma proteins, the y-intercept of the drug uptake-time profile is considerably increased suggesting non-specific binding (NSB) of the drug-protein complex to the cells or labware (Kim *et al.*, 2019; Bi *et al.*, 2021).

The above observations led us to test the hypothesis that the so-called PMUE is confounded by residual albumin-drug complex in the uptake experiments (**Fig. 3.1**). Typically, drug uptake by plated OATP-expressing cells or hepatocytes is terminated by washing with ice-cold buffer thrice and the cells are lysed to determine the remaining drug. A key assumption made is that the remaining drug is predominately or exclusively taken up by the cells. However, it is impossible to distinguish between residual drug or drug-protein complex outside the cells from that taken up by the cells. When determining the PMUE, due to extensive plasma protein binding of the OATP substrate drugs, to maintain sufficient unbound drug concentration in the media, the total concentration of the drug is kept high compared to unbound drug. Thus, even a tiny fraction of any residual drug-protein complex can significantly, but erroneously, contribute to the quantity of drug taken up by the cells (**Fig. 3.1A**). That is, it can be erroneously interpreted as an increase in drug uptake into the cells and therefore an "apparent" PMUE.

To test the above hypothesis, in **CHAPTER 2** we investigated the uptake of a cocktail of five statins (atorvastatin, ATV, cerivastatin, CRV, fluvastatin, FLV, pitavastatin, PTV and rosuvastatin, RSV) by plated OATP1B1-transfected and Mock-transfected human embryonic kidney (HEK) 293 cells, in the absence and presence of human serum albumin (HSA) (Yin, Storelli, and Jashvant D. Unadkat, 2022). Consistent with our hypothesis, there was considerable amount of residual HSA (quantified by targeted proteomics) in the plate that was not removed by washing the cells thrice with ice-cold protein-free buffer. In addition, the estimated amount of statin remaining, bound to albumin (statin-HSA complex), could fully explain the observed increase in statin uptake (both active and passive) of most of the statins studied (ATV, FLV and RSV). In addition, for all the statins, the apparent PMUE was greater on the passive uptake CL *vs.* active uptake CL of the statin. These findings demonstrate that the observed *in vitro* apparent PMUE is largely confounded by the residual statin-HSA complex in the uptake assays under this cocktail assay condition and short uptake time (up to 2 min) (Yin *et al.*, 2022).

In drug development, $CL_{int,uptake}$ is routinely determined by using suspended (SHH) or plated (PHH) human hepatocytes. Therefore, it is important to determine if the apparent PMUE observed using these approaches is also confounded by any residual statin-protein complex (Miyauchi *et al.*, 2018; Li *et al.*, 2020; Liang *et al.*, 2020; Bi *et al.*, 2021). This question is particularly interesting for SHH as they are used more frequently to determine drug $CL_{int,uptake}$ and utilize a different uptake-termination strategy. This strategy involves rapid separation of the SHH from the uptake buffer by centrifuging the cells through an oil layer. We hypothesized that using this strategy will reduce or eliminate the apparent PMUE because the drug-protein complex may not be centrifuged through the oil layer (**Fig. 3.1B**). The aims of the present study (**CHAPTER 3**) were designed to answer the above questions. To do so, we first determined the total, active and passive $CL_{int.uptake}$ of a cocktail of five statins, in the absence (protein-free buffer) and presence of 2% or 5% HSA. Second, the apparent PMUE (*i.e.* $CL_{int.uptake}$ ratio in the presence *vs.* absence of HSA) on total, active and passive uptake of five statins was estimated and compared. Third, the amount of residual HSA after terminating statin uptake into the PHH or SHH was quantified by quantitative targeted proteomics. Finally, we determined how much of the apparent PMUE could be explained by the residual statin-HSA complex. For brevity, any residual statin-HSA complex will henceforth be referred to as residual statin.

3.3 MATERIALS AND METHODS

Most of the experimental procedures and bioanalysis methods used here are detailed in our previous companion article (**CHAPTER 2,** (Yin *et al.*, 2022)) and therefore are only briefly outlined here.

3.3.1 *Chemicals and Reagents*

The dithiothreitol (DTT), iodoacetamide (IAA), Pierce™ RIPA Buffer, mass spectrometry grade trypsin, total protein quantification bicinchoninic acid assay (BCA) kit were obtained from Thermo Scientific (Rockford, IL). Atorvastatin (ATV), cerivastatin (CRV), fluvastatin (FLV), pitavastatin (PTV), rosuvastatin (RSV), diclofenac sodium salt (DCL), rifampin (RIF), human serum albumin (HSA, fatty acid free, purity $\geqslant$ 96%), silicone oil, mineral oil and formic acid were purchased from Sigma-Aldrich (St. Louis, MO). Bovine serum albumin (BSA) were purchased from MP Biomedicals (Solon, OH). Synthetic signature peptides for HSA were obtained from New England Peptides (Boston, MA). Hank's Balanced Salt Solution (HBSS), High-performance liquid chromatography (HPLC)-grade acetonitrile and sodium dodecyl sulfate (SDS) were purchased from Fischer Scientific (Fair Lawn, NJ). All reagents were analytical grade. The Calbiochem ProteoExtract Native Membrane Extraction Kit and the Centrifree® Ultrafiltration Device was purchased from EMD Millipore Corporation (Billerica, MA). Corning™ BioCoat™ Collagen I 48-well Plates were purchased from Corning (Kennebunk, ME). Cryopreserved human hepatocytes (Lots AOS, FEA, and YTW; see Suppl. Table 1 of (Yin *et al.*, 2023) for demographics), In VitroGRO HT, In VitroGRO CP medium, and Krebs-Henseleit buffer (KHB) were obtained from BioIVT (Hicksville, NY).

3.3.2 *Uptake of Statins by Plated Human Hepatocytes (PHH) in the Absence or Presence of 5% HSA*

The uptake of statins by PHH (Lots AOS, FEA and YTW) was determined as described previously with some modifications (Kumar *et al.*, 2019, 2021). In brief, cryopreserved hepatocytes were thawed at 37°C in InVitroGro-HT media and seeded into collagen I–coated 48-well plates with 0.14×10^6 cells/well in a volume of 200 μL/well in InVitroGro-CP media. The hepatocytes were cultured at 37°C for 6 hours with 5% CO_2 in a

humidified incubator. Prior to the uptake assays, the hepatocytes and uptake media, including the cocktail of statins, were equilibrated at 37°C or 4°C for at least 15 minutes. The uptake media contained approximately unbound concentration of ATV 0.1 µM, CRV 0.05 µM, FLV 0.1 µM, PTV 0.1 µM and RSV 0.5 µM in HBSS (protein-free) or 5% HSA. Five % HSA (w/v, g/dL) was used as this is within the HSA concentrations observed in human blood (3.5-5.0 g/dL) (Moman *et al.*, 2022). In 5% HSA, the approximate total concentration of ATV, CRV, FLV, PTV and RSV were 1.8 µM, 2.2 µM, 33.3 µM, 12.5 µM and 3.8 µM, respectively. For the uptake assay conducted at 4°C, rifampin (unbound concentration 500 µM), was included in the uptake buffer to ensure complete inhibition of OATP transporter activity. Dimethyl sulfoxide (DMSO) was used as a solvent (<1%) to dissolve the statins and rifampin and this concentration was kept constant for all incubations. Statin uptake was initiated by adding the uptake buffer (250 µL) to the PHH. At designated time points (30s, 60s or120s; a period over which the uptake was found to be linear), uptake was terminated by aspirating the uptake solution, and rinsing the PHH with 3× with 500 µL ice-cold HBSS per well. Then, the cells were lysed either with a quenching buffer (500 µL/well, 50% acetonitrile + 50% water containing 10 nM diclofenac as the internal standard) for statin quantification or lysed with 1:1 ratio (v/v) of 2% SDS: Extraction Buffer II (from the Calbiochem membrane extraction kit; 100 µL/well) for 1 hour at 4°C for residual albumin quantification by LC-MS/MS as described in **CHAPTER 2** (Yin *et al.*, 2022). For every experiment, extra wells were included for total protein quantification by the BCA assay. Three to four independent experiments were conducted, each in triplicate. The total, unbound (and bound) statin concentration in the uptake media (HBSS or HSA) in every uptake assay was measured by ultrafiltration as described in **CHAPTER 2** (Yin *et al.*, 2022). The estimate of the unbound fraction considered any non-specific binding of the statins to the ultrafiltration equipment.

3.3.3 *Uptake of Statins by Suspended Human Hepatocytes (SHH) in the Absence or Presence of HSA*

3.3.3.1 Blank oil-spin assay

One hundred microliter aliquot of a prewarmed (37°C) cocktail of five statins containing approximately unbound 0.05 µM ATV, 0.025 µM CRV, 0.05 µM FLV, 0.05 µM PTV and 0.25 µM RSV) in KHB (protein-

free) or in the presence of 1%, 2% or 5% HSA was loaded onto a microcentrifuge tube containing 100 µL of silicone–mineral oil mixture (v/v 5:1 ratio, density of 1.015 g/ml) layered over 100 µL of 3 M ammonium acetate. The tube was immediately centrifuged at 16,900 g for 14 seconds and then placed on dry ice. The bottom frozen layer was cut (approximately 30 µL) and vortex-mixed with either 600 µL of a quenching solution (50% acetonitrile + 50% water containing 10 nM diclofenac as the internal standard) for statin quantification or 100 µL Pierce™ RIPA Buffer for residual albumin quantification. Three independent experiments were conducted, each in triplicate or quadruplicate. The total, unbound (and bound) statin concentration in the uptake buffer (HBSS or HSA) in every uptake assay was measured by ultrafiltration and LC-MS/MS as described in **CHAPTER 2**(Yin *et al.*, 2022).

3.3.3.2 High-density oil (HDO) assay

Prior to the uptake experiments, hepatocytes (lot AOS and YTW) at cell density of 2×10^6 cells/ml or the uptake buffer containing 2× unbound statin concentration (approximately 0.1 µM ATV, 0.05 µM CRV, 0.1 µM FLV, 0.1 µM PTV and 0.5 µM RSV) in KHB (protein-free) or in the presence of 10% HSA were incubated at 37°C or in an ice-cold water bath for 15 minutes. Uptake was initiated by adding the uptake media to the hepatocyte suspension (1:1 in v/v), resulting in 1× final unbound statin concentration (approximately 0.05 µM ATV, 0.025 µM CRV, 0.05 µM FLV, 0.05 µM PTV and 0.25 µM RSV) in KHB or 5% HSA and final cell density of 1×10^6 cells/ml. At 15s, 30s, or 60s, uptake was terminated by immediately aliquoting 100 µL of the incubation mixture into a microcentrifuge tube containing two layers. The upper layer contained 100 µL of silicone oil and mineral oil (v/v 8:1 ratio, density 1.027 g/ml) and the bottom layer contained 100 µL of 3 M ammonium acetate to lyse the cells. The microcentrifuge tubes were immediately centrifuged at 16,900 g for 14 seconds and then placed on dry ice. The bottom frozen layer containing the hepatocytes was cut (approximately 30 µL) and vortex-mixed with either 600 µL of a quenching solution (50% acetonitrile + 50% water with 10 nM diclofenac as internal standard) for statin quantification or 100 µL Pierce™ RIPA Buffer for residual albumin quantification as described in **CHPATER 2** (Yin *et al.*, 2022). Three independent experiments were conducted, each in triplicate or quadruplicate. The total, unbound (and bound) statin concentration in the uptake media

(HBSS or HSA) in every uptake assay was measured by ultrafiltration and LC-MS/MS as described in **CHPATER 2** (Yin *et al.*, 2022).

3.3.3.3 Standard-density oil (SDO) assay

The above *high-density oil* experimental procedure was repeated except that the oil layer was 5:1 v/v (density 1.015 g/ml) and the final HSA concentration was 2%.

3.3.4 *Data Analyses*

3.3.4.1 Determination of Apparent Transporter-Mediated and Passive Intrinsic Uptake Clearance ($CL_{int,uptake}$) of Statins

The initial uptake rate was estimated from the slope of the statin uptake *vs.* time profile (total: 37°C; passive: 4°C +/- RIF) using simple linear regression in GraphPad Prism version 9 (GraphPad Software, San Diego, CA). The apparent $CL_{int,uptake}$ was calculated as the ratio of the initial uptake rate and the measured unbound statin concentration in HBSS or HSA. Given the unbound statin concentration slightly varied across different experiments, the uptake data presented in the figures were normalized to a nominal 1 μM unbound concentration of each statin to allow comparison across the statins. The apparent active $CL_{int,uptake}$ was calculated by subtracting the apparent passive $CL_{int,uptake}$ from the apparent total $CL_{int,uptake}$.

3.3.4.2 Estimation of the Amount of Residual Statin-HSA Complex in the Cell Lysates in the Presence of HSA

The amount of residual statin-HSA complex after washing/centrifuging at each uptake time point was estimated as follows:

Residual statin-HSA complex post washing/centrifugation (pmol/well or tube) = Statin-HSA complex in the uptake media (pmol/well or tube) $\times \frac{\text{Residual HSA amount post}-\text{washing/centrifugation (pmol/well or tube)}}{\text{Total HSA amount in the uptake media (pmol/well or tube)}}$ **Eq. 3.1**

Where the total HSA amount per well or tube was calculated based on HSA molecular weight of 69367 g/mol (https://www.uniprot.org/uniprot/P02768). The amount of residual HSA post-washing/centrifugation was calculated by subtracting the residual HSA amount in the buffer condition from that in the HSA condition. The

residual HSA was quantified by quantitative targeted proteomics as described in **CHPATER 2** (Yin *et al.*, 2022). Then, the amount of bound statin as the statin-HSA complex was calculated as follows:

Bound statin (pmol/well or tube) = [Total statin concentration (µM) - unbound statin concentration (µM)] × 250 µL/well (PHH) or 100 µL/tube (SHH) **Eq. 3.2**

3.3.4.3 Calculation of Increased Apparent Uptake in the Presence vs. Absence of HSA

To take into consideration the small variation in the measured unbound statin concentration and the total protein content in HSA *vs.* HBSS or KHB uptake studies, statin uptake at each time point in these studies was corrected (**Eq. 3.3**) for these variables before estimating the increased apparent uptake in the presence *vs.* absence of HSA.

$$\text{Normalized statin uptake in HBSS or KHB (pmol/well or tube)} = \text{Apparent statin uptake in HBSS or KHB (pmol/well or tube)} \times \frac{\text{Unbound statin concentration in HSA (µM)}}{\text{Unbound statin concentration in HBSS or KHB (µM)}} \times \frac{\text{Total protein amount in HSA (mg/well)}}{\text{Total protein amount in HBSS (mg/well)}} \quad \textbf{Eq. 3.3}$$

Where the unbound statin concentration was measured using ultrafiltration and the total protein amount in the cell well was determined by the BCA assay. Of note, total protein content was normalized only for PHH. For SHH, the hepatocyte number was assumed to be identical (1×10^6 cells/ml) between KHB and HSA. Then, the increase in statin uptake in the presence of HSA *vs.* HBSS or KHB at each time point was estimated as follows:

Increased apparent uptake in the presence of HSA *vs.* HBSS or KHB (pmol/well or tube) = Apparent statin uptake in the presence of HSA (pmol/well or tube) - Normalized statin uptake in HBSS (pmol/well or tube)

Eq. 3.4

3.3.4.4 Statistical Analyses

Estimates of residual statin amount and the measured increase in statin uptake in the presence of HSA (**Fig. 3.3** & **3.5** & **3.6**; Suppl. Fig. 2&3&5&6 of (Yin *et al.*, 2023)), the residual albumin amount at different uptake time points (Suppl. Fig. 7B of (Yin *et al.*, 2023)), the $CL_{int,uptake}$ values with 5% HSA/HDO *vs.* 2% HSA/SDO (Suppl. Fig. 7C of (Yin *et al.*, 2023)), the Na^+K^+-ATPase quantification with HDO *vs.* SDO (Suppl. Fig. 7D of (Yin *et*

al., 2023)), were statistically compared by the unpaired t-test using GraphPad Prism version 9 (GraphPad Software, San Diego, CA).

3.4 RESULTS

3.4.1 *The Presence of HSA Increased the Apparent Active and Passive Uptake of Statins into PHH*

For all three hepatocyte lots, the slopes of the statin uptake – time profiles increased in the presence of 5% HSA *vs.* HBSS, suggesting an apparent PMUE on statin uptake into PHH (**Fig. 3.2;** Suppl. Fig. 1 of (Yin *et al.*, 2023)). Except for CRV, the ratio of the $CL_{int,uptake}$ (HSA/HBSS), interpreted as the PMUE, was smaller for active uptake (e.g. 1.0- to 7.1-fold for lot AOS) *vs.* passive uptake (e.g. 3.3- to 26.7-fold for lot AOS) (**Table 3.1A**; Suppl. Table. 2&3A of (Yin *et al.*, 2023)). Consequently, the % active uptake of the statins decreased in the presence of 5% HSA. The effect of 5% HSA on active uptake was greatest for CRV (6- to 7-fold). Except for RSV, the apparent PMUE on passive uptake correlated with the degree of statin protein-binding (**Fig. 3.3A**; Suppl. Fig. 2A&3A of (Yin *et al.*, 2023)). As expected, consistent with our previous finding, not only the slope, but also the y-intercept of the uptake curves was considerably increased in the presence of HSA (**Fig. 3.2**; Suppl. Fig. 1 of (Yin *et al.*, 2023)). Our data showed consistent trends across the three PHH lots (**Table 3.1A** *vs.* Suppl. Table. 2&3A of (Yin *et al.*, 2023)).

Table 3.5. Apparent PMUE on intrinsic hepatic uptake clearance of 5 statins, in the presence of HBSS/KHB or HSA, for PHH Lot AOS with 5% HSA (A), SHH with 5% HSA/HDO (B), and SHH with 2% HSA/SDO

A

	Total $CL_{int,uptake}$[a] (µL/min/mg protein)			Passive $CL_{int,uptake}$[a] (µL/min/mg protein)			Active $CL_{int,uptake}$[b] (µL/min/mg protein)			% Active Uptake[d]	
	Buffer, Mean (%CV)	5% HSA, Mean (%CV)	Apparent PMUE[c]	Buffer, Mean (%CV)	5% HSA, Mean (%CV)	Apparent PMUE	Buffer, Mean (%CV)	5% HSA, Mean (%CV)	Apparent PMUE	Buffer	5% HSA
Fluvastatin	26.8 (21)	295.0 (19)	11.3	8.3 (14)	223.9 (35)	26.7	18.6 (28)	71.1 (4.6)	4.0	68.6%	25.1%
Pitavastatin	34.4 (16)	154.0 (9)	4.5	6.7 (17)	69.5 (30)	10.8	27.7 (23)	84.5 (24)	2.4	79.8%	54.9%
Cerivastatin	39.9 (13)	268.5 (20)	6.7	9.3 (21)	50.4 (23)	5.5	30.6 (13)	218.1 (21)	7.1	76.8%	81.1%
Atorvastatin	49.3 (26)	92.9 (9)	2.0	4.0 (36)	12.3 (20)	3.3	45.3 (31)	80.6 (14)	1.9	91.2%	86.5%
Rosuvastatin	7.2 (14)	10.7 (27)	1.5	1.1 (10)	4.3 (27)	3.8	6.1 (18)	6.4 (33.4)	1.0	84.0%	59.0%

B

	Total $CL_{int,uptake}$[a] (µL/min/10^6 hepatocytes)			Passive $CL_{int,uptake}$[a] (µL/min/10^6 hepatocytes)			Active $CL_{int,uptake}$[b] (µL/min/10^6 hepatocytes)			% Active Uptake[d]	
	Buffer, Mean (%CV)	5% HSA, Mean (%CV)	Apparent PMUE[c]	Buffer, Mean (%CV)	5% HSA, Mean (%CV)	Apparent PMUE	Buffer, Mean (%CV)	5% HSA, Mean (%CV)	Apparent PMUE	Buffer	5% HSA
Fluvastatin	35.9 (34)	53.2 (13)	1.6	3.8 (25)	16.1 (22)	4.4	32.1 (40)	37.1 (10)	1.2	89.4%	69.7%
Pitavastatin	31.2 (23)	49.0 (12)	1.6	1.7 (36)	10.0 (20)	6.3	29.5 (27)	39.0 (12)	1.3	94.4%	79.6%
Cerivastatin	39.0 (25)	56.2 (31)	1.4	2.7 (10)	6.1 (23)	2.3	36.3 (27)	50.2 (37)	1.4	93.1%	89.2%
Atorvastatin	32.6 (22)	46.0 (33)	1.4	3.1 (25)	5.6 (6)	1.9	29.5 (26)	40.4 (38)	1.4	90.5%	87.8%
Rosuvastatin	3.5 (7)	3.6 (41)	1.0	0.2 (24)	0.7 (16)	3.0	3.2 (7)	2.9 (48)	0.9	93.1%	80.4%

C

	Total $CL_{int,uptake}$[a] (µL/min/10^6 hepatocytes)			Passive $CL_{int,uptake}$[a] (µL/min/10^6 hepatocytes)			Active $CL_{int,uptake}$[b] (µL/min/10^6 hepatocytes)			% Active Uptake[d]	
	Buffer, Mean (%CV)	2% HSA, Mean (%CV)	Apparent PMUE[c]	Buffer, Mean (%CV)	2% HSA, Mean (%CV)	Apparent PMUE	Buffer, Mean (%CV)	2% HSA, Mean (%CV)	Apparent PMUE	Buffer	2% HSA
Fluvastatin	55.3 (21)	73.5 (37)	1.3	3.4 (30)	15.1 (18)	4.4	51.8 (21)	58.4 (42)	1.1	93.8%	79.4%
Pitavastatin	40.2 (19)	50.1 (17)	1.2	2.2 (39)	7.5 (13)	3.4	38.0 (18)	42.6 (18)	1.1	94.5%	85.0%
Cerivastatin	54.2 (23)	58.2 (16)	1.1	3.0 (37)	5.8 (16)	1.9	51.1 (39)	52.4 (30)	1.1	94.4%	90.0%
Atorvastatin	42.9 (33)	53.9 (24)	1.3	5.5 (13)	8.2 (10)	1.5	37.4 (27)	45.6 (17)	1.3	87.1%	84.7%
Rosuvastatin	4.0 (25)	3.6 (12)	0.9	0.3 (31)	0.7 (6)	2.3	3.7 (28)	2.9 (17)	0.8	92.3%	80.4%

[a] The *in vitro* total and passive $CL_{int,uptake}$ were respectively calculated by dividing the initial uptake rate by the unbound statin concentration measured by ultrafiltration in each experiment at 37°C and 4°C. The uptake rate was estimated from the slope (linear regression) of the linear uptake phase (30s to 2min for PHH, 15s to 1min for SHH). Data are mean (%CV) of triplicates at each time point.

[b] Active $CL_{int,uptake}$ = total $CL_{int,uptake}$ - passive $CL_{int,uptake}$

[c] Apparent PMUE = $CL_{int,uptake}$ (5% HSA or 2% HSA)/$CL_{int,uptake}$ (HBSS or KHB)

[d] % active uptake = 100* active $CL_{int,uptake}$/total $CL_{int,uptake}$

3.4.2 *Except for ATV and CRV, the Residual Statin Explained the Increase in the Apparent Uptake of Statins by PHH in the Presence of 5% HSA*

Using quantitative targeted proteomics, we confirmed the presence of residual HSA in the cell lysate after the cells had been washed thrice with the ice-cold buffer (Suppl. Fig. 7B of (Yin *et al.*, 2023)). The estimated residual statin amount explained the increase in apparent total and passive uptake of FLV, PTV and RSV by the PHH in the presence of HSA (**Fig. 3.3B-E**; Suppl. Fig. 2B-2E & 3B-3E of (Yin *et al.*, 2023)). In contrast, the amount of residual CRV-HSA and ATV-HSA only partially accounted for the increase in total apparent uptake

in the presence of 5% HSA (e.g. 30%-39 and 32-41% for AOS) (**Fig. 3.3B-E**; Suppl. Fig. 2B-2E & 3B-3E of (Yin *et al.*, 2023)). However, the apparent increase in passive uptake of these two statins was accounted for by the residual statin amount (**Fig. 3.3C** & **3.3E**; Suppl. Fig. 2&3 of (Yin *et al.*, 2023)), implying that the PMUE is a real phenomenon for transporter-mediated uptake of CRV and ATV. We emphasize that the latter was increased by ~7-fold and~2-fold respectively in the presence of 5% HSA. Of note, the results of PTV showed variability across the three hepatocyte lots. The increase in total apparent PTV uptake only by lot AOS, but not by lot FEA and YTW, was statistically greater than that explained by the residual PTV-HSA (**Fig. 3.3B** *vs.* Suppl. Fig. 2B&3B of (Yin *et al.*, 2023)).

3.4.3 *In the Oil-Spin Assay, Conducted Without Hepatocytes, HSA and Statins were Detected in the Bottom Cell Lysate Layer*

Immediately after the statins plus 5% HSA, in the absence of SHH, were centrifuged through the oil layer, the oil floated to the top (**Fig. 3.4A**). That is, the integrity of the oil-spin layer was compromised. As a result, ~10% of the total HSA loaded was detected in the bottom layer (**Fig. 3.4B**). In addition, 6%-12% of the statins was found in the bottom layer (**Fig. 3.4C**). For 1% HSA and 2% HSA, although the oil layer did not float to the top, a small but variable amount of HSA (0.01%-0.02%) and statins (0.02%-0.5%) were detected in the bottom layer. These data indicate that the statin-HSA complex can be centrifuged through the oil layer even in the absence of hepatocytes.

3.4.4 *The Presence of HSA Modestly Increased the Apparent Active and Passive Uptake of Statins into SHH*

To avoid disrupting the oil layer when using 5% HSA, high-density oil (HDO) was used with 5% HSA (see **Section 3.3 Methods**) while standard-density oil (SDO) was used with 2% HSA. For simplicity, these conditions will henceforth be referred to as 5% HSA/HDO and 2% HSA/SDO.

In contrast to the PHH, the increase in total and active uptake of statins in SHH in the presence of 5% HSA/HDO or 2% HSA/SDO was small (less than 50% increase) (**Fig. 3.5A** & **3.6A**; Suppl. Fig. 4&5A&6A&7A of (Yin *et al.*, 2023)), indicating marginal or no apparent PMUE on the active uptake of statins

by SHH. However, the apparent PMUE on the passive uptake of statins was greater, especially for FLV (4.4- to 10.6-fold increase) and PTV (3.4- to 7.8-fold increase) (**Table 3.1B-3.1C**; Suppl. Fig. 4 & Suppl. Table 3B-3C of (Yin *et al.*, 2023)). Overall, the observed PMUE on total, active and passive uptake of five statins was comparable in the presence of 5% HSA/HDO *vs.* 2% HSA/SDO (**Fig. 3.7**).

3.4.5 *The Increase in the Apparent Uptake of the Majority of Statins by SHH in the Presence of 5% HSA/HDO or 2% HSA/SDO, was Largely Explained by the Residual Statin*

The residual statin explained the increase in the apparent passive uptake of all five statins by SHH in the presence of 5% HSA/HDO (**Fig. 3.5C** & **3.5E**; Suppl. Fig. 5C&5E of (Yin *et al.*, 2023)) or 2% HSA/SDO (**Fig. 3.6C** & **3.6E**; Suppl. Fig. 6C&6E of (Yin *et al.*, 2023)). In contrast, the residual CRV-HSA or ATV-HSA accounted for only a partial increase in the total uptake of CRV and ATV in the presence of 5% HSA/HDO (e.g. 23-35% and 17%-21% for lot AOS; **Fig. 3.5B** & **3.5D**, Suppl. Fig. 5B&5D of (Yin *et al.*, 2023)) or 2% HSA/SDO (e.g. 20-23% and 15%-24% for lot AOS; **Fig. 3.6B** & **3.6D**, Suppl. Fig. 6B&6D of (Yin *et al.*, 2023)).

3.5 DISCUSSION

Here, we show that the previously reported PMUE on hepatic uptake of statins is confounded by residual statin irrespective of whether PHH or SHH are used. Our study was designed to have several important features that allowed us to arrive at definitive conclusions regarding the magnitude and mechanism of the PMUE. First, both PHH and SHH were from the same donors. They were studied with different HSA concentrations (SHH only) allowing us to directly compare the results from two different hepatocyte models. Second, we expressed all our data with respect to the unbound statin concentration in the media measured by ultrafiltration. Third, for all our studies, unlike previous studies, we maintained approximately the same unbound statin concentration in the buffer *vs.* HSA conditions to keep the same driving force for uptake into the hepatocytes. This was important as we used a cocktail of statins. This approach minimized any difference between the two conditions (buffer *vs.* HSA) of competitive interaction for transport (if any) between the statins. Fourth, we measured the apparent PMUE on total, active and passive uptake of statins to rule in or out the PLI/FDM or TIPBS hypothesis (see **3.2 Introduction** and discussion below). Fifth, all our hepatocyte lots demonstrated robust OATP activity. Also, inter-lot OATP activity should not affect the interpretation of our data as all our interpretations are within lot comparisons. Finally, in contrast to previous publications on PMUE, we corrected our data for any residual statin at every time point in each experiment.

Consistent with our previous findings (**CHAPTER 2**) using plated OATP1B1-expressing HEK293 cells (Yin *et al.*, 2022), PHH (lot: AOS, FEA and YTW), also showed substantial apparent PMUE on the total uptake of statins in the presence of 5% HSA (**Fig. 3.3A**; Suppl. Fig. 2A&3A of (Yin *et al.*, 2023)). Except for CRV, this apparent PMUE was greater for passive uptake than active uptake (**Fig. 3.3A**; Suppl. Fig. 2A&3A of (Yin *et al.*, 2023)). This discrepancy in the magnitude contradicts the PLI/FDM hypothesis. In addition, the presence of PMUE on passive uptake of the statins, contradicts the TIPBS hypothesis. However, our residual statin hypothesis can explain this apparent PMUE on the passive uptake of the statins (**Fig. 3.3B-E**, Suppl. Fig. 2B-2E&3B-3E of (Yin *et al.*, 2023)). In contrast, although our residual statin hypothesis can explain the PMUE on the total uptake of FLV, PTV and RSV, it can only partially explain such effect on the total uptake of CRV (20%-39%) and ATV (16-41%). Even for CRV and ATV, these numerical differences between the increase in

statin uptake and residual statin were not consistently significant across the hepatocyte lots, raising doubts about whether the PMUE observed for these statins is real. To determine if this effect is real or largely confounded by other factors, we examined this PMUE on statin uptake by SHH where the oil layer should theoretically reduce such confounding factors. Conversely, if this PMUE on CRV and ATV uptake is real, its magnitude should remain the same irrespective of whether PHH or SHH are used. This is because, in both instances, HSA (hence the PMUE) is present before the washing (PHH) or the oil-spin step (SHH).

The oil-spin method assumes that only the hepatocytes, and not the bound or unbound statins, will be centrifuged through the standard-density oil layer (density of 1.015 g/mL) and the integrity of the oil layer will remain intact. These assumptions are incorrect. In the absence of hepatocytes, but in the presence of 2% HSA, a fraction of both HSA and statins (presumably as HSA-statin complex), was centrifuged through the SDO layer (**Fig. 3.4B-3.4C**). In addition, when using 5% HSA, the oil-layer floated to the top and the uptake buffer merged with the bottom aqueous layer (**Fig. 3.4A**). To avoid this from occurring, for all subsequent experiments, we increased the density of the oil layer (HDO) for the 5% HSA condition. In addition, since the SDO is used routinely with SHH, to compare the PMUE when the SDO is used *vs.* when the HDO is used, we used the SDO with a reduced HSA concentration (2%). At this reduced HSA concentration, we and others have reported a PMUE on the uptake of statins (Miyauchi *et al.*, 2018; Yin *et al.*, 2022).

When 5% HSA/HDO and 2% HSA/SDO were used to determine the uptake of statins by SHH, compared with PHH, the apparent PMUE on total and active statin uptake was almost completely abolished (**Fig. 3.3A** & **3.5A** & **3.6A**; Suppl. Fig. 3A&4&5A&6A&7A of (Yin *et al.*, 2023)). While the PMUE on passive uptake remained, it too was reduced. These data suggest that the oil-spin method is more efficient at removing the residual statin than the washing steps used in PHH. Moreover, residual statin could explain all the apparent PMUE on passive uptake. Similar to PHH, though the residual statin accounted for PMUE on the total uptake of FLV, PTV and RSV, it did so only partially for CRV (20%-56%) and ATV (25%-28%). In addition, the apparent PMUE (on total, active, passive) was comparable for 5% HSA/HDO and 2% HSA/SDO, which is inconsistent with any proposed PMUE mechanism (**Fig. 3.7**). According to the PLI/FDM or TIPBS hypotheses, the PMUE should be positively correlated with the HSA concentration and therefore increase (not remain the same) as the

percentage of HSA increases. Provided the HDO does not reduce the passage of hepatocytes through the oil layer, this increase should be independent of the oil density as the true PMUE should occur before the oil-spin step. Quantitative targeted proteomics of Na^+K^+-ATPase, a surrogate marker of the quantity of hepatocytes that passaged through HDO vs. SDO layer, was not significantly different (Suppl. Fig. 7D of (Yin *et al.*, 2023)) indicating that the HDO does not reduce the passage of hepatocytes through the oil layer.

We conclude from our data that the so-called PMUE on hepatic uptake of statins by both the PHH and the SHH is largely confounded by residual statin. This raises an interesting question, why does the amount of residual statin increase with time (Suppl. Fig. 7B of (Yin *et al.*, 2023))? Is time-dependent endocytosis of the statin-HSA complex playing a role? No data are available to show that the liver endocytoses HSA. Such endocytosis can occur in the kidneys and therefore may have contributed to our data on OATP1B1-expressing HEK293 cells in **CHAPTER 2** (Yin *et al.*, 2022). However, the reported albumin endocytosis rate by kidney proximal tubule cells is approximately 0.06 μg/min/mg total protein (calculated from (Brunskill *et al.*, 1998)), minimal compared to the measured residual HSA amount (20 μg/min/mg total protein) in HEK293 cells using a short incubation time (up to 2 min). Thus, we conclude that the apparent PMUE is due to the time-dependent binding of the statin-HSA complex to the cells (PHH and SHH) and labware (PHH) under the current experimental condition (cocktail of 5 statins and short incubation time).

Our studies have some limitations. First, we used a cocktail of statins. Though the unbound concentrations of the statins were all kept below their respective unbound K_m values for OATP uptake (Bi *et al.*, 2021), the total concentration of the statins collectively may have resulted in some competition for transport. To obviate any confounding effect of such competition, we kept the unbound statin concentration in the presence of HSA the same as the total concentration in the buffer condition. Data from our OATP1B1-expressing cells show that our results are similar, irrespective of whether a single statin is used or a cocktail (Yin *et al.*, 2022). To determine the residual statin, we assumed that the extent of the binding of the statins to HSA in our uptake assays was identical to that determined by ultrafiltration. We also assumed little or no non-specific binding of the unbound statins to the hepatocytes. This is a reasonable assumption as the residual statin explained the PMUE on passive uptake of all statins. Although our data can explain the observed *in vitro* apparent PMUE (by HEK293 cells or

hepatocytes), they cannot explain the observed PMUE in several in situ–isolated rat perfused liver studies. These studies have reported more efficient hepatic uptake of highly protein-bound compounds in the presence vs. absence of albumin, such as sulfobromophthalein, warfarin, rose bengal, and taurocholate (Forker and Luxon, 1981, 1983; Weisiger *et al.*, 1984; Tsao *et al.*, 1988). Therefore, mechanisms other than the PLI/FDM need to be explored to explain these observations.

In summary, based on the following findings, we conclude that the residual statin largely confounds the apparent PMUE on uptake of statins: 1) The observed apparent PMUE is significantly larger for passive *vs.* total or active uptake of the statins. This contradicts the PLI/FDM and TIPBS hypothesis and other hypotheses such as channeling (Nelson *et al.*, 2016; Yabut and Isoherranen, 2022) and allosteric effect (Kindla *et al.*, 2011). For the latter three, based on the free drug hypothesis, only the active uptake of the statins should be affected. 2) The apparent PMUE on active, passive and total uptake of the statins using the PHH decreases dramatically when SHH are used. If the PMUE is real, such a reduction should not be observed as the real PMUE should occur prior to centrifugation. These data suggest that the residual statin quantification may not have accounted for other possible artifacts present with PHH. 3) With SHH, the true PMUE on active uptake in the presence of 5% HSA is marginal (<50%). This magnitude of PMUE cannot bridge the gap in IVIVE of transporter-mediated CL_h of drugs, including statins(Kim *et al.*, 2019; Li *et al.*, 2020, 2021; Bi *et al.*, 2021). Therefore, we recommend using SHH and the oil-spin method (rather than PHH) for future uptake studies conducted with HSA or plasma given that less residual HSA was observed using this method. HSA or plasma should be included only when significant true PMUE is demonstrated using the methods outlined here. Based on all the data presented above and in **CHAPTER 2**, we conclude that the free drug hypothesis for *in vitro* transport-mediated uptake of statins remains intact.

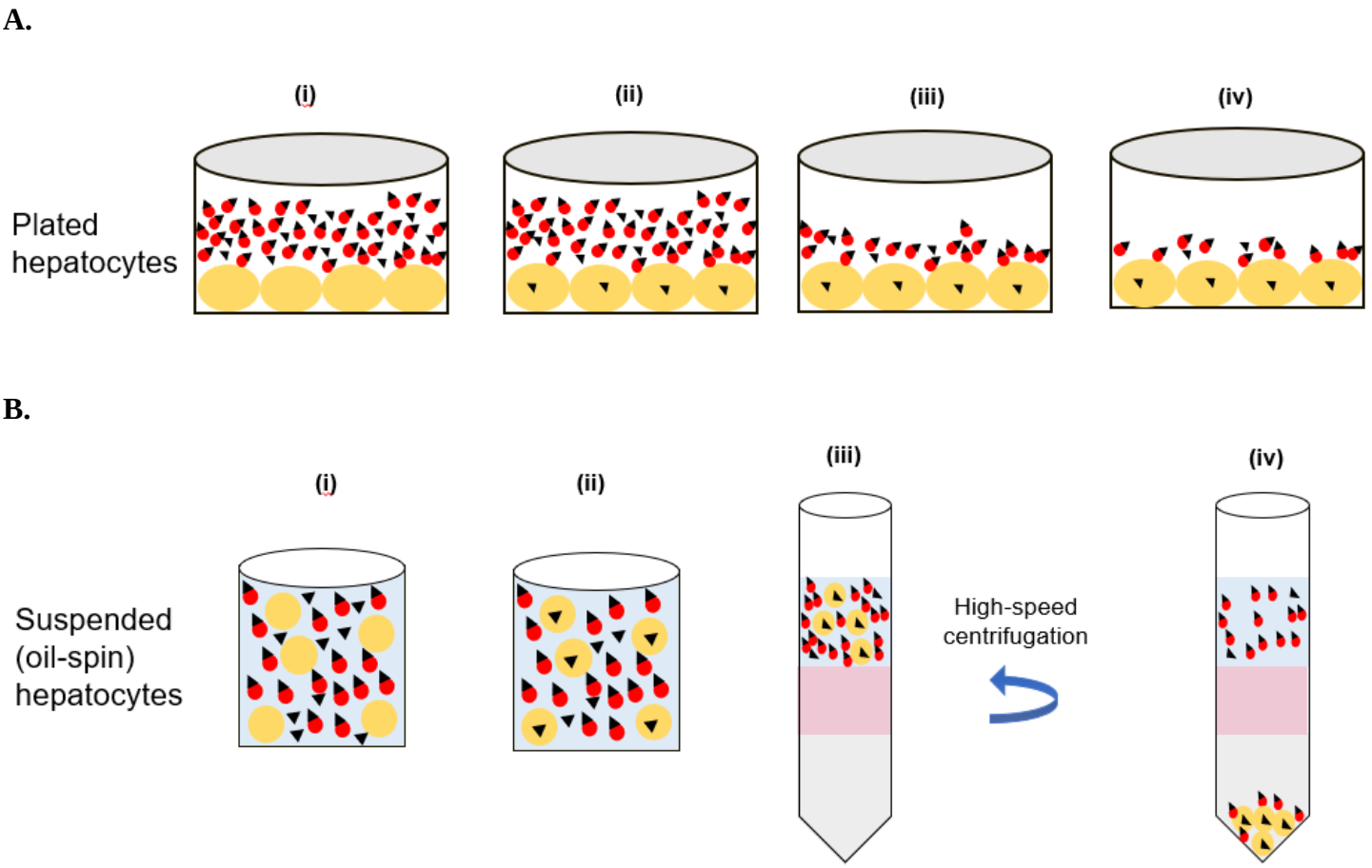

Figure 3.1. Residual drug-albumin complex hypothesis.

*Hepatic uptake of drug by plated human hepatocytes **(A)**:* The drug-HSA solution is added to the plate containing hepatocytes to initiate drug uptake **(i)**. After a designated time period (within the linear range), according to the free-drug hypothesis, the unbound drug is taken up by the hepatocytes **(ii).** Then the drug solution is removed **(iii)**. Finally, the hepatocytes are washed three times with ice-cold HBSS buffer **(iv)** and are lysed for intracellular drug amount quantification, with the assumption that all the drug or drug-HSA complex is washed away completely. However, if there is residual drug-HSA complex remaining in the plate, non-specifically bound to the hepatocytes or labware **(iv)**, it will "contaminate" the real drug uptake, resulting in an apparent "PMUE". *Hepatic uptake of drugs by suspended human hepatocytes **(B)**:* The hepatic uptake is initiated by mixing the hepatocytes and HSA solution with the drug **(i)**. After a designated time period (within the linear range), according to the free-drug hypothesis, the unbound drug is taken up by the hepatocytes **(ii).** To terminate the uptake, the hepatocytes-drug mixture is immediately loaded onto a microcentrifuge tube containing 3M ammonium acetate overlaid by a silicone-mineral oil mixture **(iii)** and is centrifuged to the

bottom by a high-speed centrifugal force for drug quantification **(iv)**. This approach assumes that only the hepatocytes are centrifuged to the bottom layer. However, if the drug-HSA complex can be centrifuged together with the hepatocytes, it will "contaminate" the real drug uptake **(iv),** resulting in an apparent "PMUE".

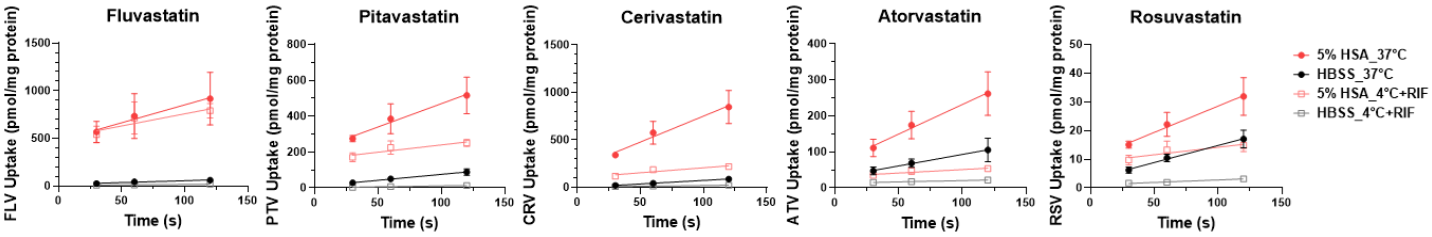

Figure 3.2. Statin uptake-time curves for a representative PHH lot (AOS) in the absence (HBSS) or presence of 5% HSA at 37°C or 4°C + rifampin (RIF; unbound concentration 500 µM).

The increase in the slope of the uptake curves in the presence of HSA *vs.* HBSS suggests an apparent PMUE on the $CL_{int,uptake}$ of the statins. The increased intercept in the presence of HSA indicates the residual statin-HSA complex non-specifically bound to the cells/labware. The data shown are mean±SD (triplicates) of statin uptake (normalized to 1 µM unbound concentration as the protein binding of the statins varies) and representative of 3 independent experiments.

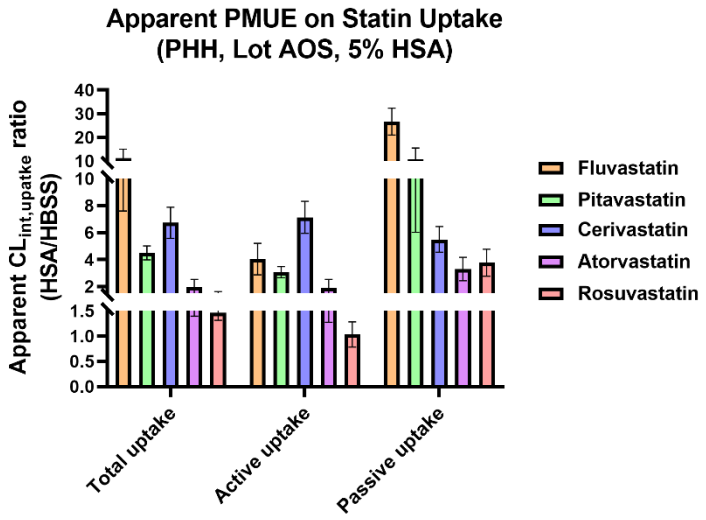

Figure 3.3. Apparent PMUE on total (37°C), active (37°C) and passive uptake (4°C + RIF) of five statins by PHH lot AOS in the presence of 5% HSA (A) and the contribution of residual statin to this apparent PMUE on the total (B, D) and passive (C, E) uptake of the statins.

The apparent PMUE on hepatic uptake follows the order passive> total> active, except for CRV (A). The increase in the passive and total uptake of FLV and RSV in the presence of 5% HSA (*vs.* HBSS) can be explained by the residual statin (B-E; $p>0.05$, unpaired t-test). However, this was not the case for the total uptake of PTV, CRV and ATV. For PTV, CRV and ATV, the percent of PMUE accounted for (at 30s and 120s) by the residual statin was 56%, 58%, 39%, 30%, and 41%, 32% respectively (B). The statins are displayed in order of protein binding. The unbound fraction (mean ± SD) in 5% HSA of FLV, PTV, CRV, ATV and RSV was 0.003±0.0004, 0.014±0.001, 0.023±0.001, 0.071±0.008 and 0.184±0.013, respectively. The data shown are mean ± SD of 3 independent experiments, each conducted in triplicate. Statistical comparison was performed using the unpaired t-test (* $p<0.05$; ** $p<0.01$; *** $p<0.001$). ns- not significant.

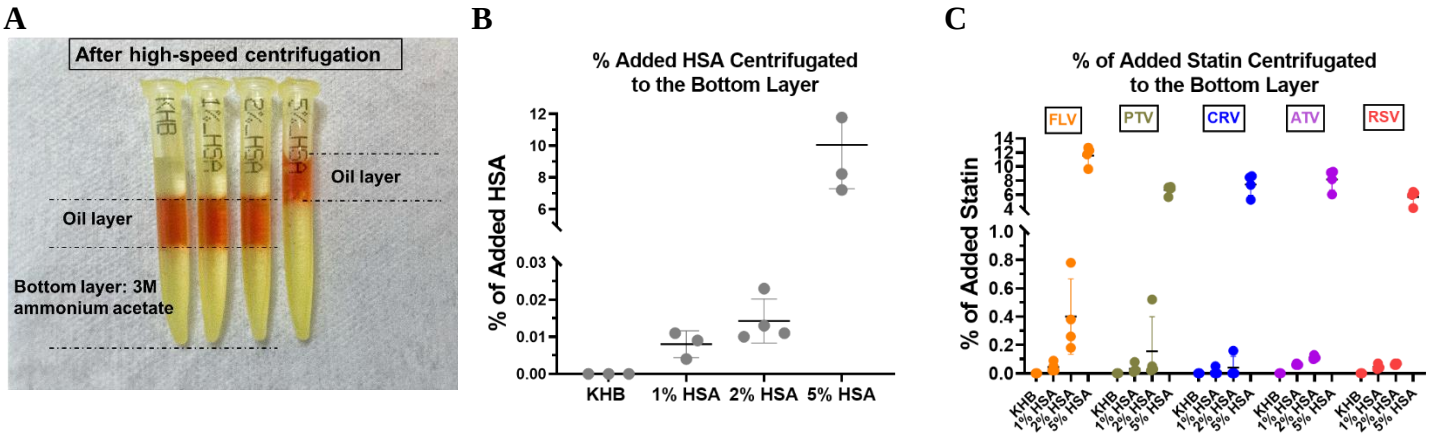

Figure 3.4. Percent of HSA and statin found in the bottom layer when the oil-spin method (standard density oil, SDO) was used without hepatocytes.

After high-speed centrifugation, in the presence of 5% HSA (but not 1% or 2% HSA), the oil layer (containing the Oil Red O dye) floated to the top (A). Consequently, with increasing percent of HSA, both the HSA (B) and statins (C) were detected in the bottom layer. These data indicate that the statin-HSA complex can be spun through the oil layer and confound the interpretation of the apparent PMUE on the uptake of statins by SHH. The data shown are representative of 3 independent experiments, each conducted in triplicate or quadruplicate. Horizontal lines in panels B and C represent the mean value with SD.

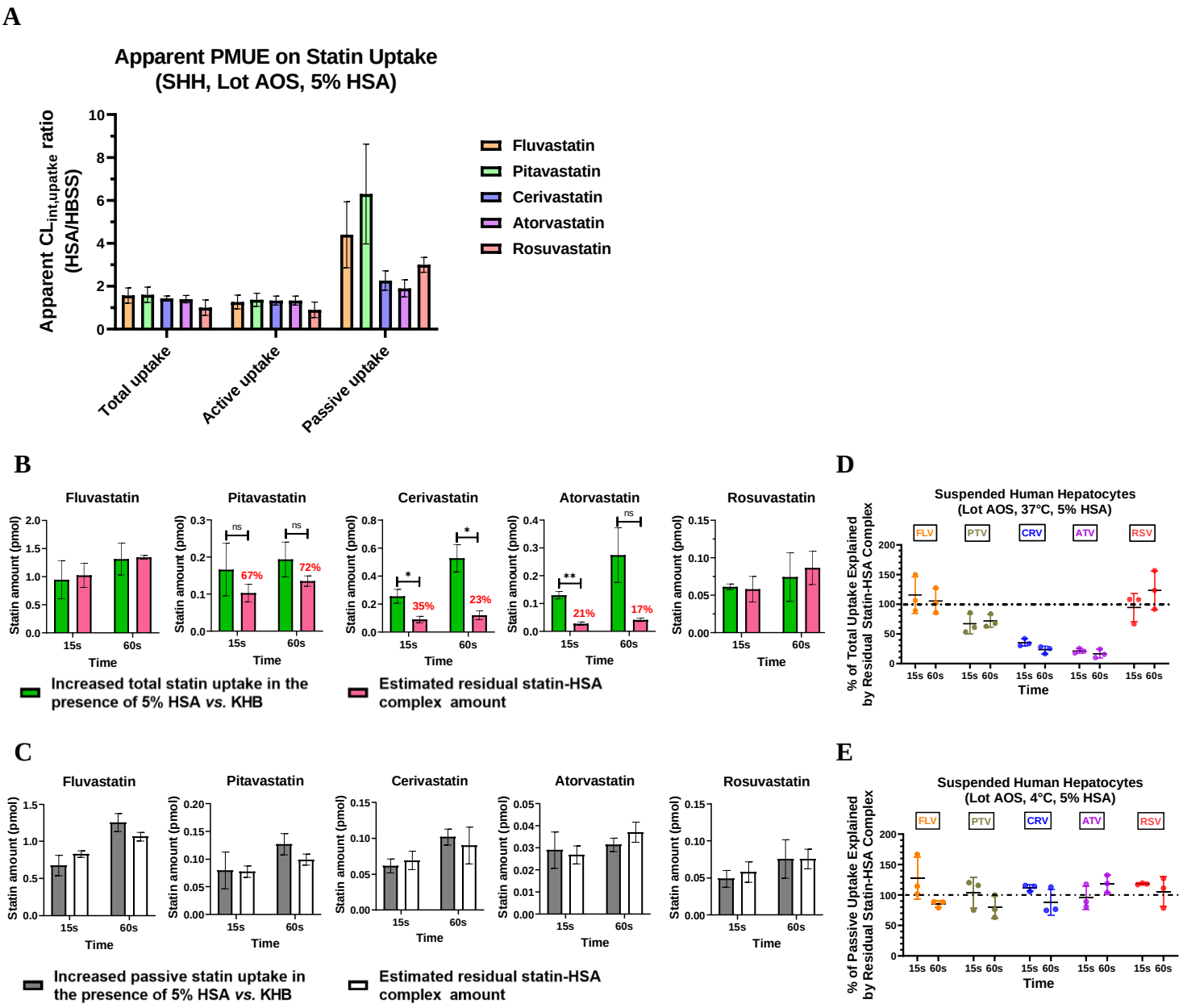

Figure 3.5. Apparent PMUE on total (37°C), active (37°C) and passive uptake (4°C) of five statins by SHH lot AOS in the presence of 5% HSA/HDO (A) and the contribution of residual statin to this apparent PMUE on the total (B, D) and passive (C, E) uptake of the statins.

The apparent PMUE on hepatic uptake follows the order passive> total ≈ active (A). The increase in the passive and total uptake of FLV, PTV and RSV in the presence of 5% HSA (*vs.* HBSS) can be explained by the residual statin (B-E; p>0.05, unpaired t-test). However, this was not the case for the total uptake of CRV and ATV (at 15s). For CRV and ATV, the percent of PMUE accounted for (at 15s and 60s) by the residual statin was 35%, 23%, and 21%, 17% respectively (B). The statins are displayed in order of protein binding. The unbound

fraction in 5% HSA of FLV, PTV, CRV, ATV and RSV were 0.004±0.0007, 0.009±0.001, 0.017±0.001, 0.057±0.003 and 0.136±0.013, respectively. The data shown are mean ± SD of 3 independent experiments, each conducted in quadruplicate. Statistical comparison was performed using the unpaired t-test (* $p<0.05$; ** $p<0.01$; *** $p<0.001$). ns- not significant.

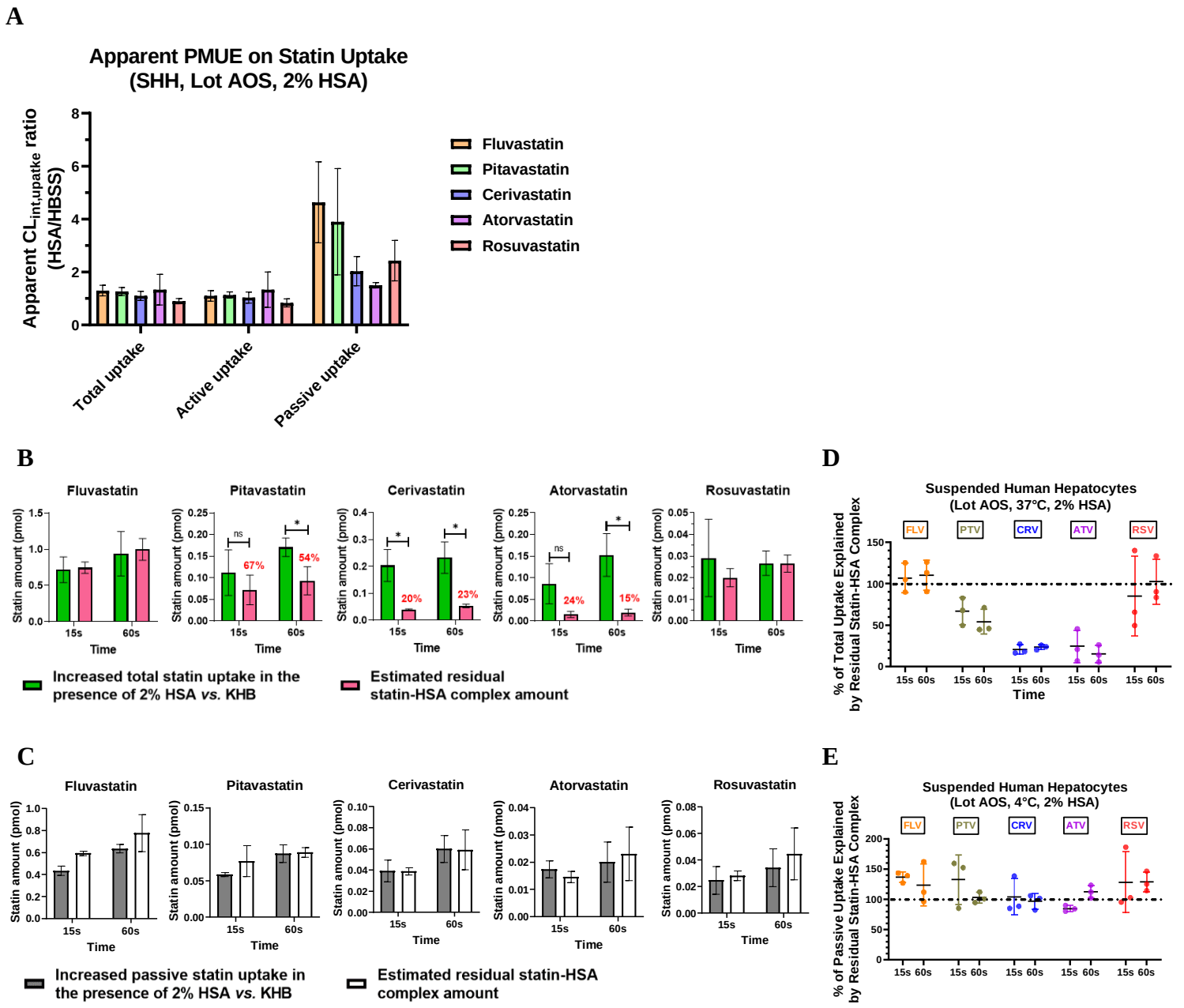

Figure 3.6. Apparent PMUE on total (37°C), active (37°C) and passive uptake (4°C) of five statins by SHH lot AOS in the presence of 2% HSA/SDO (A) and the contribution of residual statin to this apparent PMUE on the total (B, D) and passive (C, E) uptake of the statins.

The apparent PMUE on hepatic uptake follows the order passive> total ≈ active (A). The increase in the passive and total uptake of FLV, PTV (at 15s) and RSV in the presence of 2% HSA (*vs.* HBSS) can be explained by the residual statin (B-E; p>0.05, unpaired t-test). However, this was not the case for the total uptake of CRV and ATV (at 60s). For CRV and ATV, the percent of PMUE accounted for (at 15s and 60s) by the residual statin was 20%, 23%, and 24%, 15% respectively (B). The statins are displayed in order of protein binding. The

unbound fraction in 2% HSA of FLV, PTV, CRV, ATV and RSV were 0.007±0.001, 0.023±0.002, 0.053±0.007, 0.136±0.021 and 0.339±0.026, respectively. The data shown are mean ± SD of 3 independent experiments, each conducted in quadruplicate. Statistical comparison was performed using the unpaired t-test (* $p<0.05$; ** $p<0.01$; *** $p<0.001$). ns- not significant.

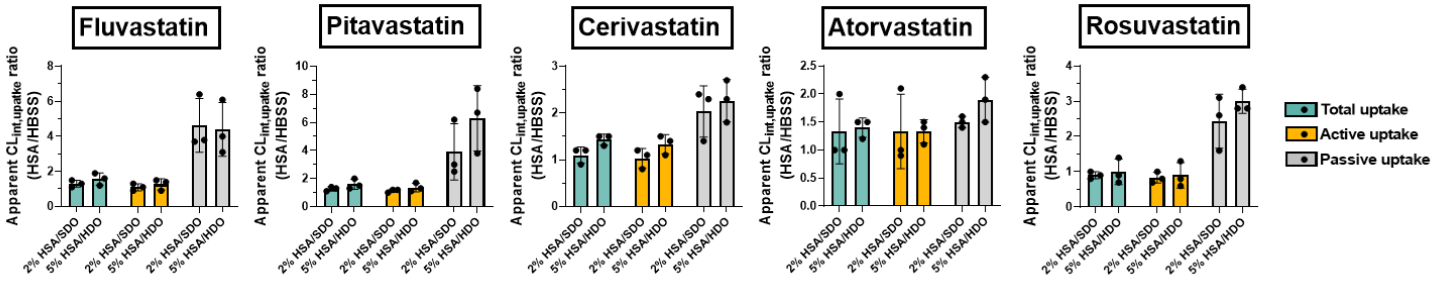

Figure 3.7. Comparison of the apparent PMUE in SHH (lot AOS) in the presence of 5% HSA/HDO *vs.* 2% HSA/SDO.

The apparent PMUE of 5% HSA/HDO was not significantly different from that of 2% HSA/SDO (p>0.05), indicating that the apparent PMUE can be manipulated by a change in oil-density, an observation supporting the residual statin hypothesis. The data shown are mean ±SD of 3 independent experiments, each conducted in quadruplicate. Statistical comparison was performed using the unpaired t-test.

3.6 ABBREVIATIONS USED

ATV, atorvastatin; BCA, bicinchoninic acid assay; CL, clearance; CL_h, hepatic clearance; $CL_{int,uptake}$, intrinsic uptake clearance; CRV: cerivastatin; DCL, diclofenac sodium salt; DMEM, Dulbecco's modified Eagle's medium; DMSO, dimethyl sulfoxide; DTT, dithiothreitol; FBS, fetal bovine serum; FLV, fluvastatin; HBSS, Hank's balanced salt solution; HEK, human embryonic kidney; HDO, high density oil; HPLC, high-performance liquid chromatography; HSA, human serum albumin; IAA, iodoacetamide; IVIVE, *in vitro* to *in vivo* extrapolation; KHB, Krebs-Henseleit buffer; LC-MS/MS, liquid chromatography tandem mass spectrometry; NSB, non-specific binding; OATP, organic anion transporting polypeptide; PHH, plated human hepatocytes; PLI, protein-lipid interaction; PMUE, protein-mediated uptake effect; PTV, pitavastatin; RIF, rifampin; RSV, rosuvastatin; SHH, suspended human hepatocyte; SDS, sodium dodecyl sulfate; SDO, standard density oil

Chapter 4. PREDICTION AND VALIDATION OF HUMAN HEPATOBILIARY CLEARANCES AND HEPATIC CONCENTRATIONS OF TRANSPORTED DRUGS USING THE PROTEOMICS-INFORMED RELATIVE EXPRESSION FACTOR APPROACH

The work presented in this chapter was accepted by *Clinical Pharmacology & Therapeutics*. Mengyue Yin is the first author leading the research design, conducting experiments and data analysis, and wrote the manuscript. Ankit Balhara handled the proteomics work and some TEVs experiments. Solène Marie and Nicolas Tournier led the PET imaging study and helped with PET data analysis. Zsuzsanna Gáborik provided the TECs and TEVs and contributed to the writing of the manuscript. Jashvant D. Unadkat contributed to the research design and the writing of the manuscript.

4.1 ABSTRACT

Tissue drug concentrations determine the efficacy and toxicity of drugs. When a drug is the substrate of transporters that are present at the blood:tissue barrier, the steady-state unbound tissue drug concentrations cannot be predicted from their corresponding plasma concentrations. To accurately predict transporter-modulated tissue drug concentrations, all clearances (CLs) mediating the drug's entry and exit (including metabolism) from the tissue must be accurately predicted. Since primary cells of most tissues are not available, we have proposed an alternative approach to predict such CLs, that is the use of transporter-expressing cells/vesicles (TECs/TEVs) and relative expression factor (REF). REF represents the abundance of the relevant transporters in the tissue *vs.* in the TECs/TEVs. Here, we determined the transporter-based intrinsic CL of glyburide (GLB) and pitavastatin (PTV) in OATP1B1, OATP1B3, OATP2B1, and NTCP-expressing cells and MRP3-, BCRP-, P-gp- and MRP2- expressing vesicles and scaled these CLs to *in vivo* using REF. These predictions fell within *a priori* set 2-fold range of the hepatobiliary CLs of GLB and PTV, estimated from their hepatic PET imaging data: 272.3 and 607.8 mL/min for *in vivo* hepatic sinusoidal uptake CL ($CL_{s,uptake}$), 47.8 and 17.4 mL/min for sinusoidal efflux CL ($CL_{s,efflux}$) and 0 and 4.20 mL/min for biliary efflux CL (CL_{bile}), respectively. Moreover, their predicted hepatic concentrations (AUC and C_{max}), fell within 2-fold of their mean

observed data. These data, together with our previous findings, confirm that the REF approach can successfully predict transporter-based drug CLs and tissue concentrations to enhance success in drug development.

4.2 INTRODUCTION

Failure of drug development in the clinic predominantly stems from inadequate drug efficacy and safety (Harrison, 2016). This could result from not achieving the desired drug concentrations at the site of action. Therefore, the measurement of tissue drug concentrations is critical for the assessment of drug efficacy, safety, and tissue-specific drug–drug interactions. For a highly permeable drug with only passive diffusion across the blood:tissue barrier, the tissue unbound steady-state drug concentrations can be assessed from the corresponding plasma drug concentrations which can be routinely determined through pharmacokinetic (PK) studies. However, for a membrane transporter-substrate drug, the presence of active transporters creates an asymmetry in the unbound steady-state drug concentrations between tissues and plasma (Zhang *et al.*, 2019). While positron emission tomography (PET) and other imaging modalities can allow direct measurement of tissue drug concentrations in humans, their mainstream use is limited by the high cost and the use of radioactivity (PET imaging) in humans (Zang *et al.*, 2022). Therefore, predicting drug tissue concentrations using *in vitro* approach is an alternative that can be routinely applied.

To accurately predict the tissue concentrations of a transported drug, one needs to accurately predict all the clearance (CL) pathways that mediate drug's entry into and exit (including metabolism) from the tissue. For example, to predict hepatic drug concentrations, one has to accurately predict the hepatobiliary CLs of the drug including sinusoidal uptake CL ($CL_{s,uptake}$), sinusoidal efflux CL ($CL_{s,efflux}$), metabolic CL (CL_{met}) and biliary efflux CL (CL_{bile}) (G. Patilea-Vrana and Unadkat, 2016). While success in predicting metabolic drug CL using primary cells or human liver microsomes, is well-documented (Wood *et al.*, 2017), accurate prediction of transporter-based CLs remains a challenge. Moreover, except for human hepatocytes, primary cells are not available for all tissues where transporters are present at the blood:tissue barrier. Although human hepatocytes are available and widely used to predict hepatic drug transport CLs, multiple studies have reported drastic under-/over-prediction of hepatic drug transport CLs (Wood *et al.*, 2017). Moreover, the magnitude of these mis-predictions is compound-dependent, not allowing estimation of a global empirical scaling factor for *in vitro* to *in vivo* extrapolation (IVIVE).

Given the above limitations, we have proposed a promising approach to predicting transporter-mediated drug CLs and tissue concentrations – the proteomics-informed relative expression factor (REF) approach (Kumar *et al.*, 2021; Storelli, Li, *et al.*, 2022). A key advantage of this approach is that it allows for the use of standardized assay with readily available transporter-expressing cells or vesicles (TECs/TEVs) and is independent of the availability and intrinsic variability of primary cells. In addition, this approach corrects for the transporter abundance difference between TECs/TEVs *vs.* human tissue, as measured by quantitative targeted proteomics (Storelli, Li, *et al.*, 2022). Furthermore, this approach enables the estimation of fraction transported by each transporter to inform risks associated with drug-drug interaction and allelic variants.

Using the REF approach, we have successfully predicted transporter-mediated tissue drug concentrations and/or CLs, in the human liver, brain and fetus where transporters are present (e.g. BCRP, OCT1, P-gp) (Sachar *et al.*, 2020; Anoshchenko *et al.*, 2021; Storelli *et al.*, 2021; Storelli, Li, *et al.*, 2022). However, the REF approach modestly underpredicted the $CL_{s,uptake}$ and the PET-imaged hepatic concentrations of rosuvastatin (RSV, an Organic Anion Transporting Polypeptides (OATP) substrate) (Storelli, Li, *et al.*, 2022). Interestingly, with inclusion of human plasma or human serum albumin in TEC uptake assays, the prediction of RSV's $CL_{s,uptake}$ was improved (Kumar *et al.*, 2021). This phenomenon called the "protein-mediated uptake effect (PMUE)", has been widely proposed to improve prediction of OATP-mediated hepatic drug CL. Unfortunately, further investigation of the PMUE led us to conclude that this increase in the *in vitro* $CL_{int,uptake}$ by plasma proteins is mostly an artifact of how *in vitro* transport studies are conducted (Yin *et al.*, 2022, 2023). Therefore, here we investigated if the underprediction of $CL_{s,uptake}$ using the REF approach is specific to RSV or applies to all OATP substrates. To address this question, we applied the REF approach to predict the hepatobiliary CLs and hepatic concentrations of two other transported drugs, namely, glyburide (GLB, a.k.a glibenclamide) and pitavastatin (PTV). These drugs were chosen as they are well-established OATP substrates and PET imaging data are available to validate the predictions (Marie *et al.*, 2022; Nakaoka *et al.*, 2022).

4.3 MATERIALS AND METHODS

4.3.1 *Materials*

Radioactive ^{3}H-glyburide (GLB), ^{3}H-pitavastatin (PTV), ^{3}H-estrone-3-sulfate, ^{3}H-digoxin, ^{3}H-taurocholate acid and ^{3}H-estradiol-17β-glucuronide were obtained from American Radiolabeled Chemicals (St. Louis, MO). Synthetic signature peptides for BCRP, MRP2 and P-gp and their stable isotopes were obtained from Thermo Fisher Scientific (Waltham, MA). Adenosine monophosphate, adenosine triphosphate, formic acid (MS grade) and ATPase assay kit were purchased from Sigma Aldrich (St. Louis, MO). Dulbecco's modified Eagle's medium (DMEM), fetal bovine serum (FBS), penicillin and streptomycin solution, Tris (powder), sodium chloride, Hank's Balanced Salt Solution (HBSS), dithiothreitol, iodoacetamide, ammonium bicarbonate, sodium deoxycholate, sucrose, Pierce™ Trypsin Protease, Pierce™ RIPA Buffer, methanol (MS grade), chloroform, acetonitrile (MS grade), human serum albumin (HSA), bovine serum albumin (BSA) and total protein quantification bicinchoninic acid assay (BCA) were obtained from Thermo Fisher Scientific (Waltham, MA). Liquid scintillation fluid Ecoscint® was purchased from National Diagnostics (Atlanta, GA). Magnesium chloride was obtained from TJ Baker (Phillipsburg, NJ). Deionized water was obtained from Milli-Q purification system (Bedford, MA). Human OATP1B1-, OATP1B3-, OATP2B1-, NTCP- expressing and mock HEK293 cells (TECs) and BCRP-, MRP2-, MRP3-, and P-gp- expressing-HEK293 vesicles (TEVs) were generously provided by SOLVO (Budapest, Hungary).

4.3.2 *Quantification of GLB and PTV Uptake by OATP1B1, OATP1B3, OATP2B1 or NTCP TECs and Mock HEK293 Cells*

The uptake assay by TECs or mock cells was conducted as described previously (Kumar *et al.*, 2021; Yin *et al.*, 2022). Briefly, prior to the uptake assay, the cells in 24-well plate were washed twice with 1 ml of warm HBSS (37°C, pH 7.4). Subsequently, the cells were preincubated with warm HBSS for 15 minutes on a hot plate with surface temperature of 42°C (to achieve 37°C within the wells). After the aspiration of HBSS, the drug uptake was initiated by adding 0.5 ml of drug solution containing 1 nM ^{3}H-GLB and 4 nM unlabeled GLB or 10 nM ^{3}H-PTV and 40 nM unlabeled PTV. The uptake was terminated at predetermined timepoints (15, 30, and 60

seconds, all within the linear range) by aspirating the drug solution and washing the cells three times with ice-cold HBSS. Subsequently, the cells were lysed by adding 1 mL of 2% sodium dodecyl sulfate (SDS) to each well. Then, the cell lysate was used for total protein (BCA Protein Assay Kit) and total radioactivity quantification by a Tri-Carb Liquid Scintillation Counter (PerkinElmer, Waltham, MA). For transporter quantification, approximate 5-10 million TECs (from the same experiment) not exposed to the radioactive substrates were washed twice with HBSS. The cells were then scraped and collected into 15mL Falcon tubes. Then, the tubes were centrifuged at 1000g at 4°C for 5 minutes. Following centrifugation, the supernatant was carefully aspirated and the cell pellet was dried. After drying, 800 µL of Pierce™ RIPA Buffer were incubated with the pellet at 4°C for 1 hour to lyse the cells. The cell lysate (80 µL) was subsequently used to determine the abundance of the transporters. Three independent experiments were conducted, each in triplicate.

4.3.3 *Quantification of transporter-mediated and passive $CL_{int,uptake}$ of GLB and PTV using TECs*

The initial uptake rate was estimated from the slope of the drug uptake versus time profile (total in TECs; passive in Mock cells) using simple linear regression in GraphPad Prism version 9 (GraphPad Software, San Diego, CA).

The total (in TECs) or passive (in Mock cells) $CL_{int,uptake}$ was calculated as follows:

$$CL_{int,uptake}(\mu L/min/mg) = \frac{slope\ (pmol/min)}{C_0(\mu M) \times potein\ content\ (mg)} \quad \textbf{Eq. 4.1}$$

Where the C_0 represents the measured drug concentrations in the cell plate at the initial time point. The intrinsic active uptake CL ($Cl_{int,active,uptake}$) in TECs was calculated by subtracting the intrinsic passive diffusion CL ($CL_{int,passive}$; in Mock cells) from the total $CL_{int,uptake}$.

4.3.4 *Quantification of GLB and PTV efflux transport using BCRP, MRP2, MRP3 or P-gp TEVs*

The efflux assay by TEVs was conducted as described previously (Storelli, Li, *et al.*, 2022). The GLB and PTV concentration used in the assay was 50 nM glyburide (10 nM ^{3}H-GLB + 40 nM GLB) or 500 nM PTV (100 nM ^{3}H-PTV + 400 nM PTV). Transport of the relevant positive control substrate (100 nM ^{3}H-estrone-3-sulfate for BCRP, 100 nM ^{3}H-digoxin for P-gp, and 100 nM ^{3}H-estradiol-17β-glucuronide for MRP2 and MRP3) was

quantified in parallel. The ATP-dependent (active) intravesicular accumulation was determined from the difference of intravesicular drug uptake in presence of ATP (active transport and passive diffusion) and AMP (passive diffusion), which were normalized by the concentration of the drug measured in the working solution. To evaluate nonspecific binding of the radioactivity to the filter, a control study without vesicles, was performed for each experiment. Thirty microliters of TEVs (160 µg total protein) from the same experiment that were not exposed to the radioactive substrates were incubated with 50 µL Pierce™ RIPA Buffer at 4°C for 1 hour. Then, the mixture (80 µL) was subsequently used to determine the abundance of the transporters. Three independent experiments were conducted, each in triplicate.

4.3.5 *Quantification of transporter-mediated $CL_{int,s,efflux}$ or $CL_{int,bile}$ of GLB and PTV using TEVs*

The active intrinsic sinusoidal efflux or biliary efflux clearance ($CL_{int,active,efflux}$ or $CL_{int,bile}$) of the drug was calculated under linear conditions as follows:

$$Cl_{int,active,efflux}\ (\mu L/min/mg) = \frac{(Drug\ accumulation_{ATP} - Drug\ accumulation_{AMP})/_{dt}\ (pmol/min)}{C_0\ (\mu M) \cdot Protein\ content\ (mg)} \quad \textbf{Eq. 4.2}$$

where Drug accumulation$_{ATP}$ and Drug accumulation$_{AMP}$ represent the intra-vesicular accumulation of ^{3}H-GLB or ^{3}H-PTV in the presence of ATP and AMP, respectively, and C_0 represents the concentrations of ^{3}H-GLB or ^{3}H-PTV in the buffer incubated with vesicles.

4.3.6 *Targeted proteomics quantification of OATP1B1, OATP1B3, OATP2B1, NTCP, BCRP, P-gp and MRP3 abundance in TECs or TEVs*

Trypsin digestion of the TECs/TEVs samples (80 µL of the lysate) was conducted as described previously (Anoshchenko *et al.*, 2021; Storelli *et al.*, 2021).The surrogate peptides were as follows NVTGFFQSFK (OATP1B1), NVTGFFQSLK (OATP1B3), VLAVTDSPAR (OATP2B1), GIYDGDLK (NTCP), SSLLDVLAAR (BCRP), NTTGALTTR (P-gp) and ADGALTQEEK (MRP3). Calibrators (0.16-360 fmol on-column) of the peptides were prepared by spiking 50 mM ammonium bicarbonate with 10 µL of unlabeled surrogate peptide and 20 µL of stable-labeled peptide internal standard (both in 80% acetonitrile plus 0.2%

formic acid solution). Four QC samples (0.198, 1.98, 19.8 and 198 fmol-on-column), spanning the calibration range, were prepared in the same manner.

The surrogate peptides of OATP1B1, OATP1B3, OATP2B1, NTCP, BCRP, P-gp and MRP3 in the calibrators or the samples were quantified by LC-MS/MS analysis using Waters Xevo TQ-S mass spectrometer coupled to a Waters Acquity Ultra-Performance Liquid Chromatography (UPLC) system (Waters, Milford, MA). The MS was operated in positive electrospray ionization mode for the analysis of signature peptides and their respective stable isotope-labeled peptides (**Table 4.4**). An Acquity UPLC HSS T3 column (1.8 µm, 2.1 X 100 mm) with 0.2-mm inlet frits (Waters) was used for chromatographic separation and resolution. Mobile phases (0.3 ml/min) consisted of 0.1% formic acid in water (A) and 0.1% formic acid in acetonitrile (B). The UPLC gradient was: 0-3 minutes, 3% B; 3-6 minutes, 3%-12.5% B; 6-8 minutes, 12.5%–22% B; 8-13 minutes, 22%–40% B; 13-15 minutes, 40%-70% B; 15-16 minutes, 70-80%; 16-17.1 minutes, 80%-3% B; 17.1-20 minutes, 3% B.

4.3.7 *Quantification of inside-out fraction of TEVs*

The membrane vesicles contain both inside-out (exposing the active site of the transporter) and right-side-out vesicles. To apply the REF, estimation of the fraction of inside-out vesicles (f_{IOV}) used in the uptake assay is needed. The activity of ectoenzyme 5'-nucleotidase was used to quantify the f_{IOV} as per manufacturer's instructions. Briefly, 25 µg of the membrane vesicles were incubated for 5, 15 or 30 minutes at 37 °C in a solution containing 50 mM Tris-HCl (pH 7.4), 4 mM $MgCl_2$, with or without 3 mM AMP or 0.3% Triton X-100. The phosphate released from AMP by the activity of 5'-nucleotidase enzyme was measured by the change in absorbance (at 620 nm) of malachite green on a spectrophotometer (Tecan Spark, Männedorf, Switzerland). This assay was carried out under four conditions: a) incubation with both AMP and 0.3% Triton X-100 (total activity of all 5'-nucleotidase); b) incubation with only AMP (5'-nucleotidase activity in the right-side-out vesicles); c) incubation with only 0.3% Triton X-100 (background phosphate in the system); d) without incubation of either Triton X-100 or AMP (background phosphate in the assay buffer). The f_{IOV} was calculated as follows:

$$f_{IOV} = 1 - \frac{(b-d)}{(a-c)} \quad \textbf{Eq. 4.3}$$

where (a – c) represents the total background corrected 5'-nucleotidase activity and (b – d) denotes the background corrected activity in only the right-side-out vesicles. The f_{IOV} was determined in two different experiments, each performed in triplicate.

4.3.8 *Quantification of the Relative Expression Factor (REF)*

REF for each transporter was determined as the ratio of the relative abundance of the transporters in human liver tissue (Deo *et al.*, 2012; Prasad *et al.*, 2013, 2014; Wang *et al.*, 2015; Fallon *et al.*, 2016) and in the TECs or TEVs (by quantitative targeted proteomics, see **Table 4.4**).

For TECs (uptake transporters),

$$REF = \frac{[Transporter]_{liver\ tissue}(^{pmol}/_{mg\ MP})}{[Transporter]_{TECs}\left(^{pmol}/_{mg\ protein}\right)\times f_{PMA}} \quad \textbf{Eq. 4.4}$$

For TEVs (efflux transporters),

$$REF = \frac{[Transporter]_{liver\ tissue}\left(^{pmol}/_{mg\ MP}\right)}{[Transporter]_{TEVs}\left(^{pmol}/_{mg\ protein}\right)\times f_{IOV}} \quad \textbf{Eq. 4.5}$$

Since only the transporters expressed on the plasma membrane (PM) play a role in drug transport, for TECs REF, the transporter abundance in TEC was adjusted for their plasma membrane abundance fraction (f_{PMA}), obtained from our previous publication using the biotinylation approach and the TECs used in this study (Kumar *et al.*, 2017). For TEVs, the transporter abundance was adjusted for the inside-out vesicle fraction (f_{IOV}). As the f_{PMA} of transporters in liver tissue cannot be estimated by biotinylation, it was assumed to be 1 (Kumar *et al.*, 2019).

4.3.9 *IVIVE of $CL_{s,uptake}$ using TECs and REF*

The $CL_{int,active,uptake}$ determined in TECs for each transporter were scaled to *in vivo* ($CL_{int,active,uptake,in\ vivo}$) as follows:

$$CL_{int,active,uptake,in\ vivo,i}\ (mL/min) = CL_{int,active,uptake,i}\ (\mu l/min/mg\ prot) \cdot REF_i \cdot MMPPGL\ (mg\ MP/g\ liver) \cdot Liver\ weight\ (g) \cdot 10^{-3}$$ **Eq. 4.6**

where i denotes the i^{th} transporter [i.e., OATP1B1, OATP1B3, OATP2B1 or NTCP (PTV only)]; MMPPGL, milligrams of membrane protein per gram liver, is 37.68 mg MP/g liver (Sachar *et al.*, 2020) and the liver weight is 21.4 g/kg body weight (Ito and Houston, 2005).

The $CL_{int,passive}$ determined in mock HEK293 cells ($CL_{int,passive,mock}$) was scaled to *in vivo* ($CL_{int,passive,in\ vivo}$) as follows:

$$CL_{int,passive,in\ vivo}\ (mL/min) = CL_{int,passive,mock}\ (\mu L/min/mg\ prot) \cdot MGPGL \cdot f_{SSA} \cdot Liver\ weight\ (g) \cdot 10^{-3}$$ **Eq. 4.7**

where MGPGL, milligrams of protein per gram liver, is 88 mg protein/g liver (Karlgren *et al.*, 2012); f_{SSA}, the fraction of sinusoidal surface area, is 0.37 (Esteller, 2008).

$$\text{The total } \textit{in vivo} \text{ intrinsic sinusoidal uptake CL } \left(CL_{int,s,uptake,in\ vivo}\right) = \sum_{i=0}^{n} CL_{int,active,uptake,in\ vivo,i} + CL_{int,passive,in\ vivo}$$ **Eq. 4.8**

The REF-predicted total sinusoidal uptake CL ($CL_{s,uptake,REF\text{-}pred,in\ vivo}$) was estimated using the hepatic well-stirred model:

$$CL_{s,uptake,REF-pred,in\ vivo} = \frac{Q_h \times \frac{f_{u,p}}{R_B} \times CL_{int,s,uptake,in\ vivo}}{Q_h + \frac{f_{u,p}}{R_B} \times CL_{int,s,uptake,in\ vivo}}$$ **Eq. 4.9**

Where Q_h is the liver blood flow, 1500 mL/min; $f_{u,p}$ is the unbound fraction in plasma [0.013 for GLB (Tse *et al.*, 1993; Obach *et al.*, 2008; Hebert *et al.*, 2009; Marie *et al.*, 2022); 0.008 for PTV (Keith A Riccardi *et al.*, 2019; Bowman *et al.*, 2020)]; the $R_{B:P}$ is the blood-to-plasma ratio [0.55 for GLB (Rupp *et al.*, 1972; Varma *et al.*, 2014; Keith A Riccardi *et al.*, 2019); 0.58 for PTV (Watanabe *et al.*, 2010)].

The relative contribution of each transporter and passive diffusion (*i.e.* fraction transported f_t) to total $CL_{s,uptake}$ was estimated as follows:

$$f_{t,i} = \frac{\mathrm{CL_{int,active,uptake,in\ vivo,i}}\ or\ \mathrm{CL_{int,passive,in\ vivo}}}{\mathrm{CL_{int,s,uptake,in\ vivo}}}$$ **Eq. 4.10**

4.3.10 *IVIVE of $CL_{s,efflux}$ using TEVs and REF*

Vesicle experiments showed that only PTV, but not GLB, is a substrate of MRP3. Therefore, for GLB, the total intrinsic sinusoidal efflux clearance was assumed to be only by passive diffusion ($f_{t,passive}$=1); while for PTV, the total intrinsic sinusoidal efflux clearance included both MRP3-mediated active efflux clearance in TEVs and passive diffusion in TECs.

For GLB,

Total *in vivo* intrinsic sinusoidal efflux CL $\left(CL_{int,s,efflux,in\ vivo}\right)(mL/min) = CL_{int,passive,in\ vivo}$ **Eq. 4.11**

For PTV,

$$CL_{int,MRP3,efflux,in\ vivo}\ (mL\ /\ min) = CL_{int,MRP3,efflux}\ (\mu L/min/mg\ prot) \cdot REF_{MRP3} \cdot MMPPGL\ (mg\ MP/g\ liver) \cdot Liver\ weight\ (g) \cdot 10^{-3}$$ **Eq. 4.12**

$$CL_{int,s,efflux,in\ vivo}\ (mL/min) = CL_{int,MRP3,efflux,in\ vivo} + CL_{int,passive,in\ vivo}$$ **Eq. 4.13**

Therefore, the REF-predicted total sinusoidal efflux CL ($CL_{s,efflux,REF\text{-}pred,in\ vivo}$) for both drugs was estimated as follows:

$$CL_{s,efflux,REF-pred,in\ vivo} = f_{u,liver} \times CL_{int,s,efllux,in\ vivo}$$ **Eq. 4.14**

Where $f_{u,liver}$ is unbound faction in liver homogenate [0.035 for GLB (Riccardi *et al.*, 2018, 2020); 0.036 for PTV (Yoshikado *et al.*, 2017; Riccardi *et al.*, 2018, 2020)].

The f_t of each transporter and passive diffusion of total $CL_{s,efflux}$ of PTV was estimated as follows:

$$\mathrm{f_{t,i}} = \frac{\mathrm{CL_{int,MRP3,efflux,in\ vivo}}\ \mathrm{or}\ \mathrm{CL_{int,passive,in\ vivo}}}{\mathrm{CL_{int,s,efllux,in\ vivo}}}$$ **Eq. 4.15**

4.3.11 *IVIVE of PTV CL_{bile} using TEVs and REF*

The $\mathrm{CL_{int,bile}}$ determined in TEVs for each transporter were scaled to *in vivo* ($\mathrm{CL_{int,bile,in\ vivo}}$) as follows:

$$CL_{int,bile,in\ vivo,i}\ (mL/min) = Cl_{int,bile,i}\ (\mu l/min/mg\ prot) \cdot REF_i \cdot MMPPGL\ (mg\ MP/g\ liver) \cdot Liver\ weight\ (g) \cdot 10^{-3}$$ **Eq. 4.16**

where i denotes the ith transporter (*i.e.*, BCRP or P-gp).

$$\text{Total in vivo intrinsic biliary efflux CL } \left(CL_{int,bile,in\ vivo}\right) = \sum_{i=0}^{n} CL_{int,bile,in\ vivo,i}$$ **Eq. 4.17**

The REF-predicted total sinusoidal efflux CL ($CL_{s,efflux,REF\text{-}pred,in\ vivo}$) was estimated as follows:

$$CL_{bile,REF-pred,in\ vivo} = f_{u,liver} \times CL_{int,bile,in\ vivo}$$ **Eq. 4.18**

The contribution of passive diffusion to biliary efflux of PTV was assumed to be negligible.

The f_t of each transporter to total CL_{bile} of PTV was estimated as follows:

$$f_{t,i} = \frac{CL_{int,bile,in\ vivo,i}}{CL_{int,bile,in\ vivo}}$$ **Eq. 4.19**

4.3.12 *Estimation of the in vivo ^{11}C-GLB and ^{18}F-PTV hepatobiliary CLs by Compartmental Modeling of the PET Imaging Data*

PET-imaged ^{11}C-GLB and ^{18}F-PTV blood, total liver and extra-hepatic bile duct-gallbladder radioactivity amount or concentration-time data obtained by some of us (^{11}C-GLB, n=7 male healthy Caucasians) (Marie *et al.*, 2022) or digitized from the published study ^{18}F-PTV (mean of n=7 male healthy Japanese) (Nakaoka *et al.*, 2022) were used. For ^{18}F-PTV, the size of data points in the published figures are relatively large compared to the X,Y axis scale (Nakaoka *et al.*, 2022). To avoid potential inaccuracies in digitization, particularly at early intensive sampling timepoints, 10 rounds of digitization of the data were performed and pooled to arrive at the mean data for model fitting (see below). To verify the accuracy of the digitization, we employed the integration plot approach to calculate the "$CL_{uptake,\ liver}$" and "$CL_{int,bile}$" as per the methods outlined in the ^{18}F-PTV PET study (Nakaoka *et al.*, 2022). Our estimated values for these parameters were within 15% of the published values, indicating that our digitization was reliable.

A two (for ^{11}C-GLB) or three (for ^{18}F-PTV) compartment model was fitted to the PET data using SAAM II (Nanomath, Spokane, WA) and the blood concentrations as a forcing function (*i.e.* to drive the hepatic

concentrations). The model took into consideration that the imaged liver contains blood (10% of the total blood volume (Hwang *et al.*, 2002) and therefore the PET imaging-derived hepatic concentrations of ^{11}C-GLB and ^{18}F-PTV were confounded by the blood radioactivity in the liver.

$$frac\ of\ total\ liver_{blood} = \frac{V_{blood} \times 0.1}{V_{total\ liver}} \quad \textbf{Eq. 4.20}$$

Where $frac\ of\ total\ liver_{blood}$ is the fraction of the liver that is blood, V_{blood} is the total blood volume, and $V_{total\ liver}$ is the total liver volume *i.e.* the volume blood in the liver plus the volume of the actual liver tissue.

^{11}C-GLB (two-compartmental model):

$$\frac{dX_{actual\ liver}}{dt} = k_{s,uptake} \cdot C_{blood} \cdot V_{blood} - k_{s,efflux} \cdot C_{actual\ liver} \cdot V_{actual\ liver} = k_{s,uptake} \cdot C_{blood} \cdot V_{blood} - k_{s,efflux} \cdot C_{actual\ liver} \cdot V_{total\ liver} \cdot (1 - frac\ of\ total\ liver_{blood}) \quad \textbf{Eq. 4.21}$$

^{18}F-PTV (three-compartmental model):

$$\frac{dX_{actual\ liver}}{dt} = k_{s,uptake} \cdot C_{blood} \cdot V_{blood} - k_{s,efflux} \cdot C_{actual\ liver} \cdot V_{actual\ liver} - k_{bile} \cdot C_{actual\ liver} \cdot V_{actual\ liver} = k_{s,uptake} \cdot C_{blood} \cdot V_{blood} - k_{s,efflux} \cdot C_{actual\ liver} \cdot V_{total\ liver} \cdot (1 - frac\ of\ total\ liver_{blood}) - k_{bile} \cdot C_{actual\ liver} \cdot V_{total\ liver} \cdot (1 - frac\ of\ total\ liver_{blood}) \quad \textbf{Eq. 4.22}$$

$$\frac{dX_{BD+GB}}{dt} = k_{bile} \cdot C_{actual\ liver} \cdot V_{actual\ liver} = k_{bile} \cdot C_{actual\ liver} \cdot V_{total\ liver} \cdot (1 - frac\ of\ total\ liver_{blood}) \quad \textbf{Eq. 4.23}$$

Where $\frac{dX_{actual\ liver}}{dt}$ is the change in amount of ^{11}C-GLB or ^{18}F-PTV in the actual liver tissue per unit of time. $V_{actual\ liver}$ is the actual liver tissue volume, which is $V_{total\ liver} \cdot (1 - frac\ of\ total\ liver_{blood})$ based on **Eq. 4.20**. $k_{s,efflux}$ and k_{bile} are the rate constants for sinusoidal uptake, sinusoidal efflux and biliary efflux, respectively.

For ^{11}C-GLB, C_{blood} was obtained from image-derived input function of the left ventricle and the aorta; $C_{total\ liver}$ and $C_{actual\ liver}$ represent the PET image-derived ^{11}C-GLB liver concentrations and ^{11}C-GLB concentrations in the actual liver tissue. For ^{18}F-PTV, C_{blood} , $C_{total\ liver}$ and X_{BD+GB} represent the venous blood ^{18}F-PTV concentrations (arterial concentrations were not available), PET image-derived ^{18}F-PTV liver

concentrations, and ^{18}F-PTV amount in extra-hepatic bile duct plus gallbladder, respectively (Nakaoka *et al.*, 2022)nn. $C_{actual\ liver}$ represents the ^{18}F-PTV concentrations in the actual liver tissue.

The total blood (V_{blood}) and total liver ($V_{total\ liver}$) volume were estimated based on the individual body weight for each subject studied in the ^{11}C-GLB study and the mean body weight for ^{18}F-PTV study (Feldschuh and Enson, 1977; Okudaira *et al.*, 2000; Vauthey *et al.*, 2002).

For both ^{11}C-GLB and ^{18}F-PTV:

The above compartment models were fitted to the observed data by taking into consideration the radioactivity in the blood in the liver:

$$C_{total\ liver} = \frac{X_{total\ liver}}{V_{total\ liver}} = \frac{X_{liver\ blood} + X_{actual\ liver}}{V_{total\ liver}} =$$

$$\frac{C_{blood} \cdot V_{total\ liver} \cdot frac\ of\ total\ liver_{blood} + C_{actual\ liver} \cdot V_{total\ liver} \cdot (1 - frac\ of\ total\ liver_{blood})}{V_{total\ liver}} \quad \textbf{Eq. 4.24}$$

Where $X_{total\ liver}$ is the amount of ^{11}C-GLB or ^{18}F-PTV in the total liver including the amount in liver blood ($X_{liver\ blood}$) plus the amount in actual liver ($X_{actual\ liver}$).

Then, the following parameters were derived from the estimated rate constants:

$$CL_{s,uptake} = k_{s,uptake} \cdot V_{blood} \quad \textbf{Eq. 4.25}$$

$$CL_{s,efflux} = k_{s,efflux} \cdot V_{total\ liver} \cdot (1 - fraction\ of\ total\ liver_{blood}) \quad \textbf{Eq. 4.26}$$

$$CL_{bile} = k_{bile} \cdot V_{total\ liver} \cdot (1 - fraction\ of\ total\ liver_{blood}) \quad \textbf{Eq. 4.27}$$

Where $CL_{s,uptake}$, $CL_{s,efflux}$ and CL_{bile} are the total sinusoidal uptake CL, sinusoidal efflux CL and biliary efflux CL, respectively. Since negligible metabolism for both GLB and PTV was observed within the time frame of the PET imaging studies, metabolic CL of these drugs was not included in the model (Marie *et al.*, 2022; Nakaoka *et al.*, 2022). Consistent with other data (Rydberg *et al.*, 1995; Marie *et al.*, 2022), the biliary efflux CL of ^{11}C-GLB was assumed to be negligible as the amount of ^{11}C-GLB (or its metabolites) in the gallbladder was minimal and could not be accurately quantified.

Goodness of fit of the model to the data (or estimation of the parameters) was assessed by the weighted residual plots, visual inspection of the predicted and observed data, and the coefficient of variation (%CV) of the estimates of the parameters.

4.3.13 *Comparison of REF-predicted hepatobiliary CLs and hepatic concentrations of GLB and PTV with those estimated from the PET imaging data*

GLB or PTV total hepatic concentrations were simulated using the REF-predicted hepatobiliary CLs and a two- (GLB) or three-compartmental model (PTV) (SAAM II, Nanomath, Spokane, WA, **Eq. 4.20-4.27**). Then, these predictions were compared with those estimated from the PET imaging data (**Table 4.2** & **Table 4.3**).

4.3.14 *Data analyses.*

Unless otherwise indicated, data are presented as geometric mean ± standard deviation or geometric mean (95% confidence interval). The difference between AMP- and ATP-dependent intravesicular accumulation of ^{3}H-GLB or ^{3}H-PTV and the difference between predicted value *vs.* observed value was determined by the unpaired t-test (ns $p > 0.05$, *$p < 0.05$; **$p < 0.01$; ***$p < 0.001$) using GraphPad Prism version 9 (GraphPad Software, San Diego, CA). The success criterion for both GLB and PTV was defined as predictions falling within a 2-fold range of the observed value. Additionally, for GLB, we employed a success criterion (Abduljalil *et al.*, 2014) that takes into account the inter-subject variability.

4.4 RESULTS

4.4.1 *Estimates of human ^{11}C-glyburide (GLB) and ^{18}F-pitavastatin (PTV) hepatobiliary CLs by compartmental modeling of the PET-imaged data*

The mean (n=7) *in vivo* $CL_{s,uptake}$ and $CL_{s,efflux}$ of ^{11}C-GLB was estimated to be 272.3 mL/min (CV%: 25%) and 47.8 mL/min (CV%: 40%), respectively (**Table 4.1**). The $CL_{s,uptake}$, $CL_{s,efflux}$ and CL_{bile} of ^{18}F-PTV was estimated to be 607.8 mL/min, 17.4 mL/min and 4.20 mL/min, respectively (**Table 4.1;** no variability in the estimates is provided as only the mean PET-imaged data were available for digitization). Both ^{11}C-GLB and ^{18}F-PTV parameters were estimated with a high degree of confidence as evidenced by the %CV of the estimates ranging from 0.9% to 14.0%.

4.4.2 *The $CL_{s,uptake}$ of GLB and PTV was well-predicted using the TECs/REF approach*

Unlike what has been reported by others, GLB was found to be a substrate of sinusoidal uptake transporters OATP1B1, OATP1B3, and OATP2B1 but not of NTCP (**Fig. 4.1**; **Fig. 4.2A; Fig. 4.3A**). After scaling by the REF, the $CL_{s,uptake}$ of GLB was predicted to be primarily mediated by OATPs ($f_{t,OATPs}$=82%), with OATP1B1 accounting for 45% of the total $CL_{s,uptake}$ (**Fig. 4.4A**). The REF-predicted total *in vivo* GLB $CL_{s,uptake,REF\text{-}pred,in\ vivo}$ was 250.8 mL/minute, and fell within the 2- fold range of the mean PET imaged-estimated GLB $CL_{s,uptake}$ value (**Table 4.2&4.5; Fig. 4.5A**) as well as within the success criterion proposed by Abduljalil *et al*.(Abduljalil *et al.*, 2014) (*i.e.*, 180.4-411.1 mL/min). PTV was transported not only by OATPs but also by NTCP (**Fig. 4.1&4.2B**), and the NTCP-mediated $CL_{s,uptake}$ contributed 22% of the total PTV $CL_{s,uptake,REF\text{-}pred,in\ vivo}$ (**Fig. 4.4B**). The total $CL_{s,uptake,\ REF\text{-}pred,in\ vivo}$ fell within the predefined 2-fold range of the observed PET imaged-estimated PTV $CL_{s,uptake}$ value (**Table 4.3; Fig. 4.6A**).

4.4.3 *The $CL_{s,efflux}$ of GLB and PTV was well-predicted using the TECs/TEVs/REF approach*

Unlike what has been reported by others, we found PTV, but not GLB, was a substrate of sinusoidal efflux transporter MRP3 (**Fig. 4.2C**; **Fig. 4.3B**). The *in vivo* $CL_{s,efflux}$ of GLB, assumed to be by passive diffusion only, was predicted to be 68.2 mL/min. This value fell within both the 2-fold success criterion (*i.e.*, 23.9 - 95.6

mL/min) as well as the criterion proposed by Abduljalil *et al*. (Abduljalil *et al.*, 2014) (*i.e.*, 25.0 - 91.6 mL/min) (**Fig. 4.5B**; **Table 4.2&4.5**). The PTV $CL_{s,efflux,\ REF\text{-}pred,in\ vivo}$ fell within the 2-fold of the PET imaged PTV $CL_{s,efflux}$ (22.1 mL/min *vs.* 17.4 mL/min) (**Fig. 4.6B; Table 4.3**). Although MRP3 contributed to the sinusoidal efflux of PTV, the majority (88%) of PTV $CL_{s,efflux}$ was predicted to be by passive diffusion (**Fig. 4.4C**).

4.4.4 *The CL_{bile} of PTV was well-predicted using the TEVs/REF approach*

Before scaling by REF, the BCRP-mediated CL_{bile} was larger than that by P-gp (**Fig. 4.4D & 4.4E**). However, the REF for BCRP was lower than that for P-gp because of its lower abundance in human liver tissue. Consequently, upon REF scaling, the fraction transported by P-gp accounted for 0.79 of the total CL_{bile} (**Fig. 4.6C**; **Fig. 4.4D & 4.4E**). The $CL_{bile,REF\text{-}pred,in\ vivo}$ of PTV (4.43 mL/min), fell within 2-fold range of its PET-imaged estimate (*i.e.*, 4.20 mL/min) (**Fig. 4.6C; Table 4.3**).

4.4.5 *The REF-predicted GLB and PTV hepatic concentrations, hepatic AUC and C_{max}, fell within our pre-defined acceptance criteria*

Using the REF-predicted hepatobiliary CLs, the predicted ^{11}C-GLB hepatic AUC and C_{max} fell within our predefined 2-fold success range for all 7 individuals (individual subject **Fig. 4.5D; Fig. 4.7; Table 4.5**). In addition, the average predicted hepatic AUC and C_{max} were not significantly different from the observed values (p>0.05; **Fig. 4.5C; Table 4.2**). The REF-predicted ^{18}F-PTV hepatic AUC fell within 2-fold of the observed values except for data at later time points (**Fig. 4.6E**). The hepatic AUC and hepatic C_{max} P/O were 0.58 and 0.63, respectively (**Fig. 4.6D; Table 4.3**).

4.5 DISCUSSION

To our knowledge, besides our study on rosuvastatin (RSV) (Kumar *et al.*, 2021; Storelli, Li, *et al.*, 2022), this is only the second time that the TECs/TEVs/REF approach has been successfully used to predict the hepatobiliary CLs and hepatic concentrations of OATP-transported drugs. The TECs/TEVs/ REF approach offers several advantages over the traditional physiological scaling where primary cells such as human hepatocytes (plated, PH, suspended, SH or sandwich-cultured, SCH) are used (Kumar *et al.*, 2021). First, compared to physiological scaling, the TECs/TEVs/REF approach utilizes readily accessible, reproducible, higher throughput and cost-effective TECs and TEVs. This is particularly important where primary cells (e.g. BBB, intestinal enterocytes) are not available. Second, we have previously shown that human hepatocytes (PH, SH or SCHH) underpredict the sinusoidal uptake clearance while the SCHH overpredict the biliary efflux clearance of drugs (Kumar *et al.*, 2020, 2021; Storelli, Li, *et al.*, 2022). This is because biliary efflux transporters' abundance is dramatically increased in SCHH *vs.* human liver tissue (Kumar *et al.*, 2019). Third, we determined the REF in TECs/TEVs using targeted proteomics, a highly quantitative method and adjusted the REF for the plasma membrane transporter abundance when scaling data from TECs/TEVs. Fourth, the data for mean human liver transporter abundance was derived from a large number of livers, thereby incorporating inter-individual variability in transporter abundance and providing a robust estimate that can be assumed to reflect the population mean. Fifth, unlike using the traditional MTPPGL approach, we applied the functional sinusoidal surface area (0.37 of the total hepatocyte surface area) available for passive diffusion to predict passive diffusion CL of drugs (Esteller, 2008). Sixth, the TECs/TEVs/REF approach allows determination of the relative contribution of each transporter to inform potential impact of transporter-related drug interactions or pharmacogenomics on both systemic and tissue drug concentrations. Due to lack of selectivity of transporter substrates (e.g. OATP1B1 *vs.* OATP1B3), human hepatocytes do not have this capability. Other unique aspect of our studies is that we determined if the TECs/TEVs/REF approach can successfully predict PET-imaged human hepatic concentrations of the transported drugs, ^{11}C-GLB (Marie *et al.*, 2022) and ^{18}F-PTV (Nakaoka *et al.*, 2022). Though, the ^{18}F-PTV PET and ^{11}C-GLB data have been previously modeled, the sinusoidal uptake CL was estimated using the integration plot approach; this

approach assumes negligible biliary or sinusoidal efflux CL of the drug during the initial uptake phase. Ignoring sinusoidal efflux CL when using this approach will result in underestimation of $CL_{s,uptake}$. Indeed, our estimated GLB and PTV $CL_{s,uptake}$ values, using compartmental modeling of the PET imaging data, were higher than those published (Marie *et al.*, 2022; Nakaoka *et al.*, 2022).

Using the REF approach, we successfully predicted hepatobiliary CLs and therefore hepatic concentrations of both ^{11}C-GLB and ^{18}F-PTV within 2-fold of the mean observed values (**Fig. 4.3&4.4**; **Table 4.2&4.3**). Furthermore, the REF-predicted mean GLB AUC and C_{max} were not significantly different from those observed (p>0.05). While the prediction of hepatic ^{18}F-PTV AUC and C_{max} met the success criteria, like RSV (Storelli, Li, *et al.*, 2022) the hepatic concentration-time profile was modestly underpredicted due to underprediction of its $CL_{s,uptake}$. We note that modest underprediction of this magnitude has also been widely reported for IVIVE of metabolic CL of drugs (Wood *et al.*, 2017).

The 2-fold acceptance criterion was chosen for several reasons. First, we could not use the criterion proposed by Abduljalil *et al*. (Abduljalil *et al.*, 2014) for ^{18}F-PTV as we did not have the inter-individual variability in the ^{18}F-PTV data. However, we do have these values for ^{11}C-GLB and our predictions fell within this acceptance criteria. Secondly, a 2-fold criterion is reasonable in early development of a drug until data on inter-individual variability in systemic pharmacokinetics of the drug are obtained to better inform this criterion. We want to emphasize here that the REF-predictions cannot be any better than the *in vivo* inter-individual variability in systemic concentrations which will drive the inter-individual variability in tissue drug concentrations.

To evaluate the rate-determining step in CL_h of GLB, we scaled the *in vitro* intrinsic metabolic CL of GLB (52.9 µL/min/mg protein) in human liver microsomes to *in vivo* CL_{met} (Varma *et al.*, 2014). The predicted *in vivo* GLB CL_{met} (237 min/min) was larger than its $CL_{s,efflux}$ suggesting that the GLB $CL_{s,uptake}$ is the rate-determining step in CL_h of GLB (G Patilea-Vrana and Unadkat, 2016). Indeed, drug interactions studies agree with this conclusion; IV rifampin (OATPs inhibitor) decreased GLB oral plasma CL by 54%, however, co-administration of CYP3A4 or CYP2C9 inducer/inhibitors with GLB had no effect (Fleishaker and Phillips,

1991; Lilja *et al.*, 2007; Zheng *et al.*, 2009). In contrast, all hepatobiliary CL pathways appear to be the rate-determining step in the hepatic CL of PTV.

There are a few limitations to our study. First, our study did not incorporate transporter genotyping data. For ^{18}F-PTV PET study, the subjects were Japanese males (Nakaoka *et al.*, 2022), while the human transporter abundance data was sourced from a predominantly Caucasian liver bank (Wang *et al.*, 2015). However, we can discount this concern because a study comparing PTV's PK between Japanese and Caucasian populations did not show any discernible difference in PK (Warrington *et al.*, 2011). Second, we assumed that the metabolism of ^{11}C-GLB and ^{18}F-PTV within the PET imaging timeframe was negligible. In the PET studies, a small (^{11}C-GLB; 6.8% ± 3.6 %) or zero (^{18}F-PTV) percent of radioactivity was associated with metabolites over the duration of PET imaging (Marie *et al.*, 2022; Nakaoka *et al.*, 2022). However, if any metabolites retain the radiolabel and are sequestered in the liver or biliary excreted, they will confound our estimating of hepatobiliary CLs. To explore this possibility, we fitted the respective compartmental model to the ^{11}C-GLB and ^{18}F-PTV PET imaging data collected over a shorter duration (<15 minutes when the extent of metabolism should be reduced). The estimated $CL_{s,uptake}$ and $CL_{s,efflux}$ were not significantly (p>0.05) different from those presented here (data not shown). Additionally, sensitivity analysis on GLB hepatic concentrations with respect to varying degrees of CL_{met} (including that observed in human liver microsomal studies(Varma *et al.*, 2014) indicated a minimal role for CL_{met} within the PET imaging timeframe (data not shown). Third, the liver blood supply consists of 80% portal vein blood and 20% hepatic arterial blood (SCHENK *et al.*, 1962). However, in the ^{11}C-GLB PET imaging study, the PET image-derived arterial blood concentrations (measured in the aorta + left ventricle) were used in the model (Marie *et al.*, 2022), likely overestimating the actual liver input concentrations and therefore underestimating the *in vivo* hepatic $CL_{s,uptake}$. In the ^{18}F-PTV PET imaging study, only the venous blood ^{18}F-PTV concentrations were measured (Nakaoka *et al.*, 2022). Fourth, we did not take into consideration that, due to the negative membrane potential in HEK293 cells as well as human hepatocytes, there could be asymmetry in the passive diffusion CL of the drugs across the sinusoidal membrane. Lastly, in all hepatic PET imaging studies, it is impossible to separate radioactivity in the biliary tree within the liver *vs.* that in the liver tissue, resulting in overestimation of hepatic drug concentrations and

underestimation of $CL_{s,efflux}$ and CL_{bile} (Wang *et al.*, 2021). This may be one reason why the REF-predicted approach underestimated the hepatic concentrations of both PTV and RSV and not of GLB; the latter (or its metabolites) is not significantly excreted in the bile over the duration of PET imaging.

In conclusion, using the REF approach, we have now successfully predicted $CL_{s,uptake}$, $CL_{s,efflux}$, CL_{bile}, and human hepatic concentrations of the drugs, GLB, PTV and RSV (Storelli *et al.*, 2022) that are transported by multiple transporters (OATPs, NTCP, MRP2, MRP3, BCRP, and P-gp). In addition, we have validated the ability of the TECs/REF approach to predict the brain and fetal unbound tissue-to-plasma concentration ratio of several transported substrates (Sachar *et al.*, 2020; Anoshchenko *et al.*, 2021; Storelli *et al.*, 2021). Moreover, the REF approach can be extended to include metabolic CL of drugs. Therefore, based on these successes, we propose that the REF approach can now be used with confidence to predict tissue drug concentrations, modulated by transporters present at the tissue-blood barrier, irrespective of whether the drug is substantially metabolized or not.

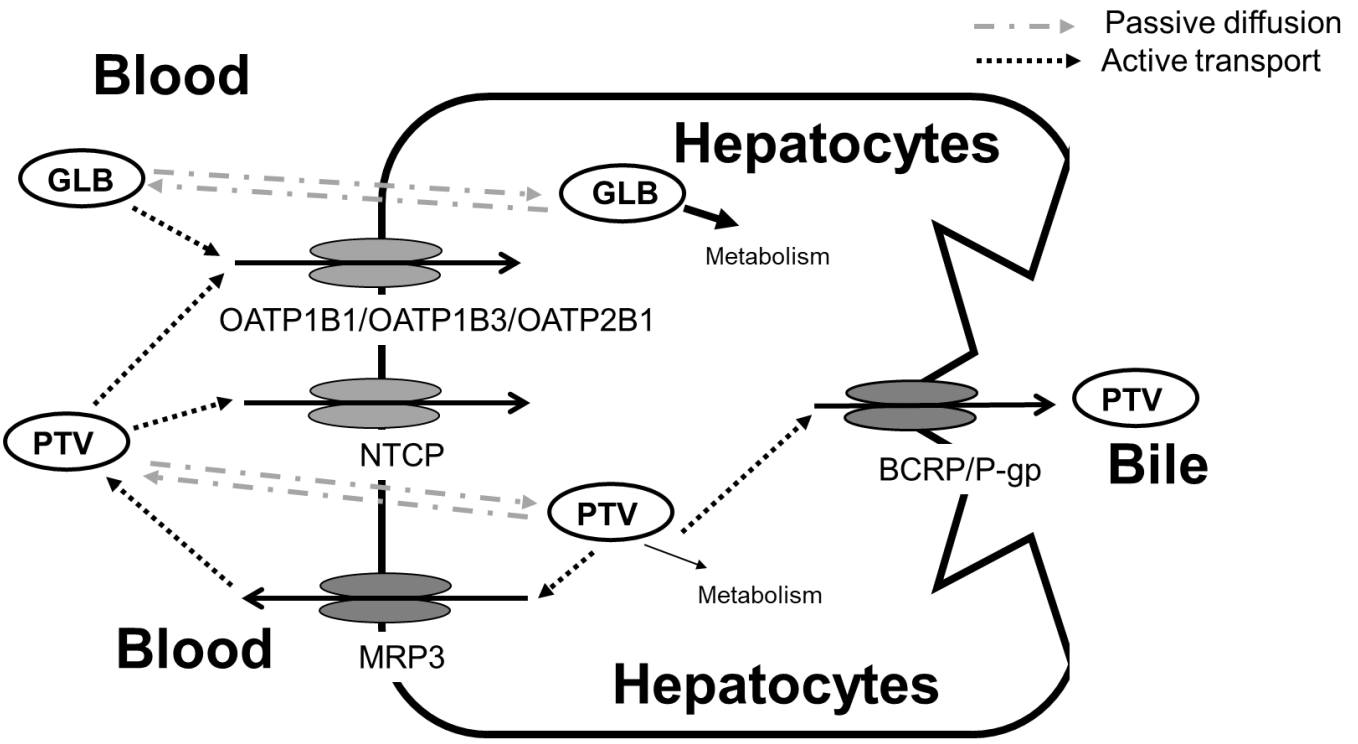

Figure 4.1. Schematic diagram of hepatic transport of glyburide (GLB) and pitavastatin (PTV) based on our data.

GLB or PTV in blood is taken up by the hepatocytes by the indicated sinusoidal transporters and by passive diffusion. Any unmetabolized GLB or PTV is returned to the blood via passive diffusion and MRP3 (PTV only). PTV is secreted into the bile by BCRP and P-gp.

A

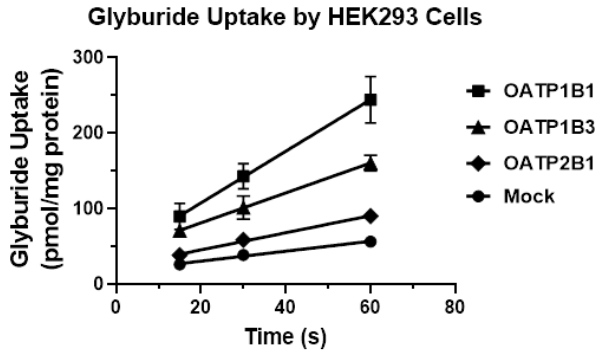

B

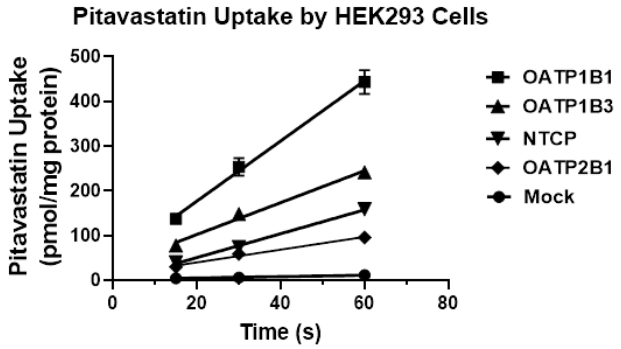

C

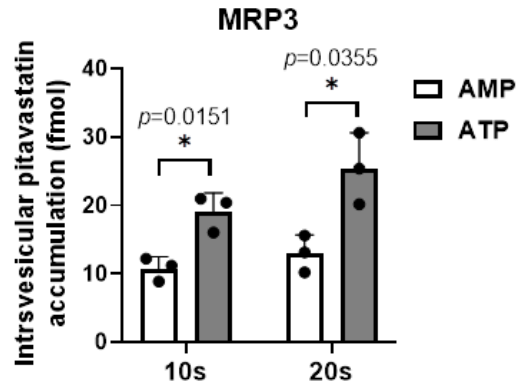

D

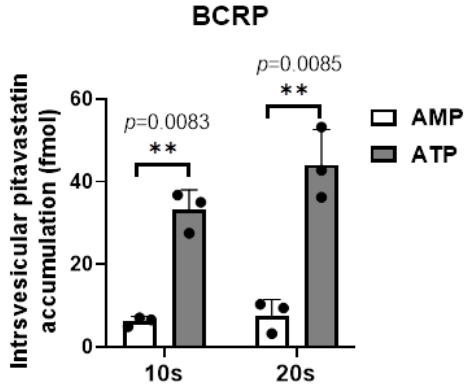

E

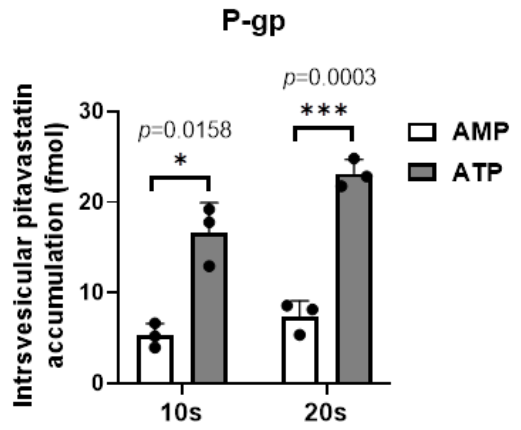

Figure 4.2. Representative plots of glyburide (A) and pitavastatin (B) uptake-time profile by TECs/mock cells or of pitavastatin by TEVs (C, D, E) in the presence of adenosine triphosphate (ATP, passive diffusion + active transport) or adenosine monophosphate (AMP, passive diffusion).

Glyburide was found not to be a NTCP-substrate. Data shown are mean ± S.D. of triplicates (normalized to 1 µM concentration for the TECs/mock cells). Statistical comparison was performed using the unpaired t-test (*p<0.05; ** p<0.01; *** p<0.001). These data were confirmed by two additional independent experiments, each conducted in triplicate.

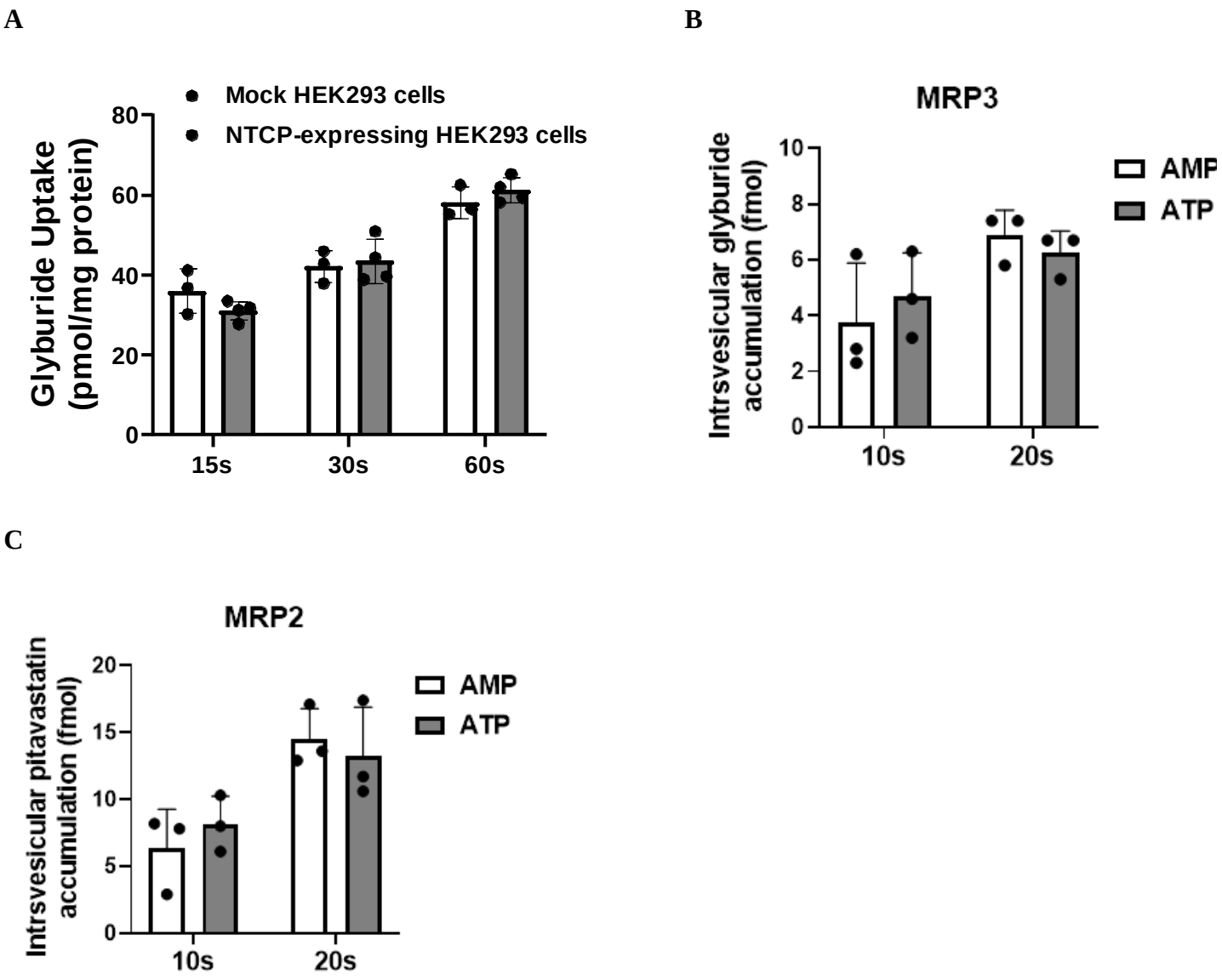

Figure 4.3. Glyburide is not transported by NTCP (A) or MRP3 (B). Representative glyburide uptake by Mock/NTCP TECs (A) or efflux by MRP3 TEVs in the presence of adenosine triphosphate (ATP, passive diffusion + MRP3 transport) or adenosine monophosphate (AMP, passive diffusion). **Pitavastatin is not transported by MRP2 (C).** Representative pitavastatin efflux by MRP2 TEVs in the presence of ATP (passive diffusion + MRP3 transport) or AMP (passive diffusion). Intravesicular accumulation was measured in the linear range. Data shown are mean±SD and were confirmed by 2 additional independent experiments, each conducted in triplicate. Statistical comparison was performed using the unpaired t-test (ns, $p > 0.05$).

A

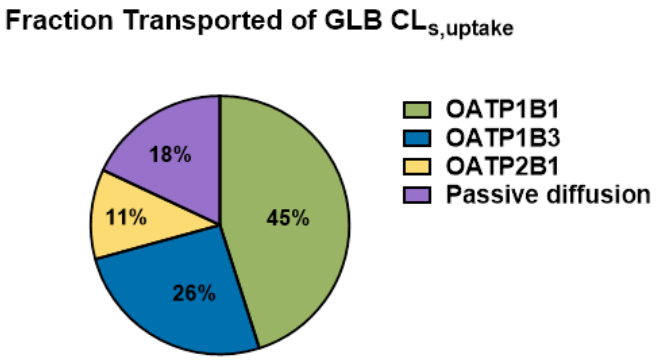
Fraction Transported of GLB $CL_{s,uptake}$
18%
11%
45%
26%
OATP1B1
OATP1B3
OATP2B1
Passive diffusion

B

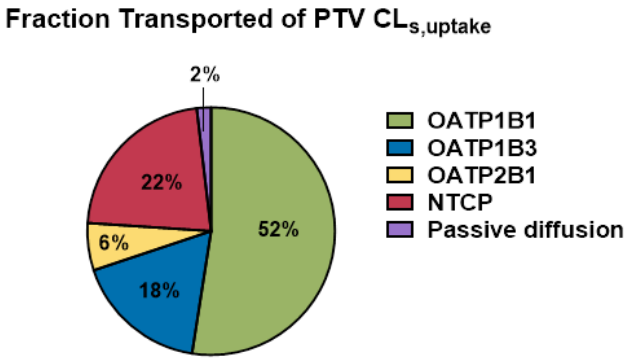
Fraction Transported of PTV $CL_{s,uptake}$
2%
22%
6%
52%
18%
OATP1B1
OATP1B3
OATP2B1
NTCP
Passive diffusion

C

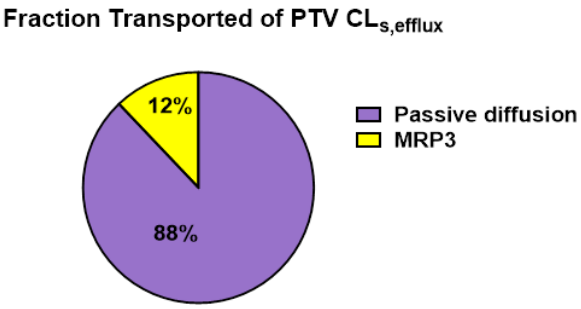
Fraction Transported of PTV $CL_{s,efflux}$
12%
88%
Passive diffusion
MRP3

D

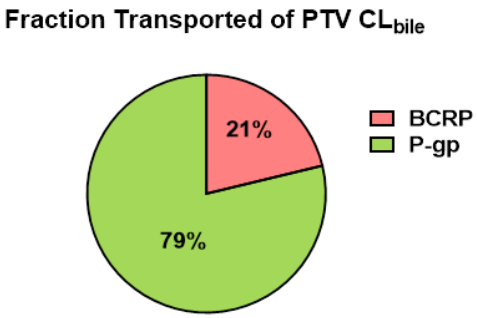
Fraction Transported of PTV CL_{bile}
21%
79%
BCRP
P-gp

E

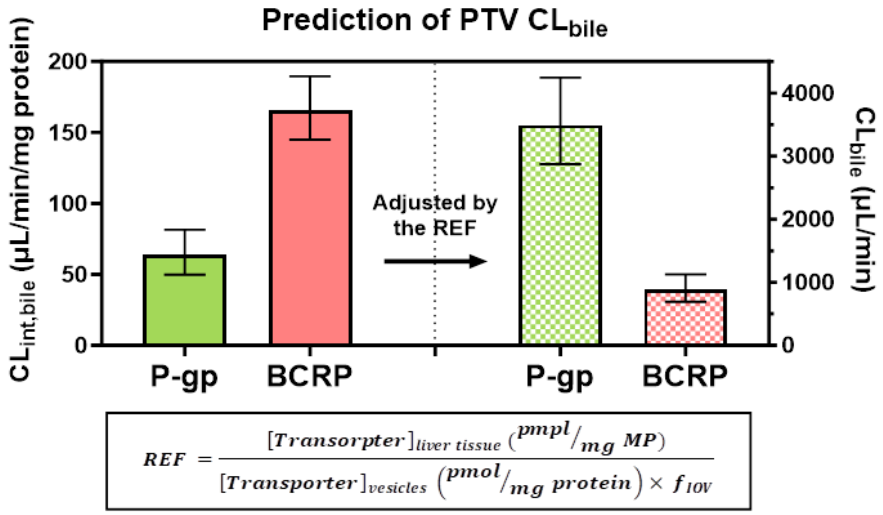
Prediction of PTV CL_{bile}
$CL_{int,bile}$ (µL/min/mg protein)
CL_{bile} (µL/min)
200
150
100
50
0
4000
3000
2000
1000
0
Adjusted by the REF
P-gp
BCRP
P-gp
BCRP
$REF = \frac{[Transorpter]_{liver\ tissue}\ (^{pmpl}/_{mg\ MP})}{[Transporter]_{vesicles}\ \left(^{pmol}/_{mg\ protein}\right) \times f_{IOV}}$

Figure 4.4. Fraction contribution of various uptake or efflux transporters as well as passive diffusion to the predicted *in vivo* glyburide (A) and pitavastatin (B) uptake clearance, pitavastatin sinusoidal efflux clearance (C), and pitavastatin biliary efflux clearance (D) in HEK293 cell lines and vesicles after adjusting by the Relative Expression Factor (REF).

Each REF was derived from targeted proteomics-measured relative plasma membrane abundance of the uptake/efflux transporters in human liver tissue *vs.* that in TECs or TEVs (see Tables 2 & 3). The human liver tissue transporter abundances were obtained from our previously published study (Deo *et al.*, 2012; Prasad *et al.*, 2013, 2014). Data shown are mean±SD of three to five independent experiments. The P-gp- and BCRP-mediated biliary intrinsic efflux CLs ($CL_{int,bile}$) of pitavastatin in vesicles was individually scaled to *in vivo* by the corresponding REF and physiological scaling factors (E).

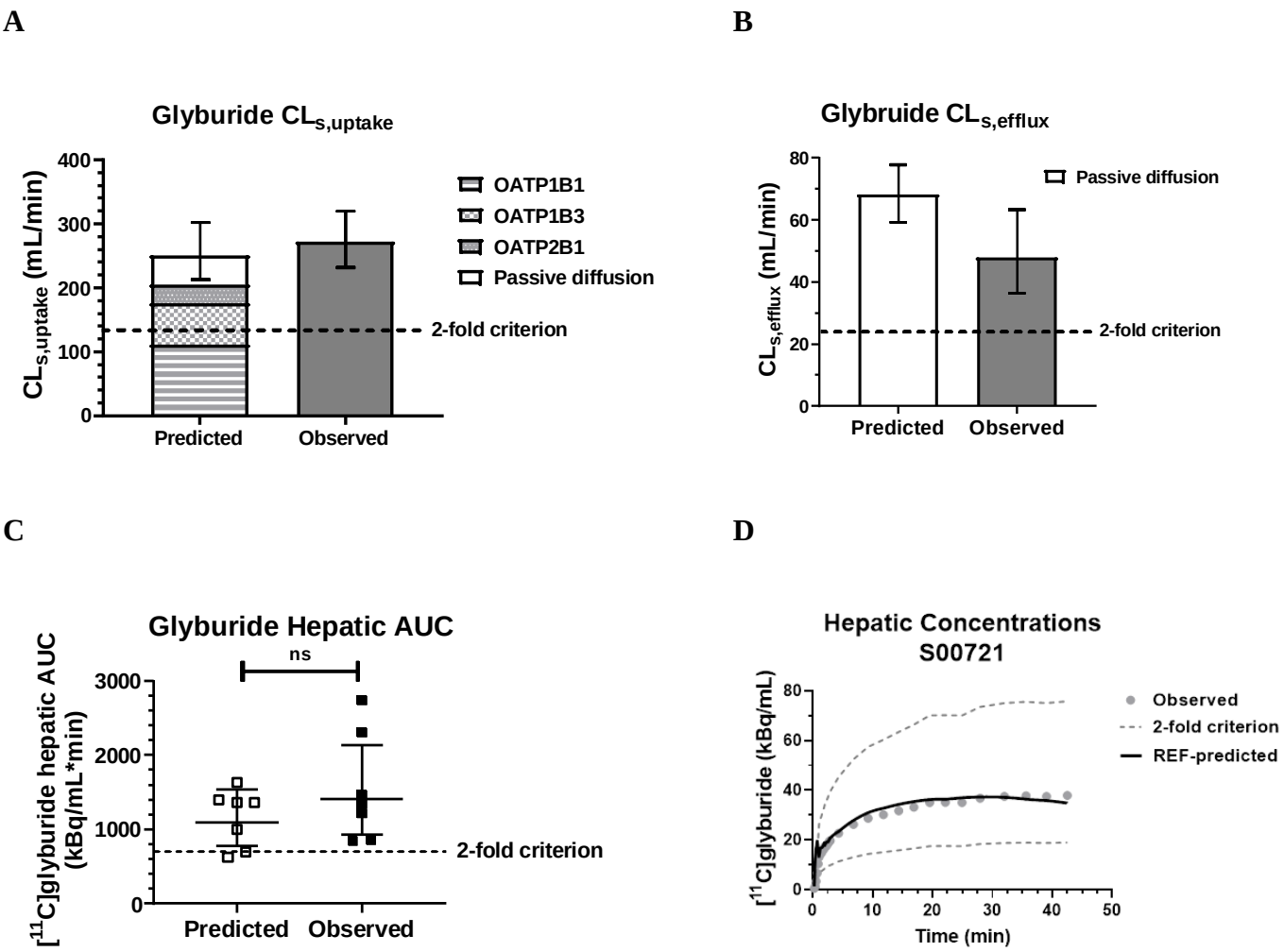

Figure 4.5. REF-predicted total glyburide (GLB) $CL_{s,uptake}$ (A), $CL_{s,efflux}$ (B), and hepatic AUC (C) fell within 2-fold of the observed value.

To illustrate, the REF-predicted (solid line) and observed (filled circles) ^{11}C-GLB hepatic concentration-time profile are shown for an individual subject (S00721; the data for the remaining 6 subjects are shown in **Fig. 4.S3**) (D; dashed lines are the 0.5- and 2-fold of the observed concentration-time profile). Solid lines in A-C indicate geometric mean and 95% confidence interval. ns- indicates predicted value not significantly different from the observed data by the unpaired Student's t-test (p=0.24).

A **B**

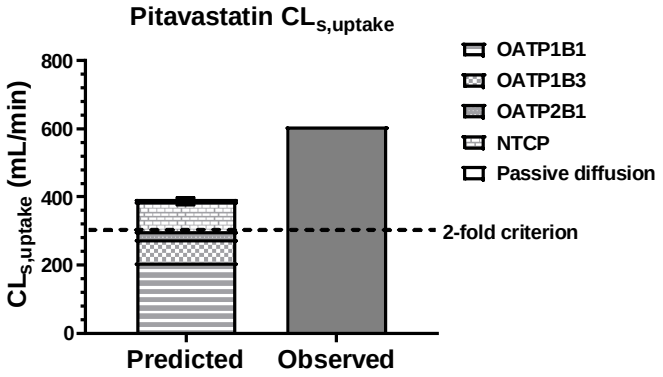

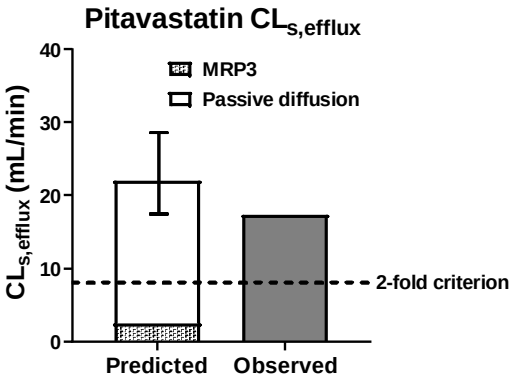

C

D

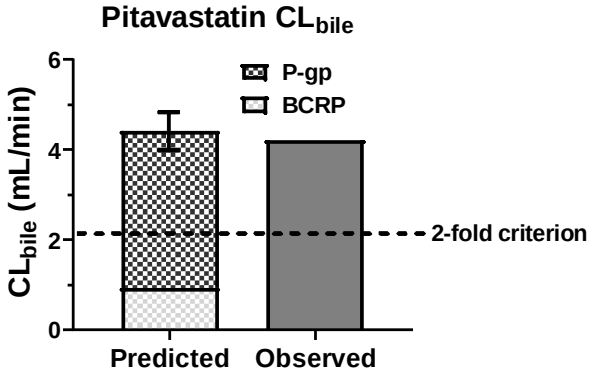

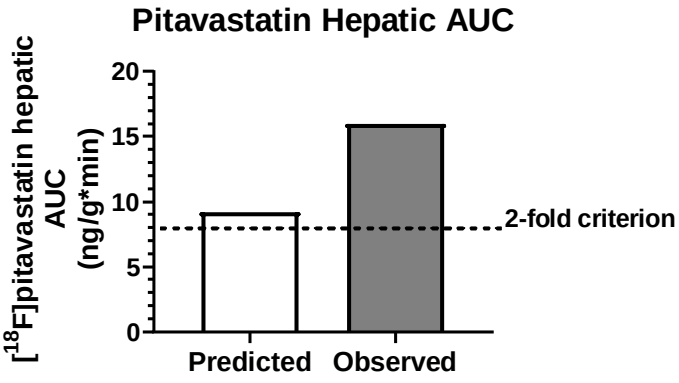

E

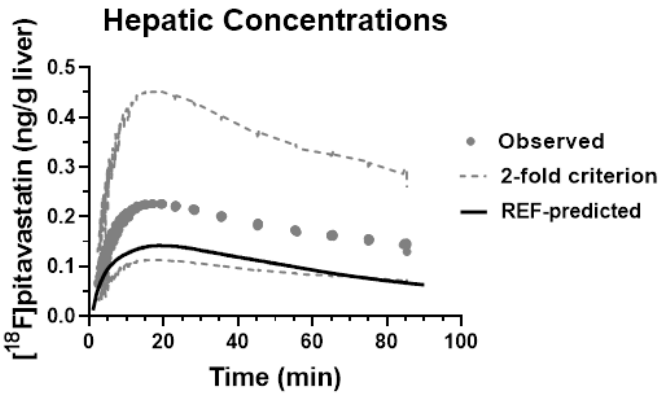

Figure 4.6. REF-predicted total pitavastatin (PTV) $CL_{s,uptake}$ (A), $CL_{s,efflux}$ (B), CL_{bile} (C) and hepatic AUC (D) fell within 2-fold of the observed value.

To illustrate, the REF-predicted (solid line) ^{18}F-PTV hepatic concentration-time profile fell within 2-fold (dashed lines) of the mean observed data (filled circles, E). Solid lines in A-C indicate geometric mean and 95% confidence interval.

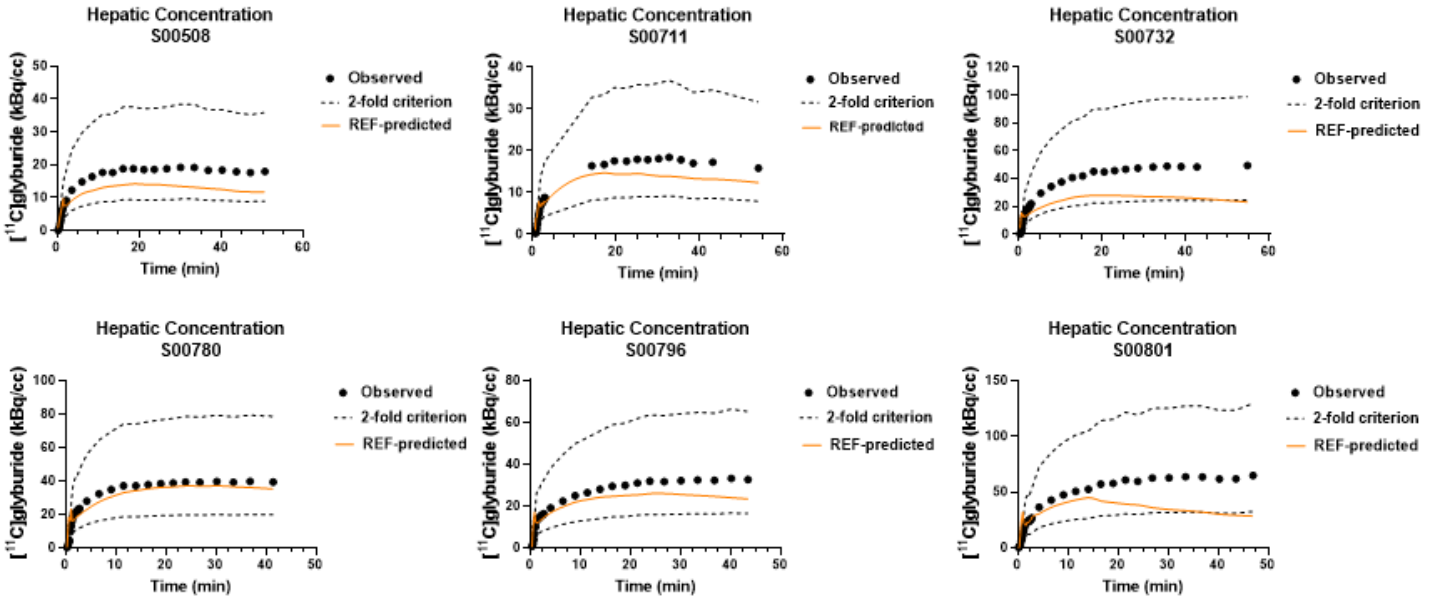

Figure 4.7. The REF (relative expression factor)–predicted hepatic ^{11}C-glyburide concentration-time profiles of 6 individual subjects.

Except for subject S00801, the predicted data agreed well with the corresponding observed PET-imaged data. The mean REF-predicted hepatic glyburide concentrations in humans (continuous lines) fell within 2-fold of the observed PET imaging data.

Tables 4.1. Estimates of ^{11}C-glyburide (GLB) and ^{18}F-pitavastatin (PTV) hepatobiliary CLs from PET imaging data and their observed hepatic exposure (AUC[a], C_{max}[b])

	^{11}C-GLB N = 7 subjects		**^{18}F-PTV**
	Geometric mean (CV%)	**95% Confidence interval (max/min)**	**Estimated from arithmetic mean of 10 rounds of digitization**
$CL_{s,uptake}$ (mL/min)	272.3 (25%)	228.1-331.5 (2.1)	607.8
$CL_{s,efflux}$ (mL/min)	47.8 (40%)	35.9-65.8 (3.6)	17.4
CL_{bile} (mL/min)	NA	NA	4.20
Hepatic AUC[a] (kBq/mL*min – GLB; ng/g liver*min - PTV)	1412.0 (51%)	1009.3-2074.3 (3.2)	16.0
Hepatic C_{max} [b] (kBq/mL – GLB; ng/g liver - PTV)	34.2 (52%)	24.6-50.7 (3.9)	0.23

$CL_{s,uptake}$, sinusoidal uptake clearance; $CL_{s,efflux}$, sinusoidal efflux clearance; CL_{bile}, biliary efflux clearance

[a] *The compartmental model-derived ^{11}C-GLB and ^{18}F-PTV hepatic area under the curve (AUC) was for 0–60 minutes and 0–90 minutes, respectively.*

[b] *C_{max} – model-derived maximal hepatic concentration.*

NA- not applicable.

Table 4.2. *In vitro* and Relative Expression Factor (REF)-predicted and observed ^{11}C-glyburide hepatobiliary CLs and hepatic exposure (AUC, C_{max})

	Transporter	*In vitro* CL_{int}[a] (µL/min/mg prot)	REF	*In vivo* $CL_{int,REF-pred}$ (ml/min)	f_t	*In vivo* $CL_{REF-pred}$ (ml/min)	Observed	P/O
$CL_{s,uptake}$	OATP1B1	118.4 (20%)	0.46	4909.4	0.44	110.4	-	-
	OATP1B3	119.3 (22%)	0.26	2830.0	0.26	65.7	-	-
	OATP2B1	43.2 (27%)	0.18	1223.4	0.11	28.8	-	-
	Passive diffusion	38.5 (19%)		1981.2	0.18	46.1	-	-
	Total	-	-	10944.0	-	250.8	272.3 [180.4-411.1][c]	0.92
$CL_{s,efflux}$	Passive diffusion only	38.5 (19%)	-	1981.2		68.2	47.8 [25.0-91.6][c]	1.43

	REF-Predicted	Observed	P/O
Hepatic AUC[b] (kBq/mL*min)	1090.9 (868.7-1437.1)	1412.0 (1009.3-2074.3) [651.0-3062.3][c]	0.77
Hepatic C_{max}[b] (kBq/mL)	26.6 (20.2-37.5)	34.2 (24.6-50.7) [16.4-71.1][c]	0.78

CL_{int}, in vitro intrinsic clearance; REF; relative expression factor; $CL_{int,REF-pred}$, REF-predicted in vivo intrinsic hepatobiliary clearance; $CL_{bile,REF-pred}$, REF-predicted in vivo hepatobiliary clearance; f_t, fraction transported; $CL_{s,uptake}$, sinusoidal uptake clearance; $CL_{s,efflux}$, sinusoidal efflux clearance; AUC, area under the concentration-time curve; C_{max}, maximum hepatic concentration; P/O, predicted-over-observed.

a - In vitro CL_{int} data shown are geometric mean (% coefficient of variation).

b - Compartmental model-derived hepatic AUC and C_{max} data shown are geometric mean (95% confidence interval).

c - The success criteria proposed by Abduljalil et al.(Abduljalil *et al.*, 2014)

Table 4.3. Relative Expression Factor (REF)-predicted and observed ^{18}F-pitavastatin hepatobiliary CLs and hepatic exposure (AUC, C_{max})

	Transporter	*In vitro* Cl_{int}[a] (µL/min/mg prot)	REF	Predicted *in vivo* $CL_{int,pred\text{-}REF}$ (ml/min)	f_t	Predicted *in vivo* $CL_{pred\text{-}REF}$ (ml/min)	Observed	P/O
$CL_{s,uptake}$	OATP1B1	410.9 (13%)	0.46	16943.0	0.52	207.1	-	-
	OATP1B3	213.0 (10%)	0.26	5141.7	0.18	68.7	-	-
	OATP2B1	62.9 (14%)	0.18	1751.9	0.06	24.4	-	-
	NTCP	166.4 (10%)	0.52	6532.9	0.22	87.2	-	-
	Passive diffusion	10.2 (36%)	-	548.9	0.02	7.5	-	-
	All	-	-	30918.4	-	394.6	607.8	0.65
$CL_{s,efflux}$	MRP3	58.7 (44%)	0.021	76.0	0.12	2.5	-	-
	Passive diffusion	10.2 (36%)	-	548.9	0.88	19.5	-	-
	All	-	-	624.9	-	22.1	17.4	1.27
CL_{bile}	BCRP	165.7 (5%)	0.0027	26.6	0.21	0.94	-	-
	P-gp	63.6 (10%)	0.026	97.6	0.79	3.49	-	-
	All	-	-	124.2	-	4.43	4.20	1.05
	Predicted				**Observed**			**P/O**
Hepatic AUC[b] (ng/g liver*min)	9.21				16.0			0.58
Hepatic C_{max}[b] (ng/g liver)	0.14				0.23			0.63

CL_{int}, in vitro intrinsic clearance; REF; relative expression factor; $CL_{int,REF\text{-}pred}$, REF-predicted in vivo intrinsic hepatobiliary clearance; $CL_{bile,REF\text{-}pred}$, REF-predicted in vivo hepatobiliary clearance; f_t, fraction transported; $CL_{s,uptake}$, sinusoidal uptake clearance; $CL_{s,efflux}$, sinusoidal efflux clearance; CL_{bile}, biliary efflux clearance;

AUC, area under the concentration-time curve; C_{max}, maximal hepatic concentration; P/O, predicted-over-observed.

a - In vitro CL_{int} data shown are geometric mean (% coefficient of variation).

b – The hepatic AUC and C_{max} were derived from compartmental modeling.

Table 4.4. MRM parameters of the peptides selected for quantification of human hepatic transporter abundance using quantitative targeted proteomics.

Transporter	Surrogate peptide	Parent ion (m/z)	Product ion (m/z)	Cone voltage (V)	Collision energy (V)
OATP1B1	NVTGFFQSFK	587.9	860.5, 961.4	**35**	17
	NVTGFFQSF**K**	591.9	868.5, 969.5	35	17
OATP1B3	NVTGFFQSLK	570.8	826.3, 927.5	35	17
	NVTGFFQSL**K**	574.8	834.3, 935.6	35	17
OATP2B1	VLAVTDSPAR	514.8	646.3, 816.4	30	16
	VLAVTDSPA**R**	519.9	656.3, 826.4	30	16
NTCP	GIYDGDLK	440.7	547.1, 710.1	30	13
	GIYDGDL**K**	444.7	555.3, 718.3	30	13
BCRP	SSLLDVLAAR	522.8	644.4, 757.4	40	18
	SSLLDVLAA**R**	527.8	654.4, 767.5	40	18
P-gp	NTTGALTTR	467.7	618.4, 719.4	30	16
	NTTGALTT**R**	472.7	628.4, 729.4	30	16
MRP3	ADAGLTQEEK	531.2	634.3, 747.4, 875.4	30	13
	ADAGLTQEE**K**	535.3	642.3, 755.4, 883.5	30	13

The labeled $^{13}C_6{}^{14}N_2$-lysine residues of the internal standards are shown in bold.

Table 4.5. Estimates of *in vivo* hepatobiliary clearances of ^{11}C-glyburide in 7 individuals using compartmental modeling

Subject	**Body Weight**	**$CL_{s,uptake}$ (mL/min)**	**95% confidence interval (mL/min)**	**$CL_{s,efflux}$ (mL/min)**	**95% confidence interval (mL/min)**
S00508	59 kg	248.7	220.9-276.5	43.1	35.4-50.8
S00711	73 kg	251.7	219.8-283.5	49.3	38.7-59.9
S00721	66 kg	181.9	161.5-202.3	45.4	35.1-55.6
S00732	81 kg	389.3	357.8-420.8	51.0	42.3-59.7
S00780	83 kg	346.7	312.5-380.0	92.3	77.3-107.3
S00796	61 kg	245.2	219.4-270.9	49.2	40.1-58.3
S00801	87 kg	295.1	270.5-319.6	25.7	18.5-32.9

$CL_{s,uptake}$, *sinusoidal uptake clearance*

$CL_{s,efflux}$, *sinusoidal efflux clearance*

4.6 ABBREVIATIONS USED

f_{IOV}, fraction of inside-out vesicles; AMP, adenosine monophosphate; ATP, adenosine triphosphate; AUC, area under plasma concentration-time curve; BCRP, breast cancer resistance protein; C_{blood}, blood concentration; C_{liver}, liver concentration; CL, clearance; CL_{bile}, biliary clearance; CL_h, hepatic clearance; $CL_{int,active}$, *in vitro* active clearance; CL_{int}, *in vivo* intrinsic clearance; CL_{met}, metabolic clearance; $CL_{s,efflux}$, sinusoidal efflux clearance; $CL_{s,uptake}$, sinusoidal uptake clearance; C_{max}, maximal hepatic concentration; f_t, fraction transported; $f_{u,liver}$, fraction of drug unbound in the liver; GLB, glyburide; HBSS, Hank's Balanced Salt Solution; IVIVE, *in vitro* to *in vivo* extrapolation; $k_{s,uptake}$, rate constant for sinusoidal uptake; $k_{s,efflux}$ rate constant for sinusoidal efflux; k_{bile}, rate constant for biliary efflux; MMPPGL, mg membrane protein per gram of liver; MRP2/3/4, multidrug resistance protein 2/3/4; MTPPGL, mg total protein per gram of liver; NTCP, sodium-taurocholate cotransporting polypeptide; OATP, organic anion transporting polypeptide; OCT, organic cation transporter; PET, positron emission tomography; P-gp, P-glycoprotein; PM, plasma membrane; PMA, plasma membrane abundance; RSV, rosuvastatin; P/O, predicted-over-observed ratio; PTV, pitavastatin; PMUE, protein-mediated uptake effect; REF, relative expression factor approach; SCHH, sandwich-cultured human hepatocytes; SDS, sodium dodecyl sulfate; SSA, sinusoidal surface area; TECs/TEVs, transporter-expressing cells or vesicles

Chapter 5. CONCLUSIONS AND FUTURE DIRECTIONS

Accurate measurement or prediction of tissue drug concentrations is crucial in informing a drug's safety, efficacy, and tissue-based drug-drug interactions, especially when the targets are intracellular (Zhang *et al.*, 2019). Although PET imaging offers a non-invasive and highly quantitative approach to measure tissue drug concentrations, it cannot be routinely applied due to technical and budgetary challenges (Langer, 2016). Therefore, it is important to predict (rather than measure) steady-state drug concentrations in target tissues where toxicological and therapeutic effects manifest, including the dynamic changes in these concentrations with time, especially when they are modulated by transporters. To achieve this goal, we have proposed the proteomics-informed TECs/TEVs/REF approach and verified this approach by successfully predicting CLs and tissue concentrations of several transported drugs (Storelli, Yin, *et al.*, 2022). However, using this approach, the hepatic uptake CL and hepatic concentrations of RSV, an OATP substrate, were modestly underpredicted (Storelli, Li, *et al.*, 2022). This observation led us to research whether the protein-mediated uptake effect (PMUE) was the cause of this underprediction and whether such underprediction was specific to RSV or also applied to other OATP drug substrates. Thus, our goals were to investigate the PMUE and its implications in improving IVIVE of OATP-substrate drugs (i.e., statins, including RSV) and to determine if the TECs/TEVs/REF approach also underpredicted the hepatobiliary CLs and hepatic concentrations of other OATP substrates.

In **Aim 1** (**Chapter 2)**, the uptake of a cocktail of statins by OATP1B1-expressing and mock cells, in the presence and absences of 5% albumin, showed that, except for CRV and PTV, the observed PMUE on statins was largely an artifact caused by the residual statin-albumin complex that is not completely washed away when the uptake experiment is terminated. In **Aim 2** (**Chapter 3)**, we confirmed that the observed PMUE on statins taken up by the plated and suspended human hepatocytes was also largely confounded by the residual statin-albumin complex. Additionally, the observed PMUE on statins taken up by the suspended hepatocytes was modest and much lower than that observed with plated hepatocytes. These data further confirm that the observed PMUE is largely an artifact. Given these observations, we did not pursue the possibility that PMUE

could bridge the gap in IVIVE of transporter-mediated CL and tissue concentrations of statins. To determine if the underprediction of hepatic uptake CL observed with RSV is applicable to other OATP-substrates, in **Aim 3** (**Chapter 4)**, in addition to previously studied RSV, we extended the TECs/TEVs/REF approach to two additional OATP-substrate drugs, GLB and PTV. We were successful in predicting their hepatobiliary CLs and hepatic concentrations as verified by their human PET imaging data (Marie *et al.*, 2022; Nakaoka *et al.*, 2022).

Although, the TECs/TEVs/REF approach appears superior to the use of primary cells (suspended or plated) and PSF, we acknowledge that the *in vivo* hepatic uptake CL of RSV was still modestly underpredicted. For both approaches, further refinements are needed. Here, I discuss principles and experimental factors that could potentially improve the accuracy of IVIVE of transporter-based drug disposition:

5.1 IS THE TRANSPORTER ACTIVITY IN VIVO REPLICATED IN VITRO?

One assumption made in both REF approach and primary cell/PSF approach is that the *in vitro* transporter activity reflects that of *in vivo*. However, if this is not the case, it could potentially explain the underpredictions of OATP-mediated hepatic uptake CL. Several factors might account for a difference in OATP activity *in vivo* vs. *in vitro*: **1) Co-transported substrate(s).** The transport mechanism of OATP requires the presence of a co-transported substrate(s). While the identity of this substrate remains elusive, it likely involves the exchange with an anionic intracellular compound (Stieger and Hagenbuch, 2014). If there is a difference between *in vitro* and *in vivo* intracellular concentrations of this co-transported substrate, OATP activity may be compromised. **2) Allosteric effect.** OATP transporters are shown to be allosteric (Kindla *et al.*, 2011). Therefore, it is possible that *in vivo* constituents in blood (a soluble factor or a protein) can bind to the OATP transporters, causing a conformational change of the transporter and thereby altering the drug's affinity for the transporter. In this case, if this endogenous allosteric factor is absent *in vitro*, the *in vitro* drug CL_{int} will not replicate that *in vivo*. While our preliminary studies indicate that human plasma filtrate (containing soluble factor) does not influence statin uptake by OATP1B1-expressing cells, the findings about a true (but modest) PMUE on active transport of ATV, CRV, and PTV (in **Chapter 2** and **Chapter 3**) cannot rule out a potential allosteric effect by albumin. **3) Post-translational modifications (PTMs).** PTMs can affect transporter function without altering transporter

membrane abundance (Sprowl *et al.*, 2016). Therefore, studies should be conducted to determine if transporters are differentially post-translationally modified in TECs/TEVs vs. *in vivo*.

5.2 ARE THE LOCAL UNBOUND DRUG CONCENTRATIONS IN VIVO REPLICATED IN VITRO?

Most of the potential mechanisms of the PMUE postulate that the *in vivo* local unbound drug concentrations are higher than that measured through the *in vitro* protein binding studies, due to an interaction between the drug-protein complex and the lipid membrane of the cells (Miyauchi *et al.*, 2022). Although in **Chapter 2** and **Chapter 3**, we largely discounted the PMUE as a real phenomenon, it is noteworthy that my dissertation research primarily focused on the PMUE observed *in vitro*. In contrast, original studies suggesting the PMUE were conducted using isolated perfused rat liver (IPRL), where the hepatic extraction was evaluated based on the disappearance kinetics of the compound from the perfusate (Forker and Luxon, 1983; Weisiger and Ma, 1987; Tsao *et al.*, 1988). Our residual drug-protein complex hypothesis is specific to the *in vitro* experimental conditions and does not translate directly to these *ex-vivo* studies. Therefore, the PMUE observed *ex vivo* could be a real phenomenon but is not captured by *in vitro* experiments. Collectively, it will be worthwhile to investigate if the PMUE observed in IPRL can improve prediction of hepatobiliary CLs and hepatic concentrations of statins *in vivo*, in the rat.

5.3 DOES THE LACK OF TISSUE ENVIRONMENT IN THE IN VITRO MODEL AFFECT DRUG UPTAKE?

One of the major differences between *in vitro* systems (suspended or plated cells) and *in vivo* conditions is the presence of flow and shear stress exerted on the endothelial cells of the organ of interest (e.g. liver and kidney) by the circulating blood. In this context, microphysiological models (MPS, also known as organs-on-chip) might offer potential benefits as they are designed to recapitulate the tissue environments in terms of fluid flow and shear stress (Chang *et al.*, 2016). However, these models are still in the exploratory phase. Their ability to accurately predict transporter-based drug CL is yet to be determined.

Another difference to consider is the surrounding cellular environment. For example, micro-patterned co-culture hepatocyte models (MPCC, e.g., HepatoPac®, Hμrel®) combine primary human hepatocytes with mouse fibroblasts, with the latter helping maintain the long-term functional stability of the former. Compared to 2D hepatocyte models, MPCCs have higher, and robust functional expression of major hepatic uptake transporters compared to plated mono-cultured hepatocytes without overlay (Moore *et al.*, 2016). However, their ability to accurately predict transporter-based PK of drugs is yet to be explored.

5.4 IS THE CL MODEL USED APPROPRIATELY?

The well-stirred CL model (the basis of the extended CL model) is the most widely used model in the IVIVE of drug CL because of its simplicity. However, the use of more physiologically relevant models taking into account a gradual decrease in tissue concentrations along the organ (e.g., from the periportal to the perivenous regions of the liver), such as the parallel tube or the dispersion model or a 5-compartment liver PBPK model, can yield better predictions of organ CL for intermediate to high extraction drugs (Watanabe *et al.*, 2009; Li and Jusko, 2023). But the choice of these models cannot bridge the gap between predicted and observed CL data for low extraction drugs. We compared the ability of the well-stirred model and the parallel tube model to predict the hepatic uptake CL of RSV (hepatic extraction ratio of ~0.6), and found only minor differences in the predicted values (Storelli et al., 2022). It's important to recognize that most PBPK models used for predicting tissue drug concentrations assume that all tissues are perfusion-limited instantly mixed compartments. In reality, many drugs have low permeability and hence follow permeability-limited distribution such as tenofovir. In addition, there are segmental differences and zonal heterogeneity of transporters and enzymes in the tissue (e.g. liver and intestine) (Fan *et al.*, 2010; Li and Jusko, 2023). Also, tissues are comprised of distinct components such as interstitial fluid, cells, and subcellular organelles, and the local unbound drug concentrations may vary in different parts. As PBPK modeling advances, more mechanistic-based factors should be incorporated, to accurately assess the tissue drug concentrations.

5.5 IS THE IN VIVO HEPATIC CL ESTIMATED CORRECTLY?

The observed *in vivo* organ CL is routinely used to verify the predicted transporter-mediated CL. When a drug is found to be an OATPs-substrate, its hepatic uptake CL is often assumed to be the RDS in its total hepatic CL (Kim *et al.*, 2019). However, we have shown that this assumption is usually incorrect. Consider the situation where all hepatobiliary CLs (*i.e.*, uptake, efflux and metabolic) are RDS. In this case, hepatic CL predicted by IVIVE assuming uptake is the RDS will be overpredicted. Namely, even if IVIVE underpredicts hepatic uptake CL, the hepatic CL will be erroneously assumed to be well-predicted (a good example can be found in Suppl. Fig. 2 of (Kumar *et al.*, 2021)). To compare "apples" with "apples", not "oranges", one should compare the *in vivo* hepatic uptake CL with the *in vitro* hepatic uptake CL. The only solution to this challenge is to estimate the *in vivo* hepatobiliary CLs by PET imaging, an approach undertaken in this dissertation research. Only using the correct *in vivo* verification, one can evaluate the IVIVE performance with confidence.

5.6 ARE THE IN VIVO HEPATOBILIARY CLS AND HEPATIC CONCENTRATIONS ESTIMATED CORRECTLY?

While human PET imaging offers valuable insights, it has several limitations that need to be addressed in future studies. The PET imaging can only measure total drug concentrations. According to the free-drug hypothesis, only the unbound drug exerts the PD effect. A common correction method involves using tissue homogenates to determine the fu in tissue, followed by estimation of unbound drug concentrations. However, the concentrations derived from this approach typically represent the average unbound drug concentrations across all subcellular compartments. As efficacy or toxicity depends on the drug's interaction with specific targets within the subcellular compartment, it is important to understand whether the average unbound drug concentration represents the subcellular compartment of interest. For example, the unbound drug for acidic compounds is usually found in the cytosol, while for basic compounds, it might predominantly be in the lysosomes or mitochondria. An example of heterogeneous subcellular drug distribution is metformin. Model predictions suggest that the $K_{p,uu}$ of metformin for mitochondria and the endoplasmic reticulum is 2 to 3 times higher than

that for the cytoplasm, lysosomes, and nucleus (Chien *et al.*, 2016). It is therefore important to convert fu from tissue homogenates to fu of the subcellular compartment of interest to obtain the unbound drug concentrations at the site of action.

Another potential limitation of PET imaging is its inability to effectively account for drug metabolism when the metabolites retain the radiolabel. At present, the method used to estimate *in vivo* hepatobiliary CLs of the drugs studied assumes minimal metabolism because negligible amount of metabolites were detected in plasma. However, if metabolism occurs and the radio-labeled metabolites display different transport kinetics compared to the parent drug, it could confound our estimates of both transport CLs and tissue drug concentrations. Adequately quantifying the influence of metabolism would necessitate a deeper understanding of the metabolites' transport kinetics and the establishment of a distinct compartment for metabolites in the model.

In addition, as discussed in **Chapter 4**, PET imaging cannot differentiate between the drug in the liver blood, intrahepatic bile canaliculi and liver tissue. This distinction is crucial for accurately estimating the transporter CLs. In our research, due to the absence of detailed kinetics information regarding drug transfer from the intrahepatic bile canaliculi to the gallbladder, we did not factor this in. This omission could result in an overestimation of the *in vivo* hepatic uptake CL, leading to the observed underprediction of RSV's hepatic uptake CL by the TECs/TEVs/REF approach.

In summary, this dissertation research investigated the *in vitro* PMUE and its implications in improving the IVIVE of transporter-mediated drug CL and hence tissue drug concentrations. We found, for the first time, that the widely reported *in vitro* PMUE on OATP-mediated statin uptake is largely an artifact of how the *in vitro* uptake experiments are conducted. Furthermore, where we found the PMUE to be real (i.e., for a few statins using the suspended hepatocytes), the effect was small and insufficient to bridge the gap in IVIVE of hepatic CL of statins. In contrast, we successfully extended the REF approach to predict the hepatobiliary CLs and hepatic concentrations of two OATP-transported drugs, GLB and PTV. These predictions were verified by human PET imaging data. These results suggest that the modest underprediction of RSV's hepatic uptake CL may be specific to RSV. Together with our previous success in using the TECs/TEVs/REF approach to predict

hepatic, brain and fetal distribution of a number of drugs transported by other transporters (e.g. OCT1, P-gp and BCRP), we propose that this approach can be employed with confidence to predict tissue drug concentrations, modulated by transporters (OATPs, NTCP, OCT1, OATPs, P-gp, MRP2 and BCRP), irrespective of whether the drug is substantially metabolized or not. We also propose that the REF approach can be used with confidence for these transporters without incurring the additional cost of PET imaging. For other transporters not explored here such as OATs, the REF approach remains to be interrogated and verified by PET imaging.

Bibliography

Abduljalil K, Cain T, Humphries H, and Rostami-Hodjegan A (2014) Deciding on success criteria for predictability of pharmacokinetic parameters from in vitro studies: an analysis based on in vivo observations. *Drug Metab Dispos* **42**:1478–1484, United States.

Anoshchenko O, Storelli F, and Unadkat JD (2021) Successful prediction of human fetal exposure to P-glycoprotein substrate drugs using the proteomics-informed relative expression factor approach and PBPK modeling and simulation. *Drug Metab Dispos* **49**:919–928, ASPET.

Baik J, and Huang Y (2015) Transporter-Induced Protein Binding Shift (TIPBS): Hypothesis and Modeling, in *Poster* p 1.

Baker KJ, and Bradley SE (1966) Binding of sulfobromophthalein (BSP) sodium by plasma albumin. Its role in hepatic BSP extraction. *J Clin Invest* **45**:281–287.

Baker M, and Parton T (2007) Kinetic determinants of hepatic clearance: Plasma protein binding and hepatic uptake. *Xenobiotica* **37**:1110–1134.

Bi Y, Qiu X, Rotter CJ, Kimoto E, Piotrowski M, Varma M V, Ei-Kattan AF, and Lai Y (2013) Quantitative assessment of the contribution of sodium-dependent taurocholate co-transporting polypeptide (NTCP) to the hepatic uptake of rosuvastatin, pitavastatin and fluvastatin. *Biopharm Drug Dispos* **34**:452–461, England.

Bi YA, Ryu S, Tess DA, Rodrigues AD, and Varma MVS (2021) Effect of human plasma on hepatic uptake of organic anion–transporting polypeptide 1B Substrates: Studies using transfected cells and primary human hepatocytes. *Drug Metab Dispos* **49**:72–83.

Billington S, Shoner S, Lee S, Clark-Snustad K, Pennington M, Lewis D, Muzi M, Rene S, Lee J, Nguyen TB, Kumar V, Ishida K, Chen L, Chu X, Lai Y, Salphati L, Hop CECA, Xiao G, Liao M, and Unadkat JD (2019) Positron Emission Tomography Imaging of [11C]Rosuvastatin Hepatic Concentrations and Hepatobiliary Transport in Humans in the Absence and Presence of Cyclosporin A. *Clin Pharmacol Ther* **106**.

Boman G, and Ringberger V (1974) Binding of Rifampicin by Human Plasma Proteins Binding of Various Concentrations o [RMP Radioassay Calculation o [Binding Binding o [RMP in Healthy Subjects Accuracy and Reproducibility o [the Method. **373**:369–373.

Bouchghoul H, Bouyer J, Senat M-V, Mandelbrot L, Letourneau A, Bourcigaux N, Becquemont L, and Verstuyft C (2021) Hypoglycemia and Glycemic Control With Glyburide in Women With Gestational Diabetes and Genetic Variants of Cytochrome P450 2C9 and/or OATP1B3. *Clin Pharmacol Ther*

110:141–148, United States.

Bowman CM, and Benet LZ (2018) An examination of protein binding and protein-facilitated uptake relating to in vitro-in vivo extrapolation. *Eur J Pharm Sci* **123**:502–514.

Bowman CM, Chen B, Cheong J, Liu L, Chen Y, and Mao J (2021) Improving the translation of organic anion transporting polypeptide substrates using hek293 cell data in the presence and absence of human plasma via physiologically based pharmacokinetic modelings. *Drug Metab Dispos* **49**:530–539.

Bowman CM, Chen E, Chen L, Chen YC, Liang X, Wright M, Chen Y, and Mao J (2020) Changes in Organic Anion Transporting Polypeptide Uptake in HEK293 Overexpressing Cells in the Presence and Absence of Human Plasma. *Drug Metab Dispos* **48**:18–24.

Bowman CM, Okochi H, and Benet LZ (2019) The presence of a transporter-induced protein binding shift: A new explanation for protein-facilitated uptake and improvement for in vitro-in vivo extrapolation. *Drug Metab Dispos* **47**:358–363.

Brunskill NJ, Stuart J, Tobin AB, Walls J, and Nahorski S (1998) Receptor-mediated endocytosis of albumin by kidney proximal tubule cells is regulated by phosphatidylinositide 3-kinase. *J Clin Invest* **101**:2140–2150.

Bteich M, Poulin P, and Haddad S (2019) The potential protein-mediated hepatic uptake: discussion on the molecular interactions between albumin and the hepatocyte cell surface and their implications for the in vitro-to-in vivo extrapolations of hepatic clearance of drugs. *Expert Opin Drug Metab Toxicol* **15**:633–658, Taylor & Francis.

Burczynski FJ, Wang GQ, Elmadhoun B, She YM, Roberts MS, and Standing KG (2001) Hepatocyte [3H]-palmitate uptake: effect of albumin surface charge modification. *Can J Physiol Pharmacol* **79**:868–875, NRC Research Press Ottawa, Canada.

Catapano AL (2010) Pitavastatin–pharmacological profile from early phase studies. *Atheroscler Suppl* **11**:3–7, Elsevier.

Chang SY, Weber EJ, Ness K Van, Eaton DL, and Kelly EJ (2016) Liver and Kidney on Chips: Microphysiological Models to Understand Transporter Function. *Clin Pharmacol Ther* **100**:464–478, United States.

Chien H-C, Zur AA, Maurer TS, Yee SW, Tolsma J, Jasper P, Scott DO, and Giacomini KM (2016) Rapid Method To Determine Intracellular Drug Concentrations in Cellular Uptake Assays: Application to Metformin in Organic Cation Transporter 1-Transfected Human Embryonic Kidney 293 Cells. *Drug Metab Dispos* **44**:356–364, United States.

Deo AK, Prasad B, Balogh L, Lai Y, and Unadkat JD (2012) Interindividual variability in hepatic expression of

the multidrug resistance-associated protein 2 (MRP2/ABCC2): quantification by liquid chromatography/tandem mass spectrometry. *Drug Metab Dispos* **40**:852–855, United States.

Doherty GJ, and McMahon HT (2009) Mechanisms of endocytosis. *Annu Rev Biochem* **78**:857–902, Annual Reviews.

Duan P, Zhao P, and Zhang L (2017) Physiologically based pharmacokinetic (PBPK) modeling of pitavastatin and atorvastatin to predict drug-drug interactions (DDIs). *Eur J Drug Metab Pharmacokinet* **42**:689–705, Springer.

Esteller A (2008) Physiology of bile secretion. *World J Gastroenterol* **14**:5641–5649, United States.

Fallon JK, Smith PC, Xia CQ, and Kim M-S (2016) Quantification of Four Efflux Drug Transporters in Liver and Kidney Across Species Using Targeted Quantitative Proteomics by Isotope Dilution NanoLC-MS/MS. *Pharm Res* **33**:2280–2288, United States.

Fan J, Chen S, CY Chow E, and Sandy Pang K (2010) PBPK modeling of intestinal and liver enzymes and transporters in drug absorption and sequential metabolism. *Curr Drug Metab* **11**:743–761, Bentham Science Publishers.

Feldman JM (1985) Glyburide: a second-generation sulfonylurea hypoglycemic agent: history, chemistry, metabolism, pharmacokinetics, clinical use and adverse effects. *Pharmacother J Hum Pharmacol Drug Ther* **5**:43–62, Wiley Online Library.

Feldschuh J, and Enson Y (1977) Prediction of the normal blood volume. Relation of blood volume to body habitus. *Circulation* **56**:605–612, United States.

Fleishaker JC, and Phillips JP (1991) Evaluation of a potential interaction between erythromycin and glyburide in diabetic volunteers. *J Clin Pharmacol* **31**:259–262, England.

Forker EL, and Luxon BA (1983) Albumin-mediated transport of rose bengal by perfused rat liver. Kinetics of the reaction of the cell surface. *J Clin Invest* **72**:1764–1771.

Forker EL, and Luxon BA (1981) Albumin helps mediate removal of taurocholate by rat liver. *J Clin Invest* **67**:1517–1522.

Francis LJ, Houston JB, and Hallifax D (2021) Impact of plasma protein binding in drug clearance prediction: A database analysis of published studies and implications for in vitro-in vivo extrapolation. *Drug Metab Dispos* **49**:188–201.

Fujino H, Saito T, Ogawa S-I, and Kojima J (2005) Transporter-mediated influx and efflux mechanisms of pitavastatin, a new inhibitor of HMG-CoA reductase. *J Pharm Pharmacol* **57**:1305–1311, England.

Fujino H, Yamada I, Shimada S, Yoneda M, and Kojima J (2003) Metabolic fate of pitavastatin, a new inhibitor

of HMG-CoA reductase: human UDP-glucuronosyltransferase enzymes involved in lactonization. *Xenobiotica* **33**:27–41, Taylor & Francis.

Harrison RK (2016) Phase II and phase III failures: 2013–2015. *Nat Rev Drug Discov* **15**:817–818.

Hay M, Thomas DW, Craighead JL, Economides C, and Rosenthal J (2014) Clinical development success rates for investigational drugs. *Nat Biotechnol* **32**:40–51, United States.

He J, Yu Y, Prasad B, Link J, Miyaoka RS, Chen X, and Unadkat JD (2014) PET imaging of oatp-mediated hepatobiliary transport of [11C] rosuvastatin in the rat. *Mol Pharm* **11**:2745–2754, American Chemical Society.

Hebert MF, Ma X, Naraharisetti SB, Krudys KM, Umans JG, Hankins GD V, Caritis SN, Miodovnik M, Mattison DR, Unadkat JD, Kelly EJ, Blough D, Cobelli C, Ahmed MS, Snodgrass WR, Carr DB, Easterling TR, and Vicini P (2009) Are we optimizing gestational diabetes treatment with glyburide? The pharmacologic basis for better clinical practice. *Clin Pharmacol Ther* **85**:607–614, United States.

Hernández Lozano I, and Langer O (2020) Use of imaging to assess the activity of hepatic transporters. *Expert Opin Drug Metab Toxicol* **16**:149–164, Taylor & Francis.

Hirano M, Maeda K, Shitara Y, and Sugiyama Y (2004) Contribution of OATP2 (OATP1B1) and OATP8 (OATP1B3) to the hepatic uptake of pitavastatin in humans. *J Pharmacol Exp Ther* **311**:139–146.

Horie T, Mizuma T, Kasai S, and Awazu S (1988) Conformational change in plasma albumin due to interaction with isolated rat hepatocyte. *Am J Physiol Liver Physiol* **254**:G465–G470.

Hoy SM (2017) Pitavastatin: a review in hypercholesterolemia. *Am J Cardiovasc Drugs* **17**:157–168, Springer.

Hwang S, Lee SG, Kim KH, Park KM, Ahn CS, Moon DB, Chu CW, Lee YJ, and Min PC (2002) Correlation of blood-free graft weight and volumetric graft volume by an analysis of blood content in living donor liver grafts, in *Transplantation proceedings* pp 3293–3294.

Ito K, and Houston JB (2005) Prediction of human drug clearance from in vitro and preclinical data using physiologically based and empirical approaches. *Pharm Res* **22**:103–112, United States.

Izumi S, Nozaki Y, Maeda K, Komori T, Takenaka O, Kusuhara H, and Sugiyama Y (2015) Investigation of the impact of substrate selection on in vitro organic anion transporting polypeptide 1B1 inhibition profiles for the prediction of drug-drug interactions. *Drug Metab Dispos* **43**:235–247.

Jones HM, Barton HA, Lai Y, Bi YA, Kimoto E, Kempshall S, Tate SC, El-Kattan A, Houston JB, Galetin A, and Fenner KS (2012) Mechanistic pharmacokinetic modeling for the prediction of transporter-mediated disposition in humans from sandwich culture human hepatocyte data. *Drug Metab Dispos* **40**:1007–1017.

Karlgren M, Vildhede A, Norinder U, Wisniewski JR, Kimoto E, Lai Y, Haglund U, and Artursson P (2012)

Classification of inhibitors of hepatic organic anion transporting polypeptides (OATPs): influence of protein expression on drug-drug interactions. *J Med Chem* **55**:4740–4763, United States.

Ke AB, Eyal S, Chung FS, Link JM, Mankoff DA, Muzi M, and Unadkat JD (2013) Modeling cyclosporine A inhibition of the distribution of a P-glycoprotein PET ligand, 11C-verapamil, into the maternal brain and fetal liver of the pregnant nonhuman primate: impact of tissue blood flow and site of inhibition. *J Nucl Med* **54**:437–446, United States.

Kesselheim AS, Hwang TJ, and Franklin JM (2015) Two decades of new drug development for central nervous system disorders. *Nat Rev Drug Discov* **14**:815–816, England.

Kim SJ, Lee KR, Miyauchi S, and Sugiyama Y (2019) Extrapolation of in vivo hepatic clearance from in vitro uptake clearance by suspended human hepatocytes for anionic drugs with high binding to human albumin: Improvement of in vitro-to-in vivo extrapolation by considering the "albumin-mediated" hepatic u. *Drug Metab Dispos* **47**:94–103.

Kindla J, Müller F, Mieth M, Fromm MF, and König J (2011) Influence of non-steroidal anti-inflammatory drugs on Organic Anion Transporting Polypeptide (OATP) 1B1- and OATP1B3-mediated drug transport. *Drug Metab Dispos* **39**:1047–1053.

Krishnan S, Ramsden D, Ferguson D, Stahl SH, Wang J, McGinnity DF, and Hariparsad N (2022) Challenges and Opportunities for Improved Drug-Drug Interaction Predictions for Renal OCT2 and MATE1/2-K Transporters. *Clin Pharmacol Ther* **112**:562–572, United States.

Kumar V, Li CY, Ishida K, Kis E, Gáborik Z, and Unadkat JD (2020) Pitfalls in Predicting Hepatobiliary Drug Transport Using Human Sandwich-Cultured Hepatocytes. *AAPS J* **22**:110.

Kumar V, Nguyen TB, Tóth B, Juhasz V, and Unadkat JD (2017) Optimization and Application of a Biotinylation Method for Quantification of Plasma Membrane Expression of Transporters in Cells. *AAPS J* **19**:1377–1386, United States.

Kumar V, Salphati L, Hop CECA, Xiao G, Lai Y, Mathias A, Chu X, Humphreys WG, Liao M, Heyward S, and Unadkat JD (2019) A Comparison of Total and Plasma Membrane Abundance of Transporters in Suspended, Plated, Sandwich-Cultured Human Hepatocytes Versus Human Liver Tissue Using Quantitative Targeted Proteomics and Cell Surface Biotinylation. *Drug Metab Dispos* **47**:350–357, United States.

Kumar V, Yin M, Ishida K, Salphati L, Hop CECA, Rowbottom C, Xiao G, Lai Y, Mathias A, Chu X, Humphreys WG, Liao M, Nerada Z, Szilvásy N, Heyward S, and Unadkat JD (2021) Prediction of Transporter-Mediated Rosuvastatin Hepatic Uptake Clearance and Drug Interaction in Humans Using Proteomics-Informed REF Approach. *Drug Metab Dispos* **49**:159 LP – 168.

Langer O (2016) Use of PET imaging to evaluate transporter-mediated drug-drug interactions. *J Clin Pharmacol* **56**:S143–S156, Wiley Online Library.

Lau YY, Okochi H, Huang Y, and Benet LZ (2006) Multiple transporters affect the disposition of atorvastatin and its two active hydroxy metabolites: application of in vitro and ex situ systems. *J Pharmacol Exp Ther* **316**:762–771, United States.

Li N, Badrinarayanan A, Ishida K, Li X, Roberts J, Wang S, Hayashi M, and Gupta A (2021) Albumin-Mediated Uptake Improves Human Clearance Prediction for Hepatic Uptake Transporter Substrates Aiding a Mechanistic In Vitro-In Vivo Extrapolation (IVIVE) Strategy in Discovery Research. *AAPS J* **23**.

Li N, Badrinarayanan A, Li X, Roberts J, Hayashi M, Virk M, and Gupta A (2020) Comparison of in vitro to in vivo extrapolation approaches for predicting transporter-mediated hepatic uptake clearance using suspended rat hepatocytes. *Drug Metab Dispos* **48**:861–872.

Li R, Bi Y, Vildhede A, Scialis RJ, Mathialagan S, Yang X, Marroquin LD, Lin J, and Varma MVS (2017) Transporter-mediated disposition, clinical pharmacokinetics and cholestatic potential of glyburide and its primary active metabolites. *Drug Metab Dispos* **45**:737–747, ASPET.

Li X, and Jusko WJ (2022) Assessing Liver-to-Plasma Partition Coefficients and In Silico Calculation Methods: When Does the Hepatic Model Matter in PBPK? *Drug Metab Dispos*, doi: 10.1124/dmd.122.000994, United States.

Li X, and Jusko WJ (2023) Exploring the Pharmacokinetic Mysteries of the Liver: Application of Series Compartment Models of Hepatic Elimination. *Drug Metab Dispos* **51**:618–628, American Society for Pharmacology and Experimental Therapeutics.

Liang X, Park Y, DeForest N, Hao J, Zhao X, Niu C, Wang K, Smith B, and Lai Y (2020) In vitro hepatic uptake in human and monkey hepatocytes in the presence and absence of serum protein and its in vitro to in vivo extrapolation. *Drug Metab Dispos* **48**:1283–1292.

Lilja JJ, Niemi M, Fredrikson H, and Neuvonen PJ (2007) Effects of clarithromycin and grapefruit juice on the pharmacokinetics of glibenclamide. *Br J Clin Pharmacol* **63**:732–740, England.

Link E, Parish S, Armitage J, Bowman L, Heath S, Matsuda F, Gut I, Lathrop M, and Collins R (2008) SLCO1B1 variants and statin-induced myopathy--a genomewide study. *N Engl J Med* **359**:789–799, United States.

Liu X (2019) Transporter-Mediated Drug-Drug Interactions and Their Significance. *Adv Exp Med Biol* **1141**:241–291, United States.

Mairinger S, Hernández-Lozano I, Zeitlinger M, Ehrhardt C, and Langer O (2022) Nuclear medicine imaging

methods as novel tools in the assessment of pulmonary drug disposition. *Expert Opin Drug Deliv* **19**:1561–1575, Taylor & Francis.

Mao J, Doshi U, Wright M, Hop CECA, Li AP, and Chen Y (2018) Prediction of the Pharmacokinetics of Pravastatin as an OATP Substrate Using Plateable Human Hepatocytes With Human Plasma Data and PBPK Modeling. *CPT Pharmacometrics Syst Pharmacol* **7**:251–258.

Marie S, Breuil L, Chalampalakis Z, Becquemont L, Verstuyft C, Lecoq A-L, Caillé F, Gervais P, Lebon V, Comtat C, Bottlaender M, and Tournier N (2022) [(11)C]glyburide PET imaging for quantitative determination of the importance of Organic Anion-Transporting Polypeptide transporter function in the human liver and whole-body. *Biomed Pharmacother* **156**:113994, France.

Mathialagan S, Piotrowski MA, Tess DA, Feng B, Litchfield J, and Varma M V (2017) Quantitative Prediction of Human Renal Clearance and Drug-Drug Interactions of Organic Anion Transporter Substrates Using In Vitro Transport Data: A Relative Activity Factor Approach. *Drug Metab Dispos* **45**:409–417, United States.

Matthews PM, Rabiner EA, Passchier J, and Gunn RN (2012) Positron emission tomography molecular imaging for drug development. *Br J Clin Pharmacol* **73**:175–186, Wiley Online Library.

Mitra P, Weinheimer S, Michalewicz M, and Taub ME (2018) Prediction and quantification of hepatic transporter-mediated uptake of pitavastatin utilizing a combination of the relative activity factor approach and mechanistic modeling. *Drug Metab Dispos* **46**:953–963.

Miyauchi S, Kim S-J, Lee W, and Sugiyama Y (2022) Consideration of albumin-mediated hepatic uptake for highly protein-bound anionic drugs: Bridging the gap of hepatic uptake clearance between in vitro and in vivo. *Pharmacol Ther* **229**:107938, Elsevier.

Miyauchi S, Kim SJ, Lee W, and Sugiyama Y (2021) Consideration of albumin-mediated hepatic uptake for highly protein-bound anionic drugs: Bridging the gap of hepatic uptake clearance between in vitro and in vivo. *Pharmacol Ther* 107938, Elsevier Inc.

Miyauchi S, Masuda MM, Kim SJ, Tanaka Yuudai, Lee KR, Iwakado S, Nemoto M, Sasaki S, Shimono K, Tanaka Yoshio, and Sugiyama Y (2018) The phenomenon of albumin-mediated hepatic uptake of organic anion transport polypeptide substrates: Prediction of the in vivo uptake clearance from the in vitro uptake by isolated hepatocytes using a facilitated-dissociation model. *Drug Metab Dispos* **46**:259–267.

Moman RN, Gupta N, and Varacallo M (2022) Physiology, Albumin.[Updated 2022 Jan 4]. *StatPearls [Internet] Treasure Isl StatPearls Publ*.

Moore A, Chothe PP, Tsao H, and Hariparsad N (2016) Evaluation of the Interplay between Uptake Transport and CYP3A4 Induction in Micropatterned Cocultured Hepatocytes. *Drug Metab Dispos* **44**:1910–1919,

United States.

Morgan RE, Campbell SE, Yu CY, Sponseller CA, and Muster HA (2012) Comparison of the Safety, Tolerability, and Pharmacokinetic Profile of a Single Oral Dose of Pitavastatin 4 mg in Adult Subjects With Severe Renal Impairment Not on Hemodialysis Versus Healthy Adult Subjects. *J Cardiovasc Pharmacol* **60**.

Müller M, Schmid R, Georgopoulos A, Buxbaum A, Wasicek C, and Eichler H (1995) Application of microdialysis to clinical pharmacokinetics in humans. *Clin Pharmacol Ther* **57**:371–380, Wiley Online Library.

Nakaoka T, Kaneko K-I, Irie S, Mawatari A, Igesaka A, Uetake Y, Ochiai H, Niwa T, Yamano E, Wada Y, Tanaka M, Kotani K, Kawahata H, Kawabe J, Miki Y, Doi H, Hosoya T, Kazuya M, Kusuhara H, Sugiyama Y, and Watanabe Y (2022) Clinical evaluation of [(18)F]pitavastatin for quantitative analysis of hepatobiliary transporter activity. *Drug Metab Pharmacokinet* **44**:100449, England.

Naritomi Y, Terashita S, and Kagayama A (2004) Identification and relative contributions of human cytochrome P450 isoforms involved in the metabolism of glibenclamide and lansoprazole: evaluation of an approach based on the in vitro substrate disappearance rate. *Xenobiotica* **34**:415–427, Taylor & Francis.

Nelson CH, Peng C-C, Lutz JD, Yeung CK, Zelter A, and Isoherranen N (2016) Direct protein-protein interactions and substrate channeling between cellular retinoic acid binding proteins and CYP26B1.

Neugebauer G, Betzien G, Hrstka V, Kaufmann B, Von Möllendorff E, and Abshagen U (1985) Absolute bioavailability and bioequivalence of glibenclamide (Semi-Euglucon N). *Int J Clin Pharmacol Ther Toxicol* **23**:453–460.

Niemi M (2010) Transporter Pharmacogenetics and Statin Toxicity. *Clin Pharmacol \& Ther* **87**:130–133.

Nunes R, Kiang C-L, Sorrentino D, and Berk PD (1988) 'Albumin-receptor' uptake kinetics do not require an intact lobular architecture and are not specific for albumin. *J Hepatol* **7**:293–304.

Obach RS, Lombardo F, and Waters NJ (2008) Trend analysis of a database of intravenous pharmacokinetic parameters in humans for 670 drug compounds. *Drug Metab Dispos* **36**:1385–1405, United States.

Okudaira M, Ikawa N, Yasuhara M, Kumagai T, and Kurosu K (2000) Liver weight of adult Japanese, especially recent weight values. *Hepatol Res* **18**:95–103, Netherlands.

Otoom S, Hasan M, and Najib N (2001) The bioavailability of glyburide (glibenclamide) under fasting and feeding conditions: a comparative study. *Int J Pharm Med* **15**:117–120, Springer.

Patilea-Vrana G, and Unadkat J (2016) Transport vs. Metabolism: What Determines the Pharmacokinetics and Pharmacodynamics of Drugs? Insights From the Extended Clearance Model. *Clin Pharmacol Ther*

100:413–418, Nature Publishing Group.

Patilea-Vrana G., and Unadkat JD (2016) Transport vs. Metabolism: What Determines the Pharmacokinetics and Pharmacodynamics of Drugs? Insights From the Extended Clearance Model. *Clin Pharmacol Ther* 413–418, Nature Publishing Group.

Pearson JG (1985) Pharmacokinetics of glyburide. *Am J Med* **79**:67–71.

Poulin P, and Haddad S (2018) Extrapolation of the Hepatic Clearance of Drugs in the Absence of Albumin In Vitro to That in the Presence of Albumin In Vivo : Comparative Assessement of 2 Extrapolation Models Based on the Albumin-Mediated Hepatic Uptake Theory and Limitations and Mecha. *J Pharm Sci* **107**:1791–1797, Elsevier Ltd.

Prasad B, Evers R, Gupta A, Hop CECA, Salphati L, Shukla S, Ambudkar S V, and Unadkat JD (2014) Interindividual variability in hepatic organic anion-transporting polypeptides and P-glycoprotein (ABCB1) protein expression: quantification by liquid chromatography tandem mass spectroscopy and influence of genotype, age, and sex. *Drug Metab Dispos* **42**:78–88, United States.

Prasad B, Lai Y, Lin Y, and Unadkat JD (2013) Interindividual variability in the hepatic expression of the human breast cancer resistance protein (BCRP/ABCG2): effect of age, sex, and genotype. *J Pharm Sci* **102**:787–793, United States.

Riccardi K, Ryu S, Lin J, Yates P, Tess D, Li R, Singh D, Holder BR, Kapinos B, Chang G, and Di L (2018) Comparison of Species and Cell-Type Differences in Fraction Unbound of Liver Tissues, Hepatocytes, and Cell Lines. *Drug Metab Dispos* **46**:415–421, United States.

Riccardi K, Ryu S, Tess D, Li R, Luo L, Johnson N, Jordan S, Patel R, and Di L (2020) Comparison of Fraction Unbound Between Liver Homogenate and Hepatocytes at 4°C. *AAPS J* **22**:91, United States.

Riccardi Keith A, Tess DA, Lin J, Patel R, Ryu S, Atkinson K, Di L, and Li R (2019) A Novel Unified Approach to Predict Human Hepatic Clearance for Both Enzyme- and Transporter-Mediated Mechanisms Using Suspended Human Hepatocytes. *Drug Metab Dispos* **47**:484–492, United States.

Riccardi Keith A., Tess DA, Lin J, Patel R, Ryu S, Atkinson K, Di L, and Li R (2019) A novel unified approach to predict human hepatic clearance for both enzyme- And transporter-mediated mechanisms using suspended human hepatocytes. *Drug Metab Dispos* **47**:484–492.

Romaine SPR, Bailey KM, Hall AS, and Balmforth AJ (2010) The influence of SLCO1B1 (OATP1B1) gene polymorphisms on response to statin therapy. *Pharmacogenomics J* **10**:1–11.

Rose RH, Neuhoff S, Abduljalil K, Chetty M, Rostami-Hodjegan A, and Jamei M (2014) Application of a physiologically based pharmacokinetic model to predict OATP1B1-related variability in

pharmacodynamics of rosuvastatin. *CPT pharmacometrics Syst Pharmacol* **3**:1–9, Wiley Online Library.

Rupp W, Christ O, and Fülberth W (1972) [Studies on the bioavailability of glibenclamide]. *Arzneimittelforschung* **22**:471–473, Germany.

Rydberg T, Jönsson A, and Melander A (1995) Comparison of the kinetics of glyburide and its active metabolites in humans. *J Clin Pharm Ther* **20**:283–295, John Wiley & Sons, Ltd.

Sachar M, Kumar V, Gormsen LC, Munk OL, and Unadkat JD (2020) Successful Prediction of Positron Emission Tomography-Imaged Metformin Hepatic Uptake Clearance in Humans Using the Quantitative Proteomics-Informed Relative Expression Factor Approach. *Drug Metab Dispos* **48**:1210–1216, United States.

Saito Y (2011) Pitavastatin: an overview. *Atheroscler Suppl* **12**:271–276, Elsevier.

Sand KMK, Bern M, Nilsen J, Noordzij HT, Sandlie I, and Andersen JT (2015) Unraveling the interaction between FcRn and albumin: opportunities for design of albumin-based therapeutics. *Front Immunol* **5**:682, Frontiers.

Scharschmidt BF, Lake JR, Renner EL, Licko V, and Van Dyke RW (1986) Fluid phase endocytosis by cultured rat hepatocytes and perfused rat liver: implications for plasma membrane turnover and vesicular trafficking of fluid phase markers. *Proc Natl Acad Sci* **83**:9488–9492, National Acad Sciences.

SCHENK WGJ, McDONALD JC, McDONALD K, and DRAPANAS T (1962) Direct measurement of hepatic blood flow in surgical patients: with related observations on hepatic flow dynamics in experimental animals. *Ann Surg* **156**:463–471, United States.

Schulz JA, Stresser DM, and Kalvass JC (2023) Plasma protein-mediated uptake and contradictions to the free drug hypothesis: a critical review. *Drug Metab Rev* 1–34, Taylor & Francis.

Sluijs P Van Der, Postema B, and Meijer DKF (1987) Lactosylation of albumin reduces uptake rate of dibromosulfophthalein in perfused rat liver and dissociation rate from albumin in vitro. *Hepatology* **7**:688–695, Wiley Online Library.

Smietana K, Siatkowski M, and Møller M (2016) Trends in clinical success rates. *Nat Rev Drug Discov* **15**:379–380, England.

Soars MG, Grime K, Sproston JL, Webborn PJH, and Riley RJ (2007) Use of hepatocytes to assess the contribution of hepatic uptake to clearance in vivo. *Drug Metab Dispos* **35**:859–865.

Soars MG, McGinnity DF, Grime K, and Riley RJ (2007) The pivotal role of hepatocytes in drug discovery. *Chem Biol Interact* **168**:2–15.

Sprowl JA, Ong SS, Gibson AA, Hu S, Du G, Lin W, Li L, Bharill S, Ness RA, Stecula A, Offer SM, Diasio

RB, Nies AT, Schwab M, Cavaletti G, Schlatter E, Ciarimboli G, Schellens JHM, Isacoff EY, Sali A, Chen T, Baker SD, Sparreboom A, and Pabla N (2016) A phosphotyrosine switch regulates organic cation transporters. *Nat Commun* **7**:10880, England.

Stahl M, Bouw R, Jackson A, and Pay V (2002) Human microdialysis. *Curr Pharm Biotechnol* **3**:165–178, Bentham Science Publishers.

Stieger B, and Hagenbuch B (2014) *Organic anion-transporting polypeptides*, 1st ed., Elsevier Inc.

Storelli F, Anoshchenko O, and Unadkat JD (2021) Successful Prediction of Human Steady-State Unbound Brain-to-Plasma Concentration Ratio of P-gp Substrates Using the Proteomics-Informed Relative Expression Factor Approach. *Clin Pharmacol Ther* **110**:432–442, John Wiley and Sons Inc.

Storelli F, Li CY, Sachar M, Kumar V, Heyward S, Sáfár Z, Kis E, and Unadkat JD (2022) Prediction of Hepatobiliary Clearances and Hepatic Concentrations of Transported Drugs in Humans Using Rosuvastatin as a Model Drug. *Clin Pharmacol Ther* **112**:593–604, United States.

Storelli F, Yin M, Kumar AR, Ladumor MK, Evers R, Chothe PP, Enogieru OJ, Liang X, Lai Y, and Unadkat JD (2022) The next frontier in ADME science: Predicting transporter-based drug disposition, tissue concentrations and drug-drug interactions in humans. *Pharmacol Ther* **238**:108271, England.

Stremmel W, Potter BJ, and Berk PD (1983) Studies of albumin binding to rat liver plasma membranes: implications for the albumin receptor hypothesis. *Biochim Biophys Acta (BBA)-General Subj* **756**:20–27, Elsevier.

Tsao SC, Sugiyama Y, Sawada Y, Iga T, and Hanano M (1988) Kinetic analysis of albumin-mediated uptake of warfarin by perfused rat liver. *J Pharmacokinet Biopharm* **16**:165–181, United States.

Tse FL, Nickerson DF, and Yardley WS (1993) Binding of fluvastatin to blood cells and plasma proteins. *J Pharm Sci* **82**:942–947, United States.

Van De Steeg E, Greupink R, Schreurs M, Nooijen IHG, Verhoeck KCM, Hanemaaijer R, Ripken D, Monshouwer M, Vlaming MLH, DeGroot J, Verwei M, Russel FGM, Huisman MT, and Wortelboer HM (2013) Drug-drug interactions between rosuvastatin and oral antidiabetic drugs occurring at the level of oatp1b1s. *Drug Metab Dispos* **41**:592–601.

Varma MVS, Scialis RJ, Lin J, Bi Y-A, Rotter CJ, Goosen TC, and Yang X (2014) Mechanism-based pharmacokinetic modeling to evaluate transporter-enzyme interplay in drug interactions and pharmacogenetics of glyburide. *AAPS J* **16**:736–748, United States.

Vauthey J-N, Abdalla EK, Doherty DA, Gertsch P, Fenstermacher MJ, Loyer EM, Lerut J, Materne R, Wang X, Encarnacion A, Herron D, Mathey C, Ferrari G, Charnsangavej C, Do K-A, and Denys A (2002) Body

surface area and body weight predict total liver volume in Western adults. *Liver Transplant Off Publ Am Assoc Study Liver Dis Int Liver Transplant Soc* **8**:233–240, United States.

Walker N, Filis P, Soffientini U, Bellingham M, O'Shaughnessy PJ, and Fowler PA (2017) Placental transporter localization and expression in the human: the importance of species, sex, and gestational age differences. *Biol Reprod* **96**:733–742, Oxford University Press.

Wang L, Prasad B, Salphati L, Chu X, Gupta A, Hop CECA, Evers R, and Unadkat JD (2015) Interspecies variability in expression of hepatobiliary transporters across human, dog, monkey, and rat as determined by quantitative proteomics. *Drug Metab Dispos* **43**:367–374, United States.

Wang L, Zhu Z, Tran D, Seo SK, and Pan X (2021) Advancing estimation of hepatobiliary clearances in physiologically based pharmacokinetic models of Rosuvastatin using human hepatic concentrations. *Pharm Res* 1–12, Springer.

Warrington S, Nagakawa S, and Hounslow N (2011) Comparison of the pharmacokinetics of pitavastatin by formulation and ethnic group: an open-label, single-dose, two-way crossover pharmacokinetic study in healthy Caucasian and Japanese men. *Clin Drug Investig* **31**:735–743, New Zealand.

Watanabe T, Kusuhara H, Maeda K, Kanamaru H, Saito Y, Hu Z, and Sugiyama Y (2010) Investigation of the rate-determining process in the hepatic elimination of HMG-CoA reductase inhibitors in rats and humans. *Drug Metab Dispos* **38**:215–222.

Watanabe T, Kusuhara H, Maeda K, Shitara Y, and Sugiyama Y (2009) Physiologically based pharmacokinetic modeling to predict transporter-mediated clearance and distribution of pravastatin in humans. *J Pharmacol Exp Ther* **328**:652–662, United States.

Weisiger R, Gollan J, and Ockner R (1981) Receptor for Albumin on the Liver Cell Surface May Mediate Uptake of Fatty Acids and Other Albumin-Bound Substances. *Science (80-)* **211**:1048–1051.

Weisiger RA, and Ma WL (1987) Uptake of oleate from albumin solutions by rat liver. Failure to detect catalysis of the dissociation of oleate from albumin by an albumin receptor. *J Clin Invest* **79**:1070–1077, United States.

Weisiger RA, Zacks CM, Smith ND, and Boyer JL (1984) Effect of Albumin Binding on Extraction of Sulfobromophthalein by Perfused Elasmobranch Liver: Evidence for Dissociation-Limited Uptake. *Hepatology* **4**:492–501.

Wood FL, Houston JB, and Hallifax D (2017) Clearance prediction methodology needs fundamental improvement: Trends common to rat and human hepatocytes/microsomes and implications for experimental methodology. *Drug Metab Dispos* **45**:1178–1188.

Yabut KCB, and Isoherranen N (2022) CRABPs Alter all-trans-Retinoic Acid Metabolism by CYP26A1 via Protein-Protein Interactions. *Nutrients* **14**, Switzerland.

Yin M, Ishida K, Liang X, Lai Y, and Unadkat JD (2023) Interpretation of Protein-Mediated Uptake of Statins by Hepatocytes Is Confounded by the Residual Statin-Protein Complex. *Drug Metab Dispos* **51**:1381–1390, American Society for Pharmacology and Experimental Therapeutics.

Yin M, Storelli F, and Unadkat JD (2022) Is The Protein-Mediated Uptake Of Drugs By OATPs A Real Phenomenon Or An Artifact? *Drug Metab Dispos*, doi: 10.1124/dmd.122.000849, United States.

Yoshikado T, Toshimoto K, Nakada T, Ikejiri K, Kusuhara H, Maeda K, and Sugiyama Y (2017) Comparison of Methods for Estimating Unbound Intracellular-to-Medium Concentration Ratios in Rat and Human Hepatocytes Using Statins. *Drug Metab Dispos* **45**:779–789, United States.

Zang R, Barth A, Wong H, Marik J, Shen J, Lade J, Grove K, Durk MR, Parrott N, and Rudewicz PJ (2022) Design and measurement of drug tissue concentration asymmetry and tissue exposure-effect (Tissue PK-PD) evaluation. *J Med Chem* **65**:8713–8734, ACS Publications.

Zhang D, Hop CECA, Patilea-Vrana G, Gampa G, Seneviratne HK, Unadkat JD, Kenny JR, Nagapudi K, Di L, Zhou L, Zak M, Wright MR, Bumpus NN, Zang R, Liu X, Lai Y, and Khojasteh SC (2019) Drug Concentration Asymmetry in Tissues and Plasma for Small Molecule-Related Therapeutic Modalities. *Drug Metab Dispos* **47**:1122–1135.

Zheng HX, Huang Y, Frassetto LA, and Benet LZ (2009) Elucidating rifampin's inducing and inhibiting effects on glyburide pharmacokinetics and blood glucose in healthy volunteers: unmasking the differential effects of enzyme induction and transporter inhibition for a drug and its primary metabolite. *Clin Pharmacol Ther* **85**:78–85, United States.

Zhou L, Naraharisetti SB, Liu L, Wang H, Lin YS, Isoherranen N, Unadkat JD, Hebert MF, and Mao Q (2010) Contributions of human cytochrome P450 enzymes to glyburide metabolism. *Biopharm Drug Dispos* **31**:228–242, Wiley Online Library.

VITA

Mengyue Yin was an international Ph.D student at the University of Washington. Originally from China, she received her bachelor's degree at China Pharmaceutical University (Nanjing, China).